

University of Groningen

Securing and Maneuvering Heterogeneous Mobile Robot Formations

Chan, Nelson

DOI:
[10.33612/diss.173545061](https://doi.org/10.33612/diss.173545061)

IMPORTANT NOTE: You are advised to consult the publisher's version (publisher's PDF) if you wish to cite from it. Please check the document version below.

Document Version
Publisher's PDF, also known as Version of record

Publication date:
2021

[Link to publication in University of Groningen/UMCG research database](#)

Citation for published version (APA):

Chan, N. (2021). *Securing and Maneuvering Heterogeneous Mobile Robot Formations: Distributed Control Design and Stability Analysis*. [Thesis fully internal (DIV), University of Groningen]. University of Groningen. <https://doi.org/10.33612/diss.173545061>

Copyright

Other than for strictly personal use, it is not permitted to download or to forward/distribute the text or part of it without the consent of the author(s) and/or copyright holder(s), unless the work is under an open content license (like Creative Commons).

The publication may also be distributed here under the terms of Article 25fa of the Dutch Copyright Act, indicated by the "Taverne" license. More information can be found on the University of Groningen website: <https://www.rug.nl/library/open-access/self-archiving-pure/taverne-amendment>.

Take-down policy

If you believe that this document breaches copyright please contact us providing details, and we will remove access to the work immediately and investigate your claim.

Downloaded from the University of Groningen/UMCG research database (Pure): <http://www.rug.nl/research/portal>. For technical reasons the number of authors shown on this cover page is limited to 10 maximum.

Securing and Maneuvering Heterogeneous Mobile Robot Formations

Distributed control design and stability analysis

Nelson Chan

陈鹏举



university of
 groningen

The research described in this dissertation has been carried out at the Faculty of Science and Engineering, University of Groningen, Groningen, The Netherlands.

disc

This dissertation has been completed in partial fulfillment of the requirements of the Dutch Institute of Systems and Control (DISC) for graduate study. The author has successfully completed the educational program of DISC.



provincie
 groningen

provincie Drenthe

provinsje fryslân
 provincie fryslân

This project is cofunded by the Northern Netherlands Alliance (SNN), Regional Economic Programme.



university of
 groningen

Securing and Maneuvering Heterogeneous Mobile Robot Formations

Distributed control design and stability analysis

PhD thesis

to obtain the degree of PhD at the
 University of Groningen
 on the authority of the
 Rector Magnificus Prof. C. Wijmenga
 and in accordance with
 the decision by the College of Deans.

This thesis will be defended in public on

Friday 9 July 2021 at 14.30 hours

by

Nelson Pen Kie Chan

born on 30 November 1989
 in Paramaribo, Suriname

Supervisors

Prof. B. Jayawardhana

Prof. J.M.A. Scherpen

Assessment committee

Prof. M. Cao

Prof. M.K. Çamlıbel

Prof. D.V. Dimarogonas

To my family

父亲 陈新兴
母亲 张惠娟
姐姐 陈诗慧

Acknowledgments

At last! The train ride labeled ‘PhD’ is coming to an end. Let me sit here for some more moments to recall the past 4+ years while the train is at the destination, but not yet standing still. While doing so, allow me to address a few words to some particular individuals.

The first on my list is Bayu. Bayu, *terima kasih!* I am grateful you have taken me under your wing in the past period. You have given me freedom to explore but also make sure I stay on the rails. You always have a smile on your face during our meetings which were not limited to only discussing research. I also thank you for the support you have shown me when I asked you for permission to conduct additional teaching duties after my involvement in the course ‘Signals & Systems’.

Dear Jacquélien, I am grateful to you for the discussions we had during the start of my PhD which led to Chapter 6 of the thesis and the good time we spent in Hong Kong! Needless to mention, the annual group outing we have and the ‘nieuwjaarsrolletjes’ with cream you bring at the start of each year.

Gracias también to Hector with whom I have collaborated on different chapters of the thesis. Hector, your cheerful appearance during our e-meetings made them light-hearted.

Who is next on the list? Yes, it is you Frederika, my favorite secretary! *Dankjewel!*¹ for bringing a smile to my face whenever I see you. I look back with joy to starting the day in the secretary office with you and the other colleagues while having a sip of coffee or tea, and I will remember the stories you shared with me.

I would like to express gratitude to my reading committee members. Thank you Ming Cao, Kanat Çamlıbel, and Dimos Dimarogonas for your time and effort.

To all my former and current colleagues at DTPA, SMS, and ODS, thanks for having me! I am happy to be in your midst and occasionally also enjoy the group dynamics evolving from a spectator’s view. Special mention goes to Xiaodong,

¹‘u’ is not preferred :)

Hadi, Lulu, Hongyu, Wouter and of course my office mates Zaki, Bao, Carmen, Tabitha, and Liangming.

I came to Groningen with the knowledge that I have to start from zero in terms of building a social circle. I am fortunate to say I will still be connected to Groningen by means of the following individuals: Jeroen, Jan, Mark, and Michel. Each of you has been a source of support when I needed to talk to somebody and you have allowed me to focus on stuff non-RUG related.

I would also like to address some words to Ignaas Jimidar and Cyrano Vaseur, the two friends I have met since our Bachelor period in Suriname and with whom I enjoyed my Master period in Enschede. Thank you both for agreeing to be my paranymphs and more than that, thanks for being my friend. While we are some train hours apart, we always have lots to discuss when being together. My gratitude also to all the other people whom I have not mentioned.

爸爸，妈妈，姐姐，很感谢你们给我机会和自由去做我想做的事，走自己的路。爸爸，妈妈，儿子快毕业了，您们不需要操心了。

Last on my list is Maarten. *Dankjewel* for having my back, and for regularly pulling me out of my work environment to discover the outside world.

Nelson Chan 陈鹏举

June 2021

Contents

Acknowledgments	vi
1 Introduction	1
1.1 Review of Multi-Agent Formation Control	2
1.2 Contributions	5
1.2.1 Formation shape control with heterogeneous sensing	5
1.2.2 Formation shape control for circular robots	6
1.2.3 Formation-motion control with obstacle avoidance	6
1.2.4 Related publications	7
1.3 Outline of the Thesis	7
2 Preliminaries	9
2.1 Notation	9
2.2 Graphs & Frameworks	10
2.2.1 Frameworks	11
2.3 Cubic Equations	12
3 Stability Analysis of Gradient-Based Distributed Formation Control with Heterogeneous Sensing Mechanism: Two and Three Robot Case	15
3.1 Introduction	15
3.2 Formations and Gradient-Based Control Laws	17
3.2.1 Distance-based formation control	17
3.2.2 Bearing-only formation control	18
3.3 Problem Formulation	19
3.4 The (1D1B) Robot Setup	20
3.4.1 Characterization of the moving set \mathcal{T}_z	22
3.4.2 Local stability of the moving set \mathcal{T}_z	23
3.5 The (1D2B) Robot Setup	25

3.5.1	Equilibrium configurations	25
3.5.2	Moving configurations	26
3.5.3	Local stability of equilibrium and moving configurations . .	28
3.6	The (1B2D) Robot Setup	32
3.6.1	Equilibrium configurations	32
3.6.2	Moving configurations	33
3.6.3	Local stability of equilibrium and moving configurations . .	35
3.7	Numerical Example	37
3.7.1	(1D2B) Simulation results	38
3.7.2	(1B2D) Simulation results	38
3.8	Full Characterization of the Local Stability of Moving Configurations for the (1D2B) Robot Setup	38
3.9	Conclusions	42
4	Securing Isosceles Triangular Formations under Heterogeneous Sensing and Mixed Constraints	45
4.1	Introduction	45
4.2	Robot Configurations & Signed Area	46
4.2.1	Robot configurations	46
4.2.2	Signed area of a triangle	47
4.3	The (1D2B) Robot Setup with a Signed Area Constraint	47
4.3.1	Adding a signed area constraint to R_1	48
4.3.2	The (1D2B) robot setup with signed area control term	48
4.4	Analysis on Isosceles Triangles	50
4.4.1	Equilibrium configurations	51
4.4.2	Moving configurations	53
4.5	Acute Isosceles Triangles	55
4.5.1	Stability of equilibrium configurations	55
4.5.2	Stability of moving configurations	58
4.6	Right and Obtuse Isosceles Triangles	61
4.6.1	Stability of equilibrium configurations	61
4.6.2	Stability of moving configurations	62
4.7	Numerical Example	63
4.7.1	Numerical evaluation of (4.32)	63
4.7.2	Simulation setup	65
4.7.3	Simulation results	65
4.7.4	Extension to general triangles	66
4.8	Conclusions	66

5	Angle-Constrained Formation Control for Circular Mobile Robots	69
5.1	Introduction	69
5.2	Distance Rigidity Theory	70
5.3	Problem Formulation	71
5.4	Gradient-Based Control Design	74
5.4.1	Proposed angle-based potential function	74
5.4.2	Gradient-based control law for each robot	75
5.4.3	Gradient-based control law for the group of robots	76
5.4.4	Internal angle error system	76
5.4.5	Equilibrium sets	78
5.5	Numerical Example	79
5.5.1	Simulation setup	79
5.5.2	Simulation results	79
5.6	Conclusions	80
6	Distributed Formation with Diffusive Obstacle Avoidance Control in Coordinated Mobile Robots	83
6.1	Introduction	83
6.2	Problem Formulation	85
6.3	Distributed Obstacle Avoidance-Formation Control Design	86
6.3.1	Distributed formation control law	87
6.3.2	Coordinated group stabilization control law	87
6.3.3	Distributed obstacle avoidance control law	88
6.3.4	Stability analysis of the unified control law	90
6.4	Numerical Example	92
6.4.1	Simulation setup	92
6.4.2	Simulation results	93
6.5	Conclusions	93
7	Conclusions	95
7.1	Main Findings	95
7.2	Outlook	96
	Bibliography	98
	Summary	105
	Samenvatting	107

Chapter 1

Introduction

CONSIDER the task of moving a large rectangular table from an initial position A to a final position B. If *one person* is asked to execute this task, perhaps he will position himself halfway along one side of the table and lift it in order to not damage the floor. He might fail to do so since the table could be too heavy; hence he himself is not able to execute the task successfully. If *two people* are asked to execute this task, perhaps each of them will stand at opposite sides of the table facing each other. While carrying the table, they might adjust their walking speed by verbal communication or as a consequence of the weight of the table on their arms. Asking *four people* to move the same table, each of them will most likely start at one corner of the table and adjust their individual speed by communicating to each other or by observing the ‘pull-and-push’ effect of the table during the transition. In this way, a common pace can be attained making it easier for them to accomplish the task.

The described scenario of attaining a common pace for the group of two or four people when moving the table is an example of collective behavior. Other examples of collective behavior are audience applauding after a performance, fireflies flashing in unison, bird migration, the stop and start traffic jams, and even the bureaucracy of the European Union [46, 51], among others. Quoting Tamas Vicsek [51],

“The main features of collective behaviour are that an individual unit’s action is dominated by the influence of its neighbours - the unit behaves differently from the way it would behave on its own; and that such systems show interesting ordering phenomena as the units simultaneously change their behaviour to a common pattern.”

In our table example, each person adapts his walking speed, i.e., he walks faster or slower, depending on the other members. In doing so, they collectively reach a common pace; the team has reached a *consensus* on their walking speed. In addition, walking with a common pace preserves the relative distance between each pair of members. This collective behavior, which is particularly displayed in nature by a flock of birds or a school of fish, is classified as a *formation type* behavior [5]. According to the Merriam-Webster dictionary,

a *formation* is an arrangement of a body or group of persons or things in some prescribed manner or for a particular purpose.

In this thesis, we will consider the problem of reaching a formation, not by a flock of birds or a group of humans, but by a team of mobile robots. Recalling the example of moving the table, for the four people case, each member will initially position himself at one corner of the table. When the group members are replaced by mobile robots, what would be the strategy that each of them autonomously should follow in order to also position themselves at each corner of the table? This is the main question we will investigate in this thesis. A follow-up question after this positioning is how to maneuver the team to reach the final destination B. Before addressing these questions, we briefly review multi-agent formation control in the next section.

1.1 Review of Multi-Agent Formation Control

Formation control studies the problem of controlling the spatial deployment of teams of agents¹ in order to achieve a specific geometrical shape. By maintaining a certain geometrical shape, the teams can subsequently be deployed to perform complex missions. In the past two decades, formation control has been an active research topic within the coordination control of multi-agent systems. Recent advances in this field focus on the design of distributed algorithms such that the formation control problem can be solved by exploiting only local information; for an overview, see [1, 6, 21, 38, 41].

Deploying a formation can be beneficial; for example, in the presence of limited sensing range, certain complex tasks, such as covering a region of interest, can be executed within a smaller amount of time by letting a team of robots move in formation than when it is carried out by a single robot. In addition, each robot within the formation can be equipped with different sensors and therefore, more (local) information can be gathered [6]. Moreover, the use of small mobile robots may lead to lower costs compared to deploying a single robot. Another benefit of deploying a formation is the probability of success when carrying out a mission.

Associated with formation control, there are two problems: *formation stabilization* and *formation tracking*. In the former, the goal is to design control laws for each robot with the aim to steer the team to display a desired geometrical shape in a collective manner. The latter problem has the additional requirement that the whole formation needs to follow a given reference trajectory. In Chapters 3 to 5, we will consider the former problem while the latter will be the focus of Chapter 6.

Prior to designing control laws for the mobile robots, we need a way to describe the desired geometrical shape. In the existing literature, this desired shape can

¹Throughout this thesis, the term ‘agent’ refers to mobile robot.

be given by a set of fixed positions [38], relative positions [42], distances [28, 48], bearings² [54], or angles [16]. Each specification leads to several sensing requirements for the team of mobile robots. For example, when the desired shape is provided in terms of fixed positions in the plane, then each robot needs to have knowledge of where the *common base* is and be able to obtain the absolute position measurements with respect to this common base, i.e., it requires a common global coordinate system. After obtaining these measurements, each robot individually moves in a manner such that the error between their current position and their desired position is reduced. Notice that in this setup, the mobile robots do not necessarily have to interact with the other team members, except when they risk colliding with each other during the transition to their desired positions. However, interactions between the robots have been reported to enhance the performance of formation control [38].

When a set of distance constraints is used for describing the desired geometrical shape, then interactions among the team members is crucial. In this setup, the trajectory of one robot is influenced by the movements of the neighboring robots maintaining individual distance requirements. The robots do not necessarily require knowledge of a *common base and common direction*, i.e., each robot can take measurements relative to a local coordinate system. This local measurement may be a relative position measurement (encoding the distance and orientation between the robots) or a pure distance measurement. The goal for each member of the team is to move such that the difference between the current and the desired distance is reduced. In distance-based formation control, the desired shape is required to be *rigid*. Roughly speaking, this means that during a motion, the shape should not be able to change its form while satisfying the given set of distance constraints. Rigidity theory has also been developed for shapes described by a set of bearing [55] or angle [16] constraints.

Fig. 1.1 shows the control action (red and blue) of two robots. In Fig. 1.1(a), we see that each robot will move toward its desired absolute position in the plane. In case the robots are required to maintain a relative position, their control directions will be to minimize the error deviation in the relative position, see Fig. 1.1(b). Robots will move toward or from each other when maintaining a desired distance. In Fig. 1.1(c), the motion is toward each other since their current distance ($\sqrt{10}$) is larger than the desired distance ($\sqrt{5}$). The control action of each robot in Fig. 1.1(d) has orientation perpendicular to their relative positioning. This chosen direction can lead the robots to obtain the desired bearing relative to each other.

Recently, approaches to realize a desired geometrical shape using a mixed set of constraints have also been considered. In [31], distance and angle constraints have been employed; the paper in [10] has considered the combination of distance

²A bearing is a unit vector indicating the direction of one member with respect to another member in the team.

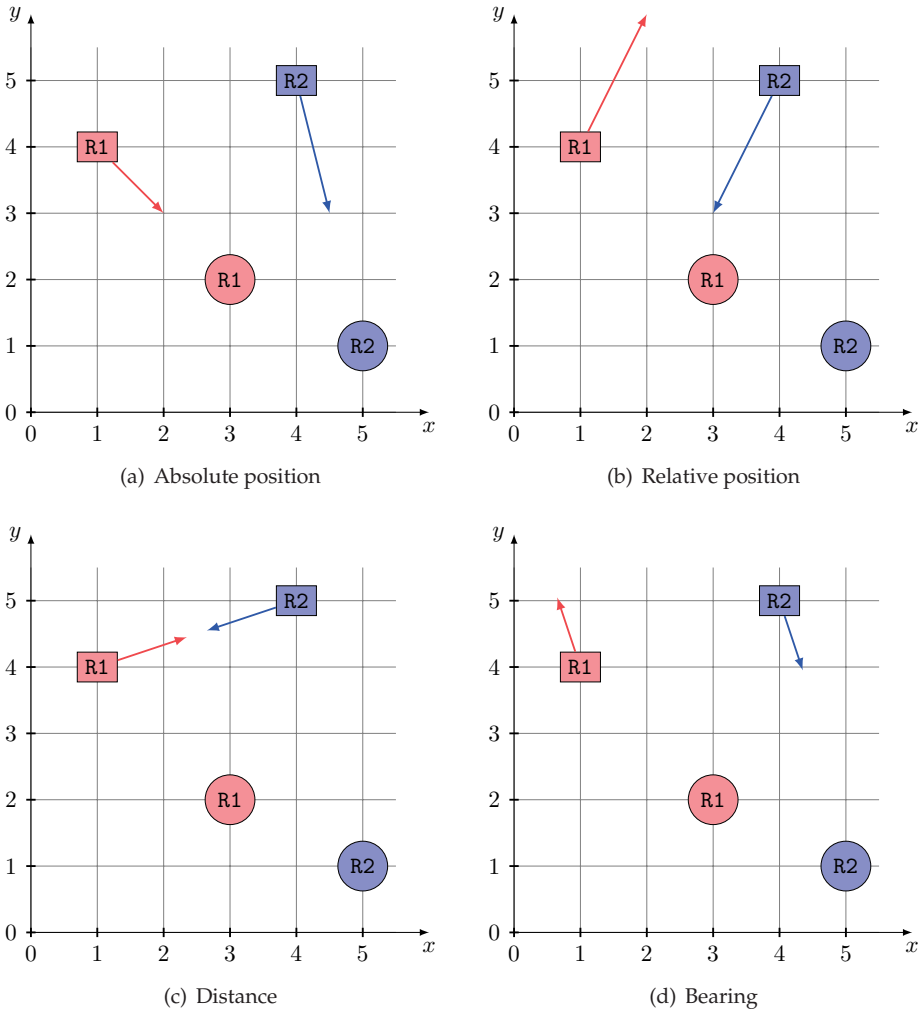


Figure 1.1: Illustration of the control action for two robots; \circ denotes desired configuration and \square is the current configuration. The control action is influenced by the (relative) quantity that the robots need to satisfy.

and bearing constraints, while the work in [29] has used distance, bearing, and angle constraints to provide a description of the desired shape. Furthermore, a series of works [3, 15, 44, 45] has focused on the combination of distance and signed area constraints. By adding signed area constraints, the authors tackle the flip and flex ambiguity problem present in distance-based formation control. A signed area constraint will also be introduced in Chapter 4 to avoid the occurrence of undesired moving geometrical shapes.

In addition, several works dealt with practical aspects when implementing the proposed control strategies in real-world settings. Among others, [34] has considered robust distance-based formation control with prescribed performance, taking into account collision avoidance and connectivity maintenance between neighboring robots while they are subjected to unknown external disturbances; [24] has considered the bearing-only formation control problem with limited visual sensing, while [18] has introduced estimators for controlling distance rigid formations under inconsistent measurements.

1.2 Contributions

The contributions of this thesis are found in Chapters 3 to 6. In Chapters 3 to 5, we focus on the formation stabilization problem (also known as formation shape control) where we propose controllers for the mobile robots within the team based on the available local sensing information they have acquired from their neighboring members. We then analyze the proposed controllers since we are interested in the shapes that the team as a collective can display. Chapter 6 provides details on the problem of steering a team of mobile robots as a collective to a predefined final destination while avoiding obstacles during the transition.

1.2.1 Formation shape control with heterogeneous sensing

In Chapter 3, we study the formation shape control problem in which the team consists of two types of mobile robots, namely *distance robots* and *bearing robots*. Each type of robots is required to maintain on the individual level some constraints relative to members of the other type, i.e., a distance (or bearing) robot is tasked to maintain distance (or bearing) constraints relative to some bearing (or distance) robots within the team. In performing these individual tasks, existing gradient-based control laws in literature [48, 53] are implemented. Curious to what collective formation the team may display, we analyze the team consisting of two and three members. During the analysis, we discover that next to the desired geometrical shape (for two members, a line and for three members, a triangle), the team may also display incorrect shape(s) (in this case, a line (or a triangle) with incorrect distance(s) and orientation(s)). The team may move as a whole with a common nonzero velocity when displaying the incorrect shape. For the team consisting of one distance robot and two bearing robots (**1D2B**), we show that one of the incorrect moving shapes is locally attractive. For the other setups, the incorrect moving shapes are found to be unstable.

Chapter 4 is closely related to Chapter 3; in particular, we devote our attention to the (**1D2B**) robot setup that is introduced in Chapter 3. In this chapter, we

include an additional control term for the distance robot with the aim to prevent the occurrence of incorrect moving shapes. Introducing this additional control term for the distance robot can be done naturally and does not require additional sensing. We identify a sufficient condition on the gain ratio R_{Ad} between the signed area and the distance control terms such that the desired shape, an isosceles triangle, is always obtained.

1.2.2 Formation shape control for circular robots

Contrary to Chapters 3 and 4 where the team consists of two types of robots, each carrying different sensing mechanisms, we assume that the mobile robots in Chapter 5 can only obtain bearing measurements from their neighbors. Furthermore, the constraints between the robots are maintained by both robots, and as a result of modeling the robots as a circular disk instead of a point mass, the robots obtain not one, but two bearing measurements from its neighbors. These are the two outer points on the neighbors' disk. Using these bearing measurements, the enclosed internal angle relative to the neighbor is obtained. We define a desired formation in terms of a set of enclosed internal angles that has a close relationship to the desired formation in terms of a set of distances. We succeed in deriving a gradient-based control law that utilizes only the available local bearing measurements. The corresponding error system has a local exponential convergence property. This implies that, when the mobile robots display a geometrical shape that is close to the desired one, then by applying the proposed control law, the team will eventually display the desired shape. One other feature of the proposed control law is that it ensures collision avoidance between the pairs of robots which actively maintain the internal angle constraints.

1.2.3 Formation-motion control with obstacle avoidance

Besides displaying the desired geometrical shape, the robots will be required to carry out different tasks, such as moving as a collective to a pre-defined final position. In fact, formation control is considered an enabler for more complex missions for the teams of robots [55]; recall the example of moving a table from position A to position B at the start of this chapter.

With this in mind, we study in Chapter 6 the multi-objective control problem in which the mobile robots collectively have to display a desired geometrical shape and reach a final position while avoiding fixed obstacles during the transition. We consider a modular approach where we design for each of the objectives a specific control law and afterward combine them together. Our main contribution here is the design of a distributed obstacle-avoidance control law which ensures that the robots avoid the obstacles while they transition to their final destination.

1.2.4 Related publications

Conference contributions

- N.P.K. Chan, B. Jayawardhana, and J.M.A. Scherpen. Distributed Obstacle Avoidance-Formation Control of Mobile Robotic Network with Coordinated Group Stabilization. *In Proceedings of the 23rd International Symposium on Mathematical Theory of Networks and Systems (MTNS)*, 722-725, 2018.
- N.P.K. Chan, B. Jayawardhana, and J.M.A. Scherpen. Distributed Formation with Diffusive Obstacle Avoidance Control in Coordinated Mobile Robots. *In Proceedings of the 57th IEEE Conference on Decision and Control (CDC)*, 4571-4576, 2018.

Journal contributions

- N.P.K. Chan, B. Jayawardhana, and H.G. de Marina. Angle-Constrained Formation Control for Circular Mobile Robots. *IEEE Control Systems Letters*, 5(1):109-114, Jan 2021.
- N.P.K. Chan, B. Jayawardhana, and H.G. de Marina. Stability Analysis of Gradient-Based Distributed Formation Control with Heterogeneous Sensing Mechanism: Two and Three Robot Case. *Submitted*, 2020.
- N.P.K. Chan, B. Jayawardhana, and H.G. de Marina. Securing Isosceles Triangular Formations under Heterogeneous Sensing and Mixed Constraints. *Submitted*, 2020.

1.3 Outline of the Thesis

The outline of the remainder of this thesis is as follows.

First, in Chapter 2, we provide notations that is used throughout the thesis. In addition to that, the necessary concepts and definitions on graph theory and frameworks and the positive roots to specific cubic equations are mentioned.

Chapter 3 starts with the problem setup of teams of n mobile robots partitioned in distance robots and bearing robots. We then focus on $n = \{2, 3\}$ robots. We identify the shapes the team can display and study the stability of these shapes.

Chapter 4 extends the analysis on the **(1D2B)** robot setup considered in Chapter 3. We introduce an additional signed area control term for the distance robot within the team. A comprehensive analysis is performed on the closed-loop formation system when the desired formation shape is an isosceles triangle.

In Chapter 5, we represent the mobile robots as circular disks in the plane. First, we present the relationship between the enclosed angle obtained from the bearing

measurements and the distance between two neighboring robots. We proceed with designing gradient control laws that only utilize the locally available bearing measurements and present local stability analysis.

Chapter 6 starts with the multi-objective formation-motion control problem in which the mobile robots are required to maintain more than one objective. We proceed with presenting a modular framework, hereby designing a specific control law for each of the objectives. Hereafter, we unify these specific controllers and perform stability analysis on the unified controller. In the numerical simulations, we compare our control law with another obstacle-avoidance control law.

The main findings of this thesis are combined in Chapter 7 where we also present some ideas for future work.

Chapter 2

Preliminaries

This chapter begins with the notation that is used throughout this thesis. We continue in Section 2.2 with recalling the necessary notions from graph theory and frameworks. Hereafter, the roots of cubic equations are provided in Section 2.3.

2.1 Notation

LET \mathbb{R} denote the set of real numbers, \mathbb{R}^n be the set of n -dimensional real vectors and $\mathbb{R}^{m \times n}$ define the set of $m \times n$ real matrices. The sets $\mathbb{R}_{\geq 0}$ and $\mathbb{R}_{> 0}$ are subsets of \mathbb{R} that contain only non-negative and positive real numbers, respectively. The cardinality of a given set \mathcal{S} is denoted by **card** (\mathcal{S}).

For a vector $x \in \mathbb{R}^n$, x_i denotes its i -th entry, x^\top is the transpose and $\|x\| = \sqrt{x^\top x}$ is the usual Euclidean norm. The vector $\mathbb{1}_n$ (or $\mathbb{0}_n$) denotes a column vector with entries being all 1s (or 0s). The set of all combinations of linearly independent vectors v_1, \dots, v_k is denoted by **span** $\{v_1, \dots, v_k\}$. In the plane \mathbb{R}^2 , the symbol $\angle v_1$ denotes the counter-clockwise angle from the x -axis of a coordinate frame Σ to the vector $v_1 \in \mathbb{R}^2$. The matrix $J = \begin{bmatrix} 0 & 1 \\ -1 & 0 \end{bmatrix}$ is the rotation matrix with angle -90° . We denote x^\perp as the perpendicular vector obtained by rotating x with a counter-clockwise angle of $+90^\circ$; we have $x^\perp = -Jx$ and $x^\top x^\perp = 0 = (x^\perp)^\top x$.

For a complex number $z = a + bi$, the numbers $a, b \in \mathbb{R}$ are the real and imaginary part of z and $i^2 = -1$. The complex conjugate of z is given by $\bar{z} = a - bi$. In polar form, we write $z = r_z \angle \varphi_z$, where $r_z = \sqrt{z\bar{z}} = \sqrt{a^2 + b^2}$ is the modulus and $\varphi_z = \tan^{-1} \left(\frac{b}{a} \right)$ is the argument corresponding to z . Furthermore, $a = r_z \cos \varphi_z$, $b = r_z \sin \varphi_z$, and $\bar{z} = r_z \angle (-\varphi_z)$. Let $y = r_y \angle \varphi_y$; we have the multiplication $yz = (r_y r_z) \angle (\varphi_y + \varphi_z)$ and the division $\frac{y}{z} = \left(\frac{r_y}{r_z} \right) \angle (\varphi_y - \varphi_z)$.

For a rectangular matrix $A \in \mathbb{R}^{m \times n}$, $[A]_{ij}$ is the i -th row and j -th column entry of A . Furthermore, **Null** (A) $\subset \mathbb{R}^n$, **Col** (A) $\subset \mathbb{R}^m$, **rank** (A), **trace** (A), and **det** (A) denote the null space, column space, rank, trace, and determinant of A , respectively. For a symmetric matrix $P \in \mathbb{R}^{n \times n}$, $P > 0$ (or $P \geq 0$) denotes a positive-definite (or positive semi-definite) matrix. The $n \times n$ identity matrix is denoted by I_n while **diag** (v) (or **blkdiag** (A_1, \dots, A_k)) is the diagonal (or block diagonal) matrix with entries of vector v (or matrices A_1, \dots, A_k) on the main

diagonal (or block). Finally, given matrices $A \in \mathbb{R}^{m \times n}$ and $B \in \mathbb{R}^{p \times q}$, $A \otimes B \in \mathbb{R}^{mp \times nq}$ is the Kronecker product of A and B and we denote $\tilde{A} = A \otimes I_d \in \mathbb{R}^{md \times nd}$.

2.2 Graphs & Frameworks

A *directed graph* (in short, *digraph*) \mathcal{G} is a pair $(\mathcal{V}, \mathcal{E})$, where $\mathcal{V} = \{1, 2, \dots, n\}$ is the finite set of *vertices* and $\mathcal{E} \subseteq \mathcal{V} \times \mathcal{V}$ is the *edge set* representing the relationships between the n vertices. For $i, j \in \mathcal{V}$, the ordered pair (i, j) represents an edge pointing *from* i to j . The set of vertices j having an edge pointing from i is denoted by $\mathcal{N}_i = \{j \in \mathcal{V} \mid (i, j) \in \mathcal{E}\}$. We assume \mathcal{G} does not have self-loops, i.e., $(i, i) \notin \mathcal{E}$ for all $i \in \mathcal{V}$ and $\mathbf{card}(\mathcal{E}) = m$. Associated to the digraph \mathcal{G} , we define the incidence matrix $H \in \{0, \pm 1\}^{m \times n}$ with rows encoding the m edges and columns encoding the n vertices. The entries of H take value $[H]_{ki} = -1$ if vertex i is the tail of edge k , $[H]_{ki} = 1$ if it is the head, and $[H]_{ki} = 0$ otherwise. Due to its structure, we have $\mathbf{span}\{\mathbb{1}_n\} \subseteq \mathbf{Null}(H)$. The digraph \mathcal{G} is *bipartite* if the vertex set \mathcal{V} can be partitioned into two subsets \mathcal{V}_1 and \mathcal{V}_2 with $\mathcal{V}_1 \cap \mathcal{V}_2 = \emptyset$ and the edge set $\mathcal{E} \subseteq (\mathcal{V}_1 \times \mathcal{V}_2) \cup (\mathcal{V}_2 \times \mathcal{V}_1)$. We assume $\mathbf{card}(\mathcal{V}_1) = n_1$ and $\mathbf{card}(\mathcal{V}_2) = n - n_1 = n_2$. For a *complete bipartite digraph*, the edge set is $\mathcal{E} = (\mathcal{V}_1 \times \mathcal{V}_2) \cup (\mathcal{V}_2 \times \mathcal{V}_1)$ and $\mathbf{card}(\mathcal{E}) = 2n_1n_2$. Fig. 2.1 depicts complete bipartite digraphs for $n = 2$ and 3 vertices and a bipartite digraph for $n = 4$ vertices.

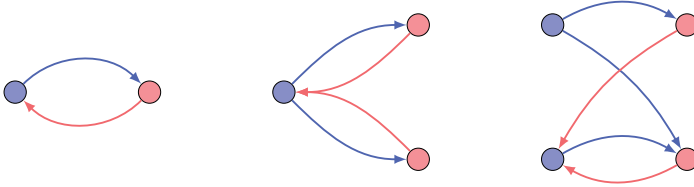


Figure 2.1: Examples of complete bipartite digraphs for $n = 2$ and 3 vertices and a bipartite digraph for $n = 4$ vertices. Without loss of generality, \bullet represents an element of \mathcal{V}_1 while \bullet is a vertex belonging to \mathcal{V}_2 . Correspondingly, the blue arrows are edges belonging to $\mathcal{V}_1 \times \mathcal{V}_2$ while the red arrows are elements of the edge set $\mathcal{V}_2 \times \mathcal{V}_1$.

If for every pair $(i, j) \in \mathcal{E}$ we have $(j, i) \in \mathcal{E}$, then the graph is *undirected*. In this case, we have $\mathcal{E} := \{\{i, j\} \mid i, j \in \mathcal{V}\}$ is the set of unordered pairs $\{i, j\}$ of the vertices. The vertices i and j are *neighbors of each other* and \mathcal{N}_i consists of all the neighbors of vertex i . Now, by assigning an arbitrary orientation to each edge of \mathcal{G} , we obtain an *oriented graph* $\mathcal{G}_{\text{orient}}$. To $\mathcal{G}_{\text{orient}}$, we can associate an incidence matrix H with the already provided rules. For a connected and undirected graph, we have $\mathbf{Null}(H) = \mathbf{span}\{\mathbb{1}_n\}$ and $\mathbf{rank}(H) = n - 1$. Each edge of the undirected graph can have a weight $w_{\{i, j\}} \in \mathbb{R}_{>0}$ corresponding to it. After indexing all the edges of \mathcal{G} , we can construct a diagonal matrix $W = \mathbf{diag}(w_1, \dots, w_m)$ with w_k being the

weight of edge k in the ordered edge index set $\mathcal{K} = \{1, 2, \dots, m\}$. The Laplacian matrix related to \mathcal{G} is the matrix product $L := H^\top W H \in \mathbb{R}^{n \times n}$. It is positive semi-definite, i.e., $L \geq 0$ and has a simple zero eigenvalue with corresponding null space $\mathbf{Null}(L) = \mathbf{span}\{\mathbb{1}_n\}$ when the graph is connected. The other $n - 1$ eigenvalues of L are positive and real and can be ordered as $\lambda_2 \leq \lambda_3 \leq \dots \leq \lambda_n$.

Lemma 2.1. *Let $Q = \frac{1}{n}\mathbb{1}_n\mathbb{1}_n^\top$ be the matrix of all ones scaled by a factor $\frac{1}{n}$ and define $K = L + Q$ where L is the Laplacian matrix related to an undirected and connected graph \mathcal{G} . Then the matrix K is a positive definite matrix, i.e., $K > 0$.*

Proof. Since \mathcal{G} is undirected and connected, we know that matrix L is positive semi-definite. Also, matrix Q is a positive semi-definite matrix. Hence the sum $K = L + Q$ is at least a positive semi-definite matrix. Matrix K is positive definite if and only if the null spaces of both matrices are disjoint, i.e.,

$$\mathbf{Null}(L) \cap \mathbf{Null}(Q) = \{0_n\}. \quad (2.1)$$

Since the graph \mathcal{G} is connected, we have the null space of L contains only $\mathbf{span}\{\mathbb{1}_n\}$. Due to L being symmetric, the range space of L is the orthogonal complement of $\mathbf{span}\{\mathbb{1}_n\}$, i.e.¹, $\mathbf{Col}(L) \perp \mathbf{Null}(L)$. Since all columns of the matrix Q are the same, it has $n - 1$ zero eigenvalues and only 1 non-zero eigenvalue with corresponding eigenvector $\mathbb{1}_n$, i.e., $\mathbf{Col}(Q) = \mathbf{span}\{\mathbb{1}_n\}$. Since Q is also symmetric, we have $\mathbf{Null}(Q) \perp \mathbf{Col}(Q)$. With $\mathbf{Null}(L) = \mathbf{Col}(Q)$, it follows $\mathbf{Null}(Q) \perp \mathbf{Null}(L)$. Hence the intersection of the null spaces contains only the zero element. This completes the proof. \square

2.2.1 Frameworks

In this thesis, we consider formation control setups in the plane, i.e., the 2-dimensional Euclidean space \mathbb{R}^2 . Here we provide some basic definitions and defer the details for the forthcoming chapters.

Let $p_i = [x_i \ y_i]^\top \in \mathbb{R}^2$ be a point and a collection of n points, called a *configuration*, be given by the stacked vector $p = [p_1^\top \ \dots \ p_n^\top]^\top \in \mathbb{R}^{2n}$. We can embed the (directed) graph $\mathcal{G}(\mathcal{V}, \mathcal{E})$ into the plane by assigning to each vertex $i \in \mathcal{V}$, a point $p_i \in \mathbb{R}^2$; the pair $\mathcal{F}_p := (\mathcal{G}, p)$ denotes a *framework* (or in the current context, a *formation*) in the 2-dimensional ambient space. We assume $p_i \neq p_j$ if $i \neq j$, i.e., no two vertices are mapped to the same position. Furthermore, for two points p_i and p_j , we define the relative position vector as $z_{ij} = p_j - p_i \in \mathbb{R}^2$, the distance as $d_{ij} = \|z_{ij}\| \in \mathbb{R}_{\geq 0}$ and the relative bearing vector, when $d_{ij} \neq 0$, as $g_{ij} = \frac{z_{ij}}{d_{ij}} \in \mathbb{R}^2$, all relative to a global coordinate frame Σ^g . It follows $z_{ji} = -z_{ij}$, $d_{ji} = d_{ij}$ and $g_{ji} = -g_{ij}$.

¹Here the symbol \perp denotes orthogonality between two subspaces.

2.3 Cubic Equations

Consider a *reduced*² cubic equation

$$y^3 + cy + d = 0, \quad (2.2)$$

where $c, d \in \mathbb{R}$. The discriminant of (2.2) is $\Delta = -4c^3 - 27d^2$. Using Δ , we determine the following properties regarding the roots:

- $\Delta > 0$; we have three distinct real roots;
- $\Delta = 0$; we have at least two equal real roots;
- $\Delta < 0$; we have a single real root and two complex roots forming a conjugate pair.

The roots of (2.2) are [22]

$$y_1 = A + B, \quad y_2 = \omega A + \omega^2 B, \quad y_3 = \omega^2 A + \omega B, \quad (2.3)$$

where

$$\begin{aligned} A &= \sqrt[3]{-\frac{d}{2} + \sqrt{R}}, & B &= \sqrt[3]{-\frac{d}{2} - \sqrt{R}}, \\ AB &= -\frac{c}{3}, & R &= \left(\frac{c}{3}\right)^3 + \left(\frac{d}{2}\right)^2 = \frac{-1}{108}\Delta, \\ \omega &= \frac{-1 + \sqrt{3}i}{2}, & \omega^2 &= \frac{-1 - \sqrt{3}i}{2}. \end{aligned} \quad (2.4)$$

Note that ω and ω^2 form a complex conjugate pair, i.e., $\bar{\omega} = \omega^2$. In polar form, we obtain $\omega = 1 \angle 120^\circ$ and $\omega^2 = 1 \angle (-120^\circ)$.

We focus on the case when the coefficients of (2.2) take values $c < 0$ and $d \geq 0$. Applying Descartes' rule of signs [22], we obtain that when the coefficient $d \leq 0$, the reduced cubic equation (2.2) always has a positive real root while for $d > 0$, it always contains a negative real root. The remaining roots for the case when d is positive depend on the discriminant Δ ; when $\Delta \geq 0$, we have two positive real roots, and otherwise, we have two complex roots. The following lemma provides the characterization of the positive real roots when $d > 0$.

Lemma 2.2. *Given a reduced cubic equation (2.2) with coefficients $c < 0$ and $d > 0$. Assume the discriminant is $\Delta \geq 0$. Then two positive real roots exist with values*

$$\begin{aligned} y_{p_1} &= 2\sqrt[3]{r_v} \cos\left(\frac{1}{3}\varphi_v - 120^\circ\right) \in (0, 1] \sqrt[3]{r_v}, \\ y_{p_2} &= 2\sqrt[3]{r_v} \cos\left(\frac{1}{3}\varphi_v\right) \in [1, \sqrt{3}) \sqrt[3]{r_v}, \end{aligned} \quad (2.5)$$

²In some texts, the term 'depressed' is used.

where $r_v = \sqrt{-\left(\frac{c}{3}\right)^3}$ and $\varphi_v = \tan^{-1}\left(\frac{-\frac{2}{d}\sqrt{\frac{\Delta}{108}}}{\frac{c}{3}}\right) \in (90^\circ, 180^\circ]$. When $\Delta = 0$, the two positive real roots are equal and have value $y_{p_1} = y_{p_2} = \sqrt[3]{r_v} = \sqrt[3]{\frac{d}{2}}$.

Proof. First, we define $v = -\frac{d}{2} + \sqrt{R}$. Since $\Delta \geq 0$ holds and $R = -\frac{1}{108}\Delta$, it follows $R \leq 0$. Hence we rewrite v as the complex number $v = -\frac{d}{2} + \sqrt{-R}i$. In polar form, we obtain $v = r_v \angle \varphi_v$ with modulus $r_v = \sqrt{-\left(\frac{c}{3}\right)^3}$ and argument $\varphi_v = \tan^{-1}\left(-\frac{2}{d}\sqrt{-R}\right)$. With $d > 0$, we know the real part of v is negative while the imaginary part is non-negative. Hence the argument φ_v is in the range $\varphi_v \in (90^\circ, 180^\circ]$ with $\varphi_v = 180^\circ$ holds when $R = 0$. Furthermore, the complex conjugate of v is $\bar{v} = -\frac{d}{2} - \sqrt{-R}i = r_v \angle (-\varphi_v)$. Substituting in (2.4), we obtain $A = \sqrt[3]{v} = \sqrt[3]{r_v} \angle \left(\frac{1}{3}\varphi_v\right)$ and $B = \sqrt[3]{\bar{v}} = \bar{A}$. Recalling $\omega^2 = \bar{\omega}$, the cubic roots (2.3) are

$$y_1 = 2\sqrt[3]{r_v} \cos\left(\frac{1}{3}\varphi_v\right), \quad y_{2,3} = 2\sqrt[3]{r_v} \cos\left(\frac{1}{3}\varphi_v \pm 120^\circ\right). \quad (2.6)$$

Corresponding to the range $\varphi_v \in (90^\circ, 180^\circ]$, we have $\frac{1}{3}\varphi_v \in (30^\circ, 60^\circ]$. The positive roots are then found to be

$$y_1 = 2\sqrt[3]{r_v} \cos\left(\frac{1}{3}\varphi_v\right), \quad y_3 = 2\sqrt[3]{r_v} \cos\left(\frac{1}{3}\varphi_v - 120^\circ\right). \quad (2.7)$$

With $\frac{1}{3}\varphi_v \in (30^\circ, 60^\circ]$, we obtain for the range of the positive roots $y_1 \in [1, \sqrt{3})\sqrt[3]{r_v}$ and $y_3 \in (0, 1]\sqrt[3]{r_v}$. The inequality $y_1 \geq y_3$ follows and equality holds when $\Delta = 0 \iff R = 0$. From (2.4), $R = 0$ is equivalent to $-\left(\frac{c}{3}\right)^3 = \left(\frac{d}{2}\right)^2$; therefore, $r_v = \frac{d}{2}$. This completes the proof. \square

Chapter 3

Stability Analysis of Gradient-Based Distributed Formation Control with Heterogeneous Sensing Mechanism: Two and Three Robot Case

In this chapter, we characterize the formation shapes that a team of mobile robots may display when each robot is tasked with maintaining either distances or bearings relative to its neighbors. For the team consisting of two or three robots, we will show that besides the desired formation shape (a line or a triangle), also incorrect shapes (a line with an erroneous distance or triangle with incorrect distances and or orientation) can be obtained when employing gradient-based control laws for reaching the individual robot objectives. Hereafter, we study the stability of the different formation shapes based on the linearization technique.

This chapter starts with an introduction. We recall the existing gradient-based control laws in Section 3.2 and formulate the problem in Section 3.3. We start our exposition of the problem by analyzing the simple two robot case in Section 3.4 and extend the analysis to the three robot case in Sections 3.5 and 3.6. Numerical simulations are presented in Section 3.7 for illustrating the various final formation shapes in the three robot case. In Section 3.8, we provide the detailed stability analysis for the robot setup considered in Section 3.5. Finally, Section 3.9 contains our conclusions.

3.1 Introduction

OVER the years, a rich body of work has been developed on the problem of realizing a formation shape by a team of mobile robots. When the formation shape is specified by inter-robot relative positions [41], then the consensus-based formation control approaches, which are linear, can be used directly. For realizing a formation shape using only distance [23, 28], bearing [53], or angle constraints [16], the notion of rigidity [6, 16, 55] for the underlying interconnection topology is required. The condition of rigidity describes the motions for the whole formation which preserve the formation shape. Gradient-based control laws are a popular approach for realizing the formation shape specified by distance [48]

or bearing constraints [53]. A formation shape can also be realized by a set of mixed constraints; see, among others, [9, 29, 31]. In distance-constrained and also distance-and-angle-constrained formation control, flip and flex ambiguities occur. To resolve this problem, signed constraints [4, 30, 44] have been introduced.

In most of the aforementioned references, the underlying interconnection topology is that of an *undirected* graph. This implies that the geometrical constraint between a robot pair, represented by an edge on the graph, is actively maintained by both robots. While the use and active maintenance of a common type of constraints (distance, bearing, or angle) between two neighboring robots have been proven to guarantee the stability of the desired formation shape, it may not be desirable in practice. Firstly, the sole use of one type of constraints on all edges implies that all robots must use the same sensing mechanism. This restriction prevents the integration of other robots carrying different sensor loads into the formation. Secondly, when multiple types of constraints need to be actively maintained by certain robots, these robots have to be equipped with multiple different sensing mechanisms corresponding to the different constraints defined on the edges connected to them. This implies that these robots have to carry extra sensor loads that can be costly and consume additional space, weight and computational load. On the other hand, it might be desirable for robots to control only distances or bearings depending on their current situation. For instance, the bearing measurement becomes less sensitive when the robots move in a large shaped formation, or the robots carrying multiple distance and bearing sensors can control the most relevant constraint depending on the accuracy or reliability of the equipped sensor for a given situation (e.g., far versus near, wide-angle versus small-angle, etc.). Lastly, if a partial sensor failure in a robot occurs, maintaining the same constraint with its neighbors may no longer be possible. For instance, in the case of a partial failure of a LIDAR sensor, which can normally provide relative position information, we may still measure bearing information with non-accurate distance information. Distance-based/bearing-based controllers are tolerant to non-accurate bearing/distance measurements [9, 55]. In this case, while it is possible to define heterogeneous constraints on the same edge that still define the same shape (e.g., one robot controls relative position while the other one controls bearing), it remains an open problem whether the application of standard local gradient-based control law based on the information available to each robot can still maintain the formation. Intuitively, the gradient-based control law will direct each robot to the direction that minimizes the local potential function and reaches the desired constraints. However, as different types of potential function may be defined for the same edge due to the heterogeneous sensing mechanisms between the two robots, the direction that is taken by each robot may not coincide anymore with the minimization of the combined potential functions.

In this chapter, we consider the formation stabilization problem in which

the desired formation shape is specified by a mixed set of distance and bearing constraints. Different from [9], we consider the setup where each constraint is actively maintained by *only* one robot, i.e., the underlying interconnection topology is a *directed* graph. Each robot within the team has the individual task of maintaining a subset of either the distance or bearing constraints. As a starting point, we focus on teams consisting of two and three robots in different setups. Using standard gradient-based control laws specific to the constraints each robot has to maintain, we analyze the stability, particularly, the local asymptotic stability of the desired formation shape. It is of interest to study the applicability of these control laws without modifying their local potential functions to incorporate the different constraints on the edges since it allows us to design distributed control laws for each robot that is completely dependent on the available local information to the robot and is independent of the eventual deployment of the robot in the formation (provided the desired admissible constraints are available to the robot).

3.2 Formations and Gradient-Based Control Laws

We consider a team consisting of n mobile robots in which \mathbb{R}_i is the label assigned to robot i . The robots are moving in the plane according to the single integrator dynamics, i.e.,

$$\dot{p}_i = u_i, \quad i \in \{1, \dots, n\}, \quad (3.1)$$

where $p_i \in \mathbb{R}^2$ (a point in the plane) and $u_i \in \mathbb{R}^2$ represent the position of and the control input for \mathbb{R}_i , respectively. For convenience, all spatial variables are given relative to a global coordinate frame Σ^g . The group dynamics is obtained as $\dot{p} = u$ with the stacked vectors $p = [p_1^\top \ \dots \ p_n^\top]^\top \in \mathbb{R}^{2n}$ representing the team *configuration* and $u = [u_1^\top \ \dots \ u_n^\top]^\top \in \mathbb{R}^{2n}$ being the collective input. The interactions among the robots is described by a fixed graph $\mathcal{G}(\mathcal{V}, \mathcal{E})$ with \mathcal{V} being the team of robots and \mathcal{E} containing the neighboring relationships. The pair $\mathcal{F}_p = (\mathcal{G}, p)$ denotes a *framework* (or equivalently a *formation*) in \mathbb{R}^2 .

3.2.1 Distance-based formation control

In *distance-based* formation control, a *desired formation* is characterized by a set of *inter-robot distance constraints*. Assume the desired distance between a robot pair (i, j) of the formation is d_{ij}^* and let $d_{ij}(t)$ be the current distance at time t . Let us define the *distance error* signal as $e_{ijd}(t) = d_{ij}^2(t) - (d_{ij}^*)^2$. A distance-based potential function used for deriving the gradient-based control law for the robot pair (i, j) takes the form $V_{ijd}(e_{ijd}) = \frac{1}{4}e_{ijd}^2$ [23, 28]. It has a minimum at the desired edge distance d_{ij}^* ; i.e., $V_{ijd}(e_{ijd}) \geq 0$ and $V_{ijd}(e_{ijd}) = 0 \iff d_{ij} = d_{ij}^*$. In

this case, the corresponding gradient-based control law for maintaining a desired inter-robot distance for the robot pair (i, j) is

$$u_{ijd} = -\left(\frac{\partial V_{ijd}}{\partial p_i}\right)^\top = e_{ijd}z_{ij},$$

where z_{ij} is the measurement that R_i obtains from its neighbor $j \in \mathcal{N}_i$. Thus, the distanced-based formation control law for robot R_i in (3.1) is given by

$$u_{id} = \sum_{j \in \mathcal{N}_i} e_{ijd}z_{ij}. \quad (3.2)$$

It is well-studied in literature that the above control law guarantees the local exponential stability of the desired formation shape when the desired shape is infinitesimally distance rigid. We refer interested readers to [48] for the exposition of standard distance-based formation control and its local exponential stability property.

3.2.2 Bearing-only formation control

In *bearing-only* formation control, the desired formation is characterized by a set of *inter-robot bearing* constraints. Consider the i -th robot (with label R_i) in this setup. Robot R_i is able to obtain the bearing measurement $g_{ij}(t)$ to its neighbors $j \in \mathcal{N}_i$ and its goal is to achieve desired bearings g_{ij}^* s with all neighbors $j \in \mathcal{N}_i$. In this case, the *bearing error* signal for a robot pair (i, j) can be defined by $e_{ijb}(t) = g_{ij}(t) - g_{ij}^*$. As before, the corresponding potential function that can be used to design the gradient-based control law is $V_{ijb}(e_{ijb}) = \frac{1}{2}d_{ij}\|e_{ijb}\|^2$. Note that $V_{ijb}(e_{ijb}) \geq 0$ and it is only zero when $d_{ij} = 0$ or $e_{ijb} = \mathbb{0}_2 \iff g_{ij} = g_{ij}^*$. (In forthcoming analysis, we will show that $d_{ij} = 0$, where robots R_i and R_j are at the same position, is not a viable option.). It can be verified that

$$u_{ijb} = -\left(\frac{\partial V_{ijb}}{\partial p_i}\right)^\top = e_{ijb}$$

is the gradient-based control law derived from $V_{ijb}(e_{ijb})$ for the robot pair (i, j) . The bearing-only formation control law for robot R_i in (3.1) is then given by

$$u_{ib} = \sum_{j \in \mathcal{N}_i} e_{ijb}. \quad (3.3)$$

In [53], it has been shown that the above control law ensures the global asymptotic stability of the desired formation shape provided the formation shape is infinitesimally bearing rigid.

3.3 Problem Formulation

As discussed in the Introduction section of this chapter, we study the setup in which the robots possess heterogeneous sensing, and each robot, depending on its own local information, maintains the prescribed distance or bearing with its neighbors using the aforementioned distance-based or bearing-only formation control law. Thus, in the current setup, each robot fulfills either a *distance task* or a *bearing task*. As before, consider a pair of robots with labels R_i and R_j . In case R_i is assigned a *distance task*, its goal is to maintain a desired distance $d_{ij}^* \in \mathbb{R}_{>0}$ with R_j . The robot R_i possesses an *independent local coordinate frame* Σ^i which is *not necessarily aligned* with that of R_j or the *global coordinate frame* Σ^g . Within its local coordinate frame Σ^i , R_i is able to measure the relative position vector $z_{ij} \in \mathbb{R}^2$ relative to R_j . On the other hand, when R_j is assigned a *bearing task*, its goal is to maintain a desired bearing $g_{ji}^* \in \mathbb{R}^2$ with R_i . The robot R_j is able to obtain the relative bearing measurement g_{ji} of R_i in its *local coordinate frame* Σ^j which is *aligned* with Σ^g . Since robot R_i is assigned the distance task, we term it a *distance robot*. Correspondingly, R_j is a *bearing robot*. For the interconnection topology, we assume each robot has only neighbors of the opposing category, i.e., a distance robot can only have edges with bearing robot(s) and vice versa. As a result, the team of n robots can be partitioned into two sets, namely the set of distance robots \mathcal{D} and bearing robots \mathcal{B} with $\mathcal{D} \neq \emptyset$ and $\mathcal{B} \neq \emptyset$. The edge set is given by $\mathcal{E} \subseteq (\mathcal{D} \times \mathcal{B}) \cup (\mathcal{B} \times \mathcal{D})$; the underlying structure is a bipartite digraph.

For the moment, we focus on the cases in which the team of $n \in \{2, 3\}$ robots has a *complete bipartite digraph* topology, i.e., the edge set is $\mathcal{E} = (\mathcal{D} \times \mathcal{B}) \cup (\mathcal{B} \times \mathcal{D})$. For the two robot case, we only have one feasible setup, namely the setup consisting of *one distance and one bearing (1D1B)* robot, while for the three robot case we have two feasible robot setups, namely the *one distance and two bearing (1D2B)* and the *one bearing and two distance (1B2D)* setup; see Fig. 3.1 for an illustration of these setups.

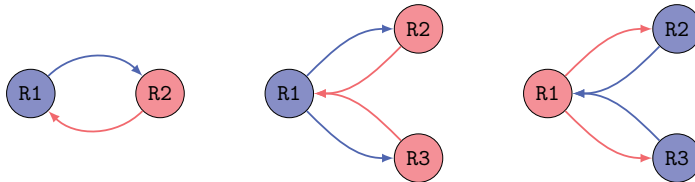


Figure 3.1: Setups for the two and three robot case; \bullet represents a distance robot and \circ represents a bearing robot. Correspondingly, blue arrows are sensing carried out by the distance robots \bullet while red arrows represents the edges from the bearing robots \circ . From left to right, we have the (1D1B), (1D2B), and (1B2D) setup.

We are interested in studying the stability of the formation when the distance-

based formation control law (3.2) for the distance robot(s) and the bearing-only formation control law (3.3) for the bearing robot(s) are used. In this case, we do not modify the standard gradient-based control law for the different tasks. Consequently, we analyze whether i). the equilibrium set contains undesired shape and/or group motion; ii). the desired shape is (exponentially) stable; and iii). the undesired shape and/or group motion (if any) is attractive. The first and last questions are motivated by the robustness issues of the distance- and displacement-based controllers as studied in [8, 17, 35, 47] where a disagreement between neighboring robots about desired values or measurements can lead to an undesired group motion and deformation of the formation shape. Since we are considering heterogeneous sensing mechanisms with corresponding heterogeneous potential functions, it is of interest whether such undesired behavior can co-exist. Such knowledge on the effect of heterogeneity in the control law can potentially be useful to design simultaneous formation and motion controller as pursued recently in [19].

3.4 The (1D1B) Robot Setup

We first focus on the case of two robots in the (1D1B) setup as depicted in Fig. 3.1. The analysis of this seemingly simple setup serves as a prelude for the setups with three robots. Without loss of generality, robot R1 takes the role of the distance robot and R2 is the bearing robot. Considering gradient-based control laws for the robot-specific tasks, the closed-loop dynamics is given by

$$\begin{bmatrix} \dot{p}_1 \\ \dot{p}_2 \end{bmatrix} = \begin{bmatrix} K_d e_{12d} z_{12} \\ K_b e_{21b} \end{bmatrix}, \quad (3.4)$$

where $K_d > 0$ and $K_b > 0$ are control gains for robots R1 and R2, respectively, the bearing error satisfies $e_{21b} = -e_{12b}$ in Σ^g , and the error vector is $e = [e_{12d} \ e_{12b}^\top]^\top \in \mathbb{R}^3$. It is of interest to note that when physical dimension is taken into account with [L] as the unit of length and [T] the unit of time, the control gain K_d has dimension $[L]^{-2} [T]^{-1}$ while K_b is expressed in $[L] [T]^{-1}$.

In the remainder of this section, we provide the analysis of the closed-loop formation system (3.4), hereby focusing on the three questions raised in Section 3.3. First, we have the following result on the equilibrium configurations.

Proposition 3.1 ((1D1B) Equilibrium Configurations). *The equilibrium configurations for the closed-loop formation system (3.4) belong to the set*

$$\mathcal{S}_p = \{p \in \mathbb{R}^4 \mid e = 0_3\}. \quad (3.5)$$

Proof. Solving for $\dot{p}_1 = \mathbb{0}_2$ and $\dot{p}_2 = \mathbb{0}_2$, we obtain $K_d e_{12d} z_{12} = \mathbb{0}_2 \iff e_{12d} = 0 \vee z_{12} = \mathbb{0}_2$ and $-K_b e_{12b} = \mathbb{0}_2 \iff g_{12} = g_{12}^*$, respectively. With $g_{12} = g_{12}^*$ implying $d_{12} \neq 0$, it follows the option $z_{12} = \mathbb{0}_2$ is not feasible. Hence, $\dot{p} = \mathbb{0}_4 \iff e = \mathbb{0}_3$. This completes the proof. \square

Following $e = \mathbb{0}_3$, the inter-robot relative position z_{12} equals the desired relative position $z_{12}^* = d_{12}^* g_{12}^*$ when both the robots attain their individual task. Furthermore, note the set \mathcal{S}_p is invariant under translations in the plane; therefore, such a set is non-compact.

We proceed the analysis by determining the stability of the equilibrium configurations (3.5). To this end, we take as Lyapunov function candidate $V(e)$ of the form

$$V(e) = V_{12d}(e_{12d}) + V_{21b}(e_{21b}) = \frac{1}{4} K_d e_{12d}^2 + \frac{1}{2} K_b d_{21} \|e_{21b}\|^2. \quad (3.6)$$

Observe that $V(e)$ is the sum of the task-specific potential functions. Since $V_{12d}(e_{12d}) \geq 0$ and $V_{21b}(e_{21b}) \geq 0$, it follows that $V(e) \geq 0$. Moreover, $V(e) = 0 \iff V_{12d}(e_{12d}) = 0 \wedge V_{21b}(e_{21b}) = 0$. When considered separately, we know $V_{12d}(e_{12d}) = 0 \iff d_{12} = d_{12}^*$ and $V_{21b}(e_{21b}) = 0 \iff d_{21} = 0 \vee e_{21b} = \mathbb{0}_2$. Combining both potential functions, we conclude that $d_{21} = 0$ is not a feasible option since then $V_{12d}(e_{12d}) > 0$. Therefore, the minimum value of $V(e)$ is attained in \mathcal{S}_p , i.e., $V(e) = 0 \iff \hat{p} \in \mathcal{S}_p$. The derivative of (3.6) evaluates to

$$\begin{aligned} \dot{V}(e) &= \frac{d}{dt} (V_{12d}(e_{12d}) + V_{21b}(e_{21b})) \\ &= \begin{bmatrix} \frac{\partial}{\partial p_1} V_{12d} & \frac{\partial}{\partial p_2} V_{12d} \end{bmatrix} \begin{bmatrix} \dot{p}_1 \\ \dot{p}_2 \end{bmatrix} + \begin{bmatrix} \frac{\partial}{\partial p_1} V_{21b} & \frac{\partial}{\partial p_2} V_{21b} \end{bmatrix} \begin{bmatrix} \dot{p}_1 \\ \dot{p}_2 \end{bmatrix} \\ &= \begin{bmatrix} -\dot{p}_1^\top & \dot{p}_1^\top \end{bmatrix} \begin{bmatrix} \dot{p}_1 \\ \dot{p}_2 \end{bmatrix} + \begin{bmatrix} \dot{p}_2^\top & -\dot{p}_2^\top \end{bmatrix} \begin{bmatrix} \dot{p}_1 \\ \dot{p}_2 \end{bmatrix} \\ &= -\|\dot{z}_{12}\|^2 \leq 0, \end{aligned} \quad (3.7)$$

where we use $\dot{p}_i = -\left(\frac{\partial}{\partial p_i} V_{ij\bullet}\right)^\top \iff -\dot{p}_i^\top = \frac{\partial}{\partial p_i} V_{ij\bullet}$ and $\frac{\partial}{\partial p_j} V_{ij\bullet} = -\frac{\partial}{\partial p_i} V_{ij\bullet}$ for $i, j \in \{1, 2\}$ and $\bullet \in \{b, d\}$. From (3.7), we have $\dot{V}(e)$ is negative semi-definite and $\dot{V}(e) = 0 \iff \dot{p}_1 = \dot{p}_2$. The following are invariant sets corresponding to $\dot{V}(e) = 0$:

1. $\dot{p}_1 = \dot{p}_2 = \mathbb{0}_2$; these are the previously obtained equilibrium configurations $\hat{p} \in \mathcal{S}_p$;
2. $\dot{p}_1 = \dot{p}_2 = w \neq \mathbb{0}_2$; in this scenario, the robots move with a (yet to be determined) constant velocity $w \in \mathbb{R}^2$.

Let the set of configurations $p \in \mathbb{R}^4$ yielding robots to move with the (yet to be determined) constant velocity w be given as

$$\mathcal{T}_p = \{p \in \mathbb{R}^4 \mid \dot{p}_1 = \dot{p}_2 = w, w \neq 0_2\}. \quad (3.8)$$

Note the set \mathcal{T}_p is also non-compact, since if $\hat{p} \in \mathcal{T}_p$, then $\hat{p} + c(\mathbb{1}_2 \otimes w) \in \mathcal{T}_p$ with $c \in \mathbb{R}$. As both the equilibrium set \mathcal{S}_p and the *moving* set \mathcal{T}_p are non-compact and the expression for the Lyapunov derivative (3.7) is expressed in the dynamics of the *link* z_{12} , we continue the analysis by exploring the *link dynamics* \dot{z}_{12} , obtained as

$$\dot{z}_{12} = -(K_b e_{12b} + K_d e_{12d} z_{12}), \quad (3.9)$$

instead of the robot dynamics \dot{p} . Mapping the sets of interest \mathcal{S}_p and \mathcal{T}_p to the *link space* yields $\mathcal{S}_z = \{z_{12} \in \mathbb{R}^2 \mid z_{12} = z_{12}^*\}$ and $\mathcal{T}_z = \{z_{12} \in \mathbb{R}^2 \mid z_{12} = z_{12_M}\}$, where $z_{12_M} = d_{12_M} g_{12_M}$ is the inter-robot relative position vector as they move with the (yet unknown) velocity w in the plane. The set \mathcal{S}_z contains only a single point, and therefore it is compact.

3.4.1 Characterization of the moving set \mathcal{T}_z

In this part, we make the effort to characterize the moving set \mathcal{T}_z (and implicitly \mathcal{T}_p). To this end, we provide the following proposition:

Proposition 3.2 ((1D1B) Moving Configurations). *The closed-loop formation system (3.4) moves with a constant velocity $w = 2K_b g_{12}^*$ when the error vector e is of the form*

$$\begin{bmatrix} e_{12d} \\ e_{12b} \end{bmatrix} = - \begin{bmatrix} \frac{2}{d_{12}} R_{bd} \\ 2g_{12}^* \end{bmatrix}. \quad (3.10)$$

Proof. Solving for $\dot{z}_{12} = 0_2$ results in the expression $(K_d e_{12d} d_{12} + K_b) g_{12} = K_b g_{12}^*$. We distinguish two cases. The case $g_{12} = g_{12}^*$ and $K_d e_{12d} d_{12} + K_b = K_b \iff K_d e_{12d} d_{12} = 0$ corresponds to the equilibrium configurations $\hat{p} \in \mathcal{S}_p$. On the other hand, we have $g_{12} = -g_{12}^*$ and $K_d e_{12d} d_{12} + K_b = -K_b \iff e_{12d} d_{12} + 2R_{bd} = 0$, where $R_{bd} = \frac{K_b}{K_d}$ is the ratio of the control gains. Substituting in the robot dynamics (3.4) yields $\dot{p}_1 = \dot{p}_2 = 2K_b g_{12}^*$, i.e., robots are moving with a common velocity $w = 2K_b g_{12}^*$. Therefore, moving formations occur at the relative orientation $g_{12} = -g_{12}^*$. By definition, we obtain $e_{12b} = -2g_{12}^*$ and the distance error $e_{12d} d_{12} + 2R_{bd} = 0 \iff e_{12d} = -\frac{2}{d_{12}} R_{bd}$. This completes the proof. \square

Proposition 3.2 provides a characterization of the moving set \mathcal{T}_z in terms of the error vector e . We also obtain that the inter-robot bearing for moving formations to occur is $g_{12_M} = -g_{12}^*$. For a complete characterization of \mathcal{T}_z in terms

of the vector z_{12M} , it remains to obtain the distance d_{12M} by solving the expression $e_{12d}d_{12} + 2R_{bd} = 0$. Expanding it, we obtain the following cubic equation in d_{12} :

$$d_{12}^3 - (d_{12}^*)^2 d_{12} + 2R_{bd} = 0. \quad (3.11)$$

Compared with (2.2), the coefficients are $c = -(d_{12}^*)^2 < 0$ and $d = 2R_{bd} > 0$. We infer the solution set to (3.11) contains positive real roots given by Lemma 2.2 when the corresponding discriminant is non-negative. This is equivalent to the constraint $d_{12}^* \geq \hat{d}$ with $\hat{d} = \sqrt[3]{3\sqrt[3]{R_{bd}}}$.

Remark 3.3. When the desired distance $d_{12}^* < \hat{d}$, the moving set $\mathcal{T}_z = \emptyset$ since a feasible distance between robots such that they move with the common velocity w does not exist. This implies $\dot{V}(e) = 0 \iff \hat{p} \in \mathcal{S}_p$. With $\dot{V}(e) < 0$ when $p \notin \mathcal{S}_p$, we conclude that for all initial configurations $p(0) \in \mathbb{R}^4$ satisfying $p_1(0) \neq p_2(0)$, we have global asymptotic convergence to the desired equilibrium set \mathcal{S}_p .

Remark 3.4. The threshold value \hat{d} is proportional to the gain ratio $\sqrt[3]{R_{bd}}$; increasing R_{bd} leads to a larger value for \hat{d} . Therefore, increasing the value of R_{bd} ‘‘delays’’ the occurrence of the moving set \mathcal{T}_p since there exists a larger range of values for d_{12}^* satisfying $d_{12}^* < \hat{d}$.

Assume the desired distance satisfies $d_{12}^* \geq \hat{d}$. Lemma 2.2 provides us the positive roots, and thus the feasible distances d_{12} satisfying (3.11). For the specific values $c = -(d_{12}^*)^2$ and $d = 2R_{bd}$, we obtain $r_v = \sqrt{\frac{(d_{12}^*)^6}{27}}$ and $\varphi_v = \tan^{-1}(-R_{bd}^{-1}\sqrt{-R})$. Substituting in (2.5) yields

$$y_{p_1} = \frac{2}{3}\sqrt{3}d_{12}^* \cos\left(\frac{1}{3}\varphi_v - 120^\circ\right), \quad y_{p_2} = \frac{2}{3}\sqrt{3}d_{12}^* \cos\left(\frac{1}{3}\varphi_v\right). \quad (3.12)$$

When $d_{12}^* = \hat{d}$, the positive root (with multiplicity 2) corresponding to the cubic equation (3.11) is $d_{12} = \frac{1}{3}\sqrt{3}\hat{d} = \sqrt[3]{R_{bd}}$. The characterization of the moving set \mathcal{T}_z for $d_{12}^* \geq \hat{d}$ is

$$\mathcal{T}_z = \{z_{12} \in \mathbb{R}^2 \mid z_{12} = -yg_{12}^*, y \text{ satisfies (3.12)}\}. \quad (3.13)$$

3.4.2 Local stability of the moving set \mathcal{T}_z

After characterizing the set \mathcal{T}_z for $d_{12}^* \geq \hat{d}$, we continue with determining the local stability of \mathcal{T}_z . First, we obtain the Jacobian of the right hand side (RHS) of the link dynamics (3.9) as the matrix

$$A = -(K_b A_{12b} + K_d A_{12d}), \quad (3.14)$$

where $A_{12b} = \frac{1}{d_{12}}(I - g_{12}g_{12}^\top)$ and $A_{12d} = e_{12d}I + 2z_{12}z_{12}^\top$.

Lemma 3.5. *The closed-loop formation system (3.4) at any feasible point \hat{z}_{12} in the moving set \mathcal{T}_z is unstable.*

Proof. From Proposition 3.2, we know that all feasible points $\hat{z}_{12} \in \mathcal{T}_z$ satisfies $e_{12d} = -2\frac{1}{d_{12}}R_{bd} < 0$ and $g_{12} = -g_{12}^*$. Let the inter-robot bearing be given as $g_{12} = \begin{bmatrix} a & b \end{bmatrix}^\top$ with the norm constraint $\|g_{12}\| = \sqrt{a^2 + b^2} = 1$; we obtain $g_{12}g_{12}^\top = \begin{bmatrix} a^2 & ab \\ ab & b^2 \end{bmatrix} = g_{12}^*g_{12}^{*\top}$. Substituting in (3.14) yields

$$A = \begin{bmatrix} x + (x - y)a^2 & (x - y)ab \\ (x - y)ab & x + (x - y)b^2 \end{bmatrix}, \quad (3.15)$$

where we define $x = K_b \frac{1}{d_{12}}$ and $y = 2K_d d_{12}^2$, both being positive. For a 2×2 matrix A , the characteristic polynomial $\chi(\lambda)$ is given by

$$\chi(\lambda) = \lambda^2 - \mathbf{trace}(A)\lambda + \mathbf{det}(A), \quad (3.16)$$

where $\mathbf{trace}(A)$ is the trace and $\mathbf{det}(A)$ is the determinant of matrix A . With A in (3.15), we obtain $\mathbf{trace}(A) = 3x - y$ and $\mathbf{det}(A) = x(2x - y)$. It follows the roots of $\chi(\lambda)$ are $\lambda_1 = x$ and $\lambda_2 = 2x - y$. Since $\lambda_1 = x > 0$, we conclude matrix A has at least one positive eigenvalue for all feasible points $\hat{z}_{12} \in \mathcal{T}_z$. Therefore, the closed-loop formation system (3.4) is unstable at these points. This completes the proof. \square

The following theorem states the main result for the **(1D1B)** setup when the desired distance satisfies $d_{12}^* \geq \hat{d}$.

Theorem 3.6 (Almost global convergence). *Consider two robots $R1$ and $R2$ possessing heterogeneous sensing mechanisms. Let the closed-loop dynamics be given by (3.4) and the desired inter-robot distance satisfies $d_{12}^* \geq \hat{d}$. If $p_1(0) \neq p_2(0)$ and $p(0) \notin \mathcal{T}_p$, then the trajectories of the robots asymptotically converge to a point $\hat{p} \in \mathcal{S}_p$.*

Proof. In (3.7), we obtain the Lyapunov derivative $\dot{V}(e) \leq 0$. In fact, $\dot{V}(e) < 0$ when $p(t) \notin \mathcal{S}_p \cup \mathcal{T}_p$. From Lemma 3.5, we obtain that the set \mathcal{T}_z and implicitly \mathcal{T}_p is unstable. Hence, if $p(0) \notin \mathcal{T}_p$, it follows $p(t) \rightarrow \mathcal{T}_p$. This implies that $\dot{V}(e) = 0$ if and only if the trajectories reaches a point $\hat{p} \in \mathcal{S}_p$. In this scenario, $V(e) = 0$ and $\dot{p}_1 = \dot{p}_2 = \mathbf{0}_2$. This completes the proof. \square

Previously, Remark 3.3 encapsulates the stability result when $d_{12}^* < \hat{d}$ holds for the desired distance. In combination with Theorem 3.6, we have provided the full stability analysis for the **(1D1B)** setup with closed-loop dynamics given by (3.4).

We can now provide answers to the three questions raised in Section 3.3. For the the **(1D1B)** setup, we have shown that equilibrium configurations consist of only the correct inter-robot relative positions z_{12}^* and we have (almost) global

convergence towards z_{12}^* . Also, moving configurations z_{12_M} exist. However, these are locally not attractive. Moreover, as mentioned in Remark 3.4, the occurrence of moving configurations can be postponed when the gain ratio R_{bd} is increased.

3.5 The (1D2B) Robot Setup

In the previous section, we have analyzed the case of two robots in the (1D1B) setup. One observation which stands out is the fact that robots may move with a constant velocity w when they are initialized at specific points in the plane.

We consider now three robots with the specific partition $\mathcal{D} = \{1\}$ and $\mathcal{B} = \{2, 3\}$; the (1D2B) setup depicted in Fig. 3.1. The neighbor sets are found to be $\mathcal{N}_1 = \{2, 3\}$ and $\mathcal{N}_2 = \mathcal{N}_3 = \{1\}$. Utilizing gradient-based control laws for each distance or bearing task, we obtain the following closed-loop dynamics

$$\begin{bmatrix} \dot{p}_1 \\ \dot{p}_2 \\ \dot{p}_3 \end{bmatrix} = \begin{bmatrix} K_d e_{12d} z_{12} + K_d e_{13d} z_{13} \\ K_b e_{21b} \\ K_b e_{31b} \end{bmatrix}, \quad (3.17)$$

where we assume the distance robot R1 has the control gain $K_d > 0$ and the bearing robots R2 and R3 the common control gain $K_b > 0$. In the (1D1B) setup, we observe the link dynamics is also of interest. Therefore, in the current setup, we define the relative position vector $z = [z_{12}^\top \quad z_{13}^\top]^\top \in \mathbb{R}^4$. The link dynamics \dot{z} evaluates to

$$\begin{bmatrix} \dot{z}_{12} \\ \dot{z}_{13} \end{bmatrix} = - \begin{bmatrix} K_b e_{12b} + K_d e_{12d} z_{12} + K_d e_{13d} z_{13} \\ K_b e_{13b} + K_d e_{12d} z_{12} + K_d e_{13d} z_{13} \end{bmatrix}. \quad (3.18)$$

For a triangle, it holds that $z_{12} + z_{23} - z_{13} = \mathbb{0}_2$. Hence, the dynamics related to link z_{23} evaluates to $\dot{z}_{23} = -K_b (e_{13b} - e_{12b})$.

In the following subsections, we analyze the closed-loop formation system (3.17), following similar steps as we have done for the (1D1B) setup.

3.5.1 Equilibrium configurations

The following result on the equilibrium configurations is obtained.

Proposition 3.7 ((1D2B) Equilibrium Configurations). *The equilibrium configurations corresponding to the closed-loop formation system (3.17) belong to the set*

$$\mathcal{S}_p = \{p \in \mathbb{R}^6 \mid e = \mathbb{0}_6\}, \quad (3.19)$$

where $e = [e_{12d} \quad e_{13d} \quad e_{12b}^\top \quad e_{13b}^\top]^\top \in \mathbb{R}^6$.

Proof. Setting the left hand side (LHS) of each equation in (3.17) to the zero vector, we immediately obtain that at the equilibrium configurations, the bearing constraints for robots R2 and R3 are satisfied since $e_{21b} = -e_{12b} = \mathbb{0}_2$ and $e_{31b} = -e_{13b} = \mathbb{0}_2$. This implies that $d_{21} = d_{12} \neq 0$ and $d_{31} = d_{13} \neq 0$. It remains to solve for $\dot{p}_1 = \mathbb{0}_2$. With the gathered insights, we obtain $e_{12d}d_{12}g_{12}^* = -e_{13d}d_{13}g_{13}^*$. Since $g_{12}^* \neq \pm g_{13}^*$ (the robots are colinear when $g_{12} = \pm g_{13}$), the only way to satisfy the expression is when $e_{12d}d_{12} = 0$ and $e_{13d}d_{13} = 0$. Because $d_{12} \neq 0$ and also $d_{13} \neq 0$, we require $e_{12d} = 0$ and $e_{13d} = 0$ to hold. This completes the proof. \square

3.5.2 Moving configurations

During the analysis of the (1D1B) setup, we observed that robots may move with a common velocity w while the predefined constraints are not met. For the (1D2B) setup, we explore whether conditions exist such that the formation may move with a common velocity w .

Proposition 3.8 ((1D2B) Moving Configurations). *The closed-loop formation system (3.17) moves with a constant velocity $w = K_b (g_{12}^* + g_{13}^*)$ when the error vector e satisfies*

$$\begin{bmatrix} e_{12d} \\ e_{13d} \\ e_{12b} \\ e_{13b} \end{bmatrix} = - \begin{bmatrix} \frac{1}{d_{12}} R_{bd} \\ \frac{1}{d_{13}} R_{bd} \\ g_{12}^* + g_{13}^* \\ g_{12}^* + g_{13}^* \end{bmatrix}. \quad (3.20)$$

Proof. First, we solve for $\dot{z} = \mathbb{0}_4$. Since $\dot{z}_{12} = \mathbb{0}_2 = \dot{z}_{13}$, it follows $\dot{z}_{23} = \mathbb{0}_2$. This expression evaluates to $g_{12} - g_{13} = g_{12}^* - g_{13}^*$. Define $b_{\text{diff}} = g_{12} - g_{13}$ and let $\angle g_{12} = \alpha$ be the angle enclosed by g_{12} and the positive x -axis of Σ^g . Similarly, let $\angle g_{13} = \beta$. We can rewrite b_{diff} as

$$b_{\text{diff}} = \begin{bmatrix} \cos \alpha \\ \sin \alpha \end{bmatrix} - \begin{bmatrix} \cos \beta \\ \sin \beta \end{bmatrix} = 2 \cos \left(\frac{\alpha - \beta}{2} \right) \begin{bmatrix} \cos \left(\frac{\alpha + \beta}{2} \right) \\ \sin \left(\frac{\alpha + \beta}{2} \right) \end{bmatrix}, \quad (3.21)$$

where $\beta_\pi = \beta + \pi \pmod{2\pi}$. The expression $\dot{z}_{23} = \mathbb{0}_2$ can be transformed to the following set of constraints on the angles, namely

$$\begin{cases} \alpha + \beta_\pi = \alpha^* + \beta_\pi^* \\ \alpha - \beta_\pi = \alpha^* - \beta_\pi^* \end{cases} \iff \begin{cases} \alpha = \alpha^* \\ \beta = \beta^* \end{cases} \quad (3.22)$$

and

$$\begin{cases} \alpha + \beta_\pi = \alpha^* + \beta_\pi^* \\ -(\alpha - \beta_\pi) = \alpha^* - \beta_\pi^* \end{cases} \iff \begin{cases} \alpha = \beta^* + \pi \\ \beta = \alpha^* - \pi \end{cases}. \quad (3.23)$$

From (3.22), we obtain $g_{12} = g_{12}^*$ and $g_{13} = g_{13}^*$, corresponding to the equilibrium configurations in \mathcal{S}_p while the solution in (3.23) corresponds to $g_{12} = -g_{13}^*$ and $g_{13} = -g_{12}^*$. Subsequently, we obtain $e_{12b} = e_{13b} = -(g_{12}^* + g_{13}^*)$. Hence it is sufficient to consider one of the equations in (3.18). This leads to $(-K_d e_{13d} d_{13}) g_{12}^* + (-K_d e_{12d} d_{12}) g_{13}^* = K_b g_{12}^* + K_b g_{13}^*$. For it to hold, we require $-K_d e_{13d} d_{13} = K_b \iff e_{13d} = -\frac{1}{d_{13}} R_{bd}$ and $-K_d e_{12d} d_{12} = K_b \iff e_{12d} = -\frac{1}{d_{12}} R_{bd}$ with the gain ratio $R_{bd} = \frac{K_b}{K_d}$. Collecting the error constraints, we obtain (3.20). By an immediate substitution, we obtain for the dynamics of the bearing robot R2, $\dot{p}_2 = K_b (g_{12}^* + g_{13}^*) =: w$. This completes the proof. \square

Remark 3.9. The signed area for a triangle, introduced as a constraint for resolving flip and flex ambiguities in [6, 33], can be obtained using the expression $S_A = z_{12}^\top \begin{bmatrix} 0 & 1 \\ -1 & 0 \end{bmatrix} z_{13}$. The signed area of the desired formation shape evaluates to $S_A^* = d_{12}^* d_{13}^* g_{12}^{\top*} \begin{bmatrix} 0 & 1 \\ -1 & 0 \end{bmatrix} g_{13}^*$. The signed area of the moving formation shape is $S_{A_M} = d_{12} d_{13} g_{13}^\top \begin{bmatrix} 0 & 1 \\ -1 & 0 \end{bmatrix} g_{12}^* = -d_{12} d_{13} g_{12}^{\top*} \begin{bmatrix} 0 & 1 \\ -1 & 0 \end{bmatrix} g_{13}^* = -\frac{d_{12} d_{13}}{d_{12}^* d_{13}^*} S_A^*$. Since the distance error signals in (3.20) are negative, it follows $d_{ij} < d_{ij}^*$. Hence $|S_{A_M}| < |S_A|$ and the cyclic ordering of the robots is opposite to that of the desired formation shape.

Following Proposition 3.8, a characterization of the moving set \mathcal{T}_p in terms of the error vector e is

$$\mathcal{T}_p = \{p \in \mathbb{R}^6 \mid e \text{ satisfies (3.20)}\}. \quad (3.24)$$

An equivalent characterization of \mathcal{T}_p can be provided in terms of the inter-robot relative position vectors z_{12_M} and z_{13_M} where subscript M refers to ‘‘moving’’. In fact, the inter-robot bearing vectors g_{12_M} between R1 and R2 and g_{13_M} between robots R1 and R3 is known from the proof of Proposition 3.8. It remains to obtain feasible values for the inter-robot distances d_{12_M} and d_{13_M} . To this end, we find the roots satisfying the expressions for the distance error signals e_{12d} and e_{13d} in (3.20). Expanding the expressions leads to the following cubic equation

$$d_{ij}^3 - (d_{ij}^*)^2 d_{ij} + R_{bd} = 0, \quad ij \in \{12, 13\}, \quad (3.25)$$

similar to the (1D1B) setup. Compared with (2.2), we now have $c = -(d_{ij}^*)^2 < 0$ and $d = R_{bd} > 0$. In the (1D1B) setup, we had $d = 2R_{bd}$. Following the same steps as was done for (3.11), we obtain that the discriminant corresponding to (3.25) is $\Delta = 4(d_{ij}^*)^6 - 27R_{bd}^2$ and the threshold value for the desired distance d_{ij}^* such that positive roots exist is $\hat{d} = \sqrt[3]{3} \sqrt[3]{\frac{R_{bd}}{2}} \approx 1.3747 \sqrt[3]{R_{bd}}$. Similar to the (1D1B) setup, we conclude that if one of (or both) the desired distances d_{12}^* or (and) d_{13}^* has (have) a value less than \hat{d} , then no feasible value for d_{12} or (and) d_{13} satisfies $e_{12d} d_{12} = -R_{bd}$ or (and) $e_{13d} d_{13} = -R_{bd}$, implying the in-feasibility of moving formations. We conclude the set \mathcal{S}_p containing equilibrium configurations with either one of (or both) $d_{12}^* < \hat{d}$ or $d_{13}^* < \hat{d}$ is globally asymptotically stable.

When the desired distance d_{ij}^* satisfies $d_{ij}^* \geq \hat{d}$, we obtain feasible distances d_{ij} to (3.25) are given by Lemma 2.2 with the values $r_v = \sqrt{\frac{(d_{ij}^*)^6}{27}}$ and $\varphi_v = \tan^{-1}(-2R_{\text{bd}}^{-1}\sqrt{-R})$. Since we have two desired distances d_{12}^* and d_{13}^* and we have either one or two feasible value(s) d_{ij} to the cubic equation (3.25), it follows that different feasible combinations (d_{12_M}, d_{13_M}) exist. In Table 3.1, we summarize the number of feasible combinations for the different scenarios. We conclude the set $\mathcal{T}_p \neq \emptyset$ when the additional constraints $d_{12}^* \geq \hat{d}$ and $d_{13}^* \geq \hat{d}$ are satisfied.

Table 3.1: Number of feasible combinations (d_{12_M}, d_{13_M}) depending on desired distances d_{12}^* and d_{13}^*

	$d_{13}^* > \hat{d}$	$d_{13}^* = \hat{d}$
$d_{12}^* > \hat{d}$	4	2
$d_{12}^* = \hat{d}$	2	1

Recall the common velocity $w = K_b (g_{12}^* + g_{13}^*)$ for the robots in Proposition 3.8. Define $b_{\text{sum}} = g_{12} + g_{13}$. We want to write b_{sum} in the form $b_{\text{sum}} = d_{\text{sum}} g_{\text{sum}}$ with d_{sum} being the magnitude and g_{sum} the orientation of b_{sum} relative to Σ^g . By the sum-to-product identities for cosine and sine, we obtain

$$b_{\text{sum}} = \begin{bmatrix} \cos \alpha \\ \sin \alpha \end{bmatrix} + \begin{bmatrix} \cos \beta \\ \sin \beta \end{bmatrix} = 2 \cos \left(\frac{\alpha - \beta}{2} \right) \begin{bmatrix} \cos \left(\frac{\alpha + \beta}{2} \right) \\ \sin \left(\frac{\alpha + \beta}{2} \right) \end{bmatrix}. \quad (3.26)$$

Depending on the value of the angle difference $|\alpha - \beta|$, we have different expressions for d_{sum} and g_{sum} . When $|\alpha - \beta| < \pi$, we set $d_{\text{sum}} = 2 \cos \left(\frac{|\alpha - \beta|}{2} \right)$ and $\angle g_{\text{sum}} = \frac{\alpha + \beta}{2}$ while for $|\alpha - \beta| > \pi$, we set $d_{\text{sum}} = 2 \cos \left(\pi - \frac{|\alpha - \beta|}{2} \right)$ and $\angle g_{\text{sum}} = \frac{\alpha + \beta}{2} + \pi \pmod{2\pi}$. Note that $d_{\text{sum}} \in (0, 2)$ for the cases $|\alpha - \beta| \geq \pi$. If $|\alpha - \beta| = 0^\circ$, then $g_{12} = g_{13}$ and $b_{\text{sum}} = 2g_{12}$, and finally, $|\alpha - \beta| = \pi$ implies $g_{12} = -g_{13}$, and hence $b_{\text{sum}} = \mathbb{0}_2$. Since $g_{12}^* \neq \pm g_{13}^*$, the last two mentioned cases do not occur; therefore, the magnitude of w is $0 < \|w\| < 2K_b$.

3.5.3 Local stability of equilibrium and moving configurations

Assume that the desired distances satisfy $d_{12}^* \geq \hat{d}$ and $d_{13}^* \geq \hat{d}$. In this case, both the equilibrium configurations in (3.19) and moving configurations in (3.24) satisfy $\dot{z} = \mathbb{0}_4$ and are feasible. We are interested in determining the local stability around these formations. To this end, we consider the linearization of the z -dynamics

(3.18); this results in the Jacobian matrix $A \in \mathbb{R}^{4 \times 4}$ as

$$A = - \begin{bmatrix} K_b A_{12b} + K_d A_{12d} & K_d A_{13d} \\ K_d A_{12d} & K_b A_{13b} + K_d A_{13d} \end{bmatrix}, \quad (3.27)$$

where $A_{ijd} = e_{ijd} I_2 + 2z_{ij} z_{ij}^\top$ and $A_{ijb} = \frac{1}{d_{ij}} (I_2 - g_{ij} g_{ij}^\top)$, $ij \in \{12, 13\}$.

We first consider the stability analysis around the equilibrium configurations.

Theorem 3.10. *Consider a team of three robots arranged in the (1D2B) setup with closed-loop dynamics given by (3.17). Assume the desired distances satisfy $d_{12}^* \geq \hat{d}$ and $d_{13}^* \geq \hat{d}$ with $\hat{d} = \sqrt{3} \sqrt{\frac{R_{bd}}{2}}$ and the bearing vectors satisfy $g_{12}^* \neq \pm g_{13}^*$. Given an initial configuration $p(0)$ that is close to the desired formation shape, then the robot trajectories asymptotically converge to a point $\hat{p} \in \mathcal{S}_p$.*

Proof. Evaluating the Jacobian matrix (3.27) at the equilibrium configurations yields

$$A_E = -\text{diag} \left(\begin{bmatrix} x^* & x^* & p^* & p^* \end{bmatrix} \right) - \begin{bmatrix} (y^* - x^*) a^2 & (y^* - x^*) ab & q^* c^2 & q^* cd \\ (y^* - x^*) ab & (y^* - x^*) b^2 & q^* cd & q^* d^2 \\ y^* a^2 & y^* ab & (q^* - p^*) c^2 & (q^* - p^*) cd \\ y^* ab & y^* b^2 & (q^* - p^*) cd & (q^* - p^*) d^2 \end{bmatrix}, \quad (3.28)$$

where we define the variables

$$x = K_b \frac{1}{d_{12}}, \quad y = 2K_d d_{12}^2, \quad p = K_b \frac{1}{d_{13}}, \quad q = 2K_d d_{13}^2. \quad (3.29)$$

and the matrices

$$g_{12}^* g_{12}^{*\top} = \begin{bmatrix} a^2 & ab \\ ab & b^2 \end{bmatrix}, \quad g_{13}^* g_{13}^{*\top} = \begin{bmatrix} c^2 & cd \\ cd & d^2 \end{bmatrix}. \quad (3.30)$$

The starred version for x , p , y , and q is used here since we have $d_{12} = d_{12}^*$ and $d_{13} = d_{13}^*$. The characteristic polynomial $\chi_E(\lambda)$ corresponding to matrix A_E is obtained as

$$\chi_E(\lambda) = (\lambda + x^*) (\lambda + p^*) (\lambda^2 + (y^* + q^*) \lambda + y^* q^* \sin^2 \theta^*), \quad (3.31)$$

where $\sin \theta = g_{12}^\top \begin{bmatrix} 0 & 1 \\ -1 & 0 \end{bmatrix} g_{13}$. The roots of (3.31) are

$$\begin{aligned} \lambda_1 &= -x^*, & \lambda_2 &= -p^*, \\ \lambda_{3,4} &= -\frac{1}{2} (y^* + q^*) \pm \frac{1}{2} \sqrt{(y^* + q^*)^2 - 4y^* q^* \sin^2 \theta^*}. \end{aligned} \quad (3.32)$$

It can be verified that $0 < 4y^*q^*\sin^2\theta^* \leq (y^* + q^*)^2$; therefore all roots are real. Moreover, $-(y^* + q^*) + \sqrt{(y^* + q^*)^2 - 4y^*q^*\sin^2\theta^*} < 0$ and we conclude all λ s are negative; matrix A_E is Hurwitz. This implies that the link trajectories asymptotically converge to the desired relative positions, i.e., $z(t) \rightarrow z^*$ as $t \rightarrow \infty$. It also means that the robots reach their individual tasks since $z_{ij}^* = d_{ij}^*g_{ij}^*$, so $p(t) \rightarrow \mathcal{S}_p$ when $p(0)$ is close to the desired formation shape. This completes the proof. \square

We continue with determining the stability of the moving formations in the set \mathcal{T}_p . Again, the Lyapunov's indirect method is used for this task. As a first step, the characteristic polynomial corresponding to the Jacobian matrix of the moving formations is derived. Based on the characterization in (3.20), we obtain the sub-matrices $A_{12d} = -R_{bd}\frac{1}{d_{12}}I_2 + 2d_{12}^2g_{13}^*g_{13}^{*\top}$, $A_{13d} = -R_{bd}\frac{1}{d_{13}}I_2 + 2d_{13}^2g_{12}^*g_{12}^{*\top}$, $A_{12b} = \frac{1}{d_{12}}(I_2 - g_{13}^*g_{13}^{*\top})$, and $A_{13b} = \frac{1}{d_{13}}(I_2 - g_{12}^*g_{12}^{*\top})$. Substituting these sub-matrices in (3.27) yields the matrix

$$A_M = - \begin{bmatrix} (y-x)c^2 & (y-x)cd & -p+qa^2 & qab \\ (y-x)cd & (y-x)d^2 & qab & -p+qb^2 \\ -x+yc^2 & ycd & (q-p)a^2 & (q-p)ab \\ ycd & -x+yd^2 & (q-p)ab & (q-p)b^2 \end{bmatrix}, \quad (3.33)$$

where the variables are previously defined in (3.29) and (3.30). The characteristic polynomial $\chi_M(\lambda)$ corresponding to matrix A_M is obtained as the quartic polynomial

$$\chi_M(\lambda) = \lambda^4 + c_1\lambda^3 + c_2\lambda^2 + c_3\lambda + c_4 \quad (3.34)$$

with the coefficients

$$\begin{aligned} c_1 &= (y-x) + (q-p), & c_2 &= qy\sin^2\theta^* - px, \\ c_3 &= x(y-x)(q\sin^2\theta^* - p) + p(q-p)(y\sin^2\theta^* - x), \\ c_4 &= px(y-x)(q-p)\sin^2\theta^*. \end{aligned} \quad (3.35)$$

Recall from Table 3.1 that depending on the value of the desired distances d_{12}^* and d_{13}^* , we can obtain more than one feasible combination (d_{12M}, d_{13M}) for the moving configurations. Under certain conditions, we have the following result on the eigenvalues of the matrix A_M .

Lemma 3.11. *Assume the desired distances satisfy $d_{12}^* > \hat{d}$ and $d_{13}^* > \hat{d}$ and the desired bearing vectors are not perpendicular, i.e. $g_{12}^* \not\perp g_{13}^*$. Consider the feasible combination in which the distances are of the form $d_{12M} = y_{p_2}(d_{12}^*)$ and $d_{13M} = y_{p_2}(d_{13}^*)$ in Lemma 2.2. Then all eigenvalues of the matrix A_M have a negative real part if the inequality*

$$\cos^2\theta^* < \frac{mn(mq - ny)^2 + m^2n^2(m+n)(x+p)}{(m^2q + n^2y)(mqx + nyp)} \quad (3.36)$$

holds, where the variables x , y , p , and q are as defined in (3.29), and we define $m = y - x$ and $n = q - p$.

Proof. Assuming the bearing vectors are not perpendicular, we obtain that $0 < \sin^2 \theta^* < 1$. Also, since $d_{12_M} = y_{p_2} (d_{12}^*)$ and $d_{13_M} = y_{p_2} (d_{13}^*)$ and $d_{12}^* > \hat{d}$ and $d_{13}^* > \hat{d}$, we can verify that $m > 0$ and $n > 0$ by applying Proposition 3.19. We employ the Routh-Hurwitz stability criterion to justify the claim provided (3.36) holds. To this end, the Routh-Hurwitz table is formed. The first column of the Routh-Hurwitz table, which is the column of interest, contains the following values

$$\left[1 \quad c_1 \quad \frac{c_1 c_2 - c_3}{c_1} \quad \frac{(c_1 c_2 - c_3) c_3 - c_1^2 c_4}{(c_1 c_2 - c_3)} \quad c_4 \right]. \quad (3.37)$$

For all roots λ to have negative real parts, all values in (3.37) need to be positive. With $m > 0$ and $n > 0$, the coefficients c_1 and c_4 are positive. It remains to show the third and fourth entry in (3.37) is positive. In fact, it is sufficient to show the numerators are both positive. The numerator $c_1 c_2 - c_3$ evaluates to

$$\begin{aligned} c_1 c_2 - c_3 &= (m + n) (qy \sin^2 \theta^*) - mxq \sin^2 \theta^* - npy \sin^2 \theta^* \\ &= \sin^2 \theta^* (m^2 q + n^2 y) > 0, \end{aligned} \quad (3.38)$$

while $(c_1 c_2 - c_3) c_3 - c_1^2 c_4$ evaluates to

$$\begin{aligned} &(c_1 c_2 - c_3) c_3 - c_1^2 c_4 \\ &= \sin^2 \theta^* (m^2 q + n^2 y) (mx (q \sin^2 \theta^* - p) + np (y \sin^2 \theta^* - x)) \\ &\quad - (m + n)^2 (xmpn \sin^2 \theta^*) \\ &= \sin^2 \theta^* \left(\left((mq - ny)^2 + mn(m + n)(x + p) \right) mn \right. \\ &\quad \left. - (m^2 q + n^2 y) (mxq + npy) \cos^2 \theta^* \right). \end{aligned} \quad (3.39)$$

Provided (3.36) holds, it follows the numerator $(c_1 c_2 - c_3) c_3 - c_1^2 c_4 > 0$. Since the entries in (3.37) are all positive, we conclude all eigenvalues of the matrix A_M have negative real parts. This completes the proof. \square

Remark 3.12. The implication of Lemma 3.11 is that under certain conditions on the distance and bearing constraints, a subset of the moving set \mathcal{T}_p is locally asymptotically stable. Hence, initializing the robots close to the conditions for the moving formation is not desirable. An illustration of this behavior is provided in Fig. 3.3(b).

Lemma 3.11 also holds when the desired bearing vectors are perpendicular, i.e. $g_{12}^* \perp g_{13}^* \iff \sin^2 \theta^* = 1$. In this case, the coefficients in (3.35) and also all entries in (3.37) are positive; therefore, the matrix A_M will only have eigenvalues with negative real parts.

A full characterization of the remaining cases can be found in Section 3.8. In almost all cases, the matrix A_M contains at least a root with positive real part and hence it is not Hurwitz.

3.6 The (1B2D) Robot Setup

Here we focus on the formation setup with one bearing and two distance robots (1B2D) is considered. Without loss of generality, we assume robot R1 is the bearing robot while robots R2 and R3 are the distance robots. The rightmost graph in Fig. 3.1 depicts the interconnection structure for this setup. Based on the interconnection structure, the closed-loop dynamics is obtained as

$$\begin{bmatrix} \dot{p}_1 \\ \dot{p}_2 \\ \dot{p}_3 \end{bmatrix} = \begin{bmatrix} K_b e_{12b} + K_b e_{13b} \\ K_d e_{21d} z_{21} \\ K_d e_{31d} z_{31} \end{bmatrix}. \quad (3.40)$$

The corresponding link dynamics evaluates to

$$\begin{bmatrix} \dot{z}_{12} \\ \dot{z}_{13} \end{bmatrix} = - \begin{bmatrix} K_d e_{12d} z_{12} + K_b e_{12b} + K_b e_{13b} \\ K_d e_{13d} z_{13} + K_b e_{12b} + K_b e_{13b} \end{bmatrix}. \quad (3.41)$$

Also, the dynamics of the link z_{23} is found to be $\dot{z}_{23} = -K_d (e_{13d} z_{13} - e_{12d} z_{12})$. In the following, we follow similar steps as in Sections 3.4 and 3.5 for the analysis of the closed-loop formation system (3.40) focusing on equilibrium configurations, possible moving formations, and their (local) stability analysis.

3.6.1 Equilibrium configurations

When we consider the equilibrium conditions with $\dot{p} = \mathbb{0}_6$, we have the following result.

Proposition 3.13 ((1B2D) Equilibrium Configurations:). *The equilibrium configurations corresponding to the closed-loop formation system (3.40) belong to $\mathcal{S}_p^{\text{correct}} \cup \mathcal{S}_p^{\text{flipped}}$, where*

$$\begin{aligned} \mathcal{S}_p^{\text{correct}} &= \{p \in \mathbb{R}^6 \mid e = \mathbb{0}_6\}, \\ \mathcal{S}_p^{\text{flipped}} &= \left\{ p \in \mathbb{R}^6 \mid e = \begin{bmatrix} 0 & 0 & -b_{\text{diff}}^{\star\top} & b_{\text{diff}}^{\star\top} \end{bmatrix}^\top \right\}, \end{aligned} \quad (3.42)$$

with $e = [e_{12d} \quad e_{13d} \quad e_{12b}^\top \quad e_{13b}^\top]^\top \in \mathbb{R}^6$ and $b_{\text{diff}}^{\star} = g_{12}^{\star} - g_{13}^{\star}$.

Proof. Setting the LHS of each equation of the closed-loop dynamics (3.40) to the zero vector, we obtain for robot R2 that $-K_d e_{12d} z_{12} = \mathbb{0}_2 \iff e_{12d} = 0 \vee z_{12} = \mathbb{0}_2$

and similarly, we have $-K_d e_{13d} z_{13} = 0_2 \iff e_{13d} = 0 \vee z_{13} = 0_2$ for R3. The expression for R1 evaluates to $g_{12} + g_{13} = g_{12}^* + g_{13}^*$. Defining $\angle g_{12} = \alpha$, $\angle g_{13} = \beta$ as before, and recalling the RHS of (3.26), we can write the following set of constraints on the angles, namely

$$\begin{cases} \alpha + \beta = \alpha^* + \beta^* \\ \alpha - \beta = \alpha^* - \beta^* \end{cases} \iff \begin{cases} \alpha = \alpha^* \\ \beta = \beta^* \end{cases} \quad (3.43)$$

and

$$\begin{cases} \alpha + \beta = \alpha^* + \beta^* \\ -(\alpha - \beta) = \alpha^* - \beta^* \end{cases} \iff \begin{cases} \alpha = \beta^* \\ \beta = \alpha^* \end{cases}. \quad (3.44)$$

Equation (3.43) translates to $g_{12} = g_{12}^*$ and $g_{13} = g_{13}^*$ implying robot R1 satisfies its bearing tasks while (3.44) translates to the *flipped* formation shape with bearings satisfying $g_{12} = g_{13}^*$ and $g_{13} = g_{12}^*$. It follows the bearing error signals are $e_{12b} = -e_{13b} = -b_{\text{diff}}^*$. With both g_{12} and g_{13} defined, we obtain $d_{12} \neq 0$ and $d_{13} \neq 0$ and hence $z_{12} = 0_2$ and $z_{13} = 0_2$ are both not feasible. Robots R2 and R3 will stop moving when $e_{12d} = 0$ and $e_{13d} = 0$ holds, respectively, i.e., when they accomplished their individual distance task irrespective of R1. This completes the proof. \square

It can be verified that the signed area of the flipped formation satisfies $S_{A_F} = -S_A^*$.

3.6.2 Moving configurations

For the moving formations, we set the link dynamics to the zero vector and obtain the following result.

Proposition 3.14 ((1B2D) Moving Formations). *The moving formations for the (1B2D) setup occur when the robots are colinear, i.e., $g_{12} = \pm g_{13}$ and oriented in the direction of $b_{\text{sum}}^* = g_{12}^* + g_{13}^*$.*

Proof. The expression for the link z_{12} and z_{13} in (3.41) evaluates to

$$\begin{aligned} (K_d e_{12d} d_{12} + K_b) g_{12} + K_b g_{13} &= K_b b_{\text{sum}}^* \\ K_b g_{12} + (K_d e_{13d} d_{13} + K_b) g_{13} &= K_b b_{\text{sum}}^*. \end{aligned} \quad (3.45)$$

Solving for $\dot{z}_{23} = 0_2$, we obtain $e_{12d} d_{12} g_{12} = e_{13d} d_{13} g_{13}$. Two vectors are equal when they have the same magnitude and direction or opposite signs in both the magnitude and direction. Hence we distinguish the case $g_{12} = g_{13} \wedge e_{12d} d_{12} = e_{13d} d_{13}$ and $g_{12} = -g_{13} \wedge e_{12d} d_{12} = -e_{13d} d_{13}$. Since $g_{12} = \pm g_{13}$, we conclude the robots are colinear. Substituting in (3.45) yields expressions of the form $h g_{12} =$

$K_b d_{\text{sum}}^* g_{\text{sum}}^*$ where $h = K_d e_{12d} d_{12} + 2K_b$ when $g_{12} = g_{13}$ and $h = K_d e_{12d} d_{12}$ when $g_{12} = -g_{13}$. From this, we infer $g_{12} = \pm g_{\text{sum}}^*$, implying the orientation of the formation is in the direction of b_{sum}^* . This completes the proof. \square

In light of Proposition 3.14, we obtain *four* different ordering of the robots, as depicted in Fig. 3.2.

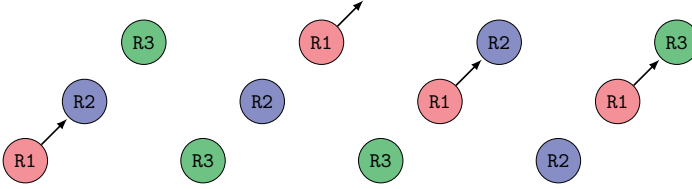


Figure 3.2: Different robot ordering for the moving configurations in the (1B2D) setup; the black arrow is the bearing vector g_{sum}^* . From left to right, we have the ordering I to IV. Despite the different colors, both R2 and R3 are distance robots.

To provide a full characterization of the moving configurations, it remains to obtain the inter-robot distances for the different ordering. We first derive expressions for the distance error signals corresponding to the different ordering from the general expression $h g_{12} = K_b d_{\text{sum}}^* g_{\text{sum}}^*$. Define $e_{12d} = \frac{s}{d_{12}} R_{\text{bd}}$ and $e_{13d} = \frac{t}{d_{13}} R_{\text{bd}}$. Table 3.2 provides the values for s and t corresponding to the different robot orderings depicted in Fig. 3.2.

Table 3.2: Values for variables s and t corresponding to the robot orderings in Fig. 3.2

Ordering	Direction	s	t
I:	$g_{12} = g_{13} = g_{\text{sum}}^*$	$-2 + d_{\text{sum}}^*$	$-2 + d_{\text{sum}}^*$
II:	$g_{12} = g_{13} = -g_{\text{sum}}^*$	$-2 - d_{\text{sum}}^*$	$-2 - d_{\text{sum}}^*$
III:	$g_{12} = -g_{13} = g_{\text{sum}}^*$	d_{sum}^*	$-d_{\text{sum}}^*$
IV:	$g_{12} = -g_{13} = -g_{\text{sum}}^*$	$-d_{\text{sum}}^*$	d_{sum}^*

When expanded, we obtain an instance of the cubic expression (2.2) with the coefficient $c = -d_{12}^*$ and $d = -s R_{\text{bd}}$ when solving for feasible distance d_{12} while coefficient $c = -d_{12}^*$ and $d = -t R_{\text{bd}}$ when we are considering distance d_{13} . Since $d_{\text{sum}}^* \in \{0, 2\}$, it follows the value for s and t can be positive or negative and hence also the coefficient d of the cubic equation. In turn, this may impose a condition on the desired distances d_{12}^* and d_{13}^* for obtaining positive values for d_{12} and d_{13} as discussed in Section 2.3. In particular, we can verify that coefficient d has range $d \in (-2, 4) R_{\text{bd}}$. Taking $d = 4R_{\text{bd}}$, we obtain that all four robot orderings in Fig. 3.2 can occur when the desired distances satisfy $d_{ij}^* \geq \sqrt[3]{3} \sqrt[3]{2R_{\text{bd}}}$.

In the next part, we will show that the colinear moving formations are unstable.

3.6.3 Local stability of equilibrium and moving configurations

We have characterized the equilibrium configurations and the moving configurations. It is of interest to study the local stability property of these different sets. Similar to the stability analysis for the (1D2B) setup, we will use Lyapunov's indirect method. The Jacobian matrix corresponding to the z -dynamics (3.41) is

$$A = - \begin{bmatrix} K_b A_{12b} + K_d A_{12d} & K_b A_{13b} \\ K_b A_{12b} & K_b A_{13b} + K_d A_{13d} \end{bmatrix}, \quad (3.46)$$

where, as before, $A_{ijd} = e_{ijd} I_2 + 2z_{ij} z_{ij}^\top$ and $A_{ijb} = \frac{1}{d_{ij}} (I_2 - g_{ij} g_{ij}^\top)$, $ij \in \{12, 13\}$.

We obtain the following result for the equilibrium configurations in (3.42).

Lemma 3.15. *The Jacobian matrix A_E at the equilibrium configurations in $\mathcal{S}_p^{\text{correct}} \cup \mathcal{S}_p^{\text{flipped}}$ is Hurwitz.*

Proof. For the correct and desired equilibrium configurations in $\mathcal{S}_p^{\text{correct}}$, the Jacobian matrix (3.46) evaluates to

$$A_E^{\text{correct}} = -\mathbf{diag}([x^* \quad x^* \quad p^* \quad p^*]) - \begin{bmatrix} (y^* - x^*) a^2 & (y^* - x^*) ab & p^* d^2 & -p^* cd \\ (y^* - x^*) ab & (y^* - x^*) b^2 & -p^* cd & p^* c^2 \\ x^* b^2 & -x^* ab & (q^* - p^*) c^2 & (q^* - p^*) cd \\ -x^* ab & x^* a^2 & (q^* - p^*) cd & (q^* - p^*) d^2 \end{bmatrix}, \quad (3.47)$$

where x, y, p, q and the bearing matrices are previously defined in (3.29) and (3.30). Also, for the flipped equilibrium configurations in $\mathcal{S}_p^{\text{flipped}}$, we obtain

$$A_E^{\text{flipped}} = -\mathbf{diag}([x^* \quad x^* \quad p^* \quad p^*]) - \begin{bmatrix} (y^* - x^*) c^2 & (y^* - x^*) cd & p^* b^2 & -p^* ab \\ (y^* - x^*) cd & (y^* - x^*) d^2 & -p^* ab & p^* a^2 \\ x^* d^2 & -x^* cd & (q^* - p^*) a^2 & (q^* - p^*) ab \\ -x^* cd & x^* c^2 & (q^* - p^*) ab & (q^* - p^*) b^2 \end{bmatrix}. \quad (3.48)$$

The characteristic polynomial $\chi_E(\lambda)$ corresponding to the Jacobian matrices A_E^{correct} and A_E^{flipped} is the same, namely

$$\chi_E(\lambda) = (\lambda + q^*)(\lambda + y^*)(\lambda^2 + (p^* + x^*)\lambda + p^* x^* \sin^2 \theta^*). \quad (3.49)$$

The roots of (3.49) are

$$\begin{aligned}\lambda_1 &= -q^*, & \lambda_2 &= -y^*, \\ \lambda_{3,4} &= -\frac{1}{2}(p^* + x^*) \pm \frac{1}{2}\sqrt{(p^* + x^*)^2 - 4p^*x^*\sin^2\theta^*}\end{aligned}\quad (3.50)$$

We can verify that $0 < 4p^*x^*\sin^2\theta^* \leq (p^* + x^*)^2$. This implies that all λ s are real. Also, $-(p^* + x^*) + \sqrt{(p^* + x^*)^2 - 4p^*x^*\sin^2\theta^*} < 0$, and hence we conclude that all roots are negative real. This completes the proof. \square

This leads to the following main result:

Theorem 3.16. *Consider a team of three robots arranged in the (1B2D) setup with closed-loop dynamics given by (3.40). Given an initial configuration $p(0)$ that is close to the desired formation shape, then the robot trajectories asymptotically converge to a point $\hat{p} \in \mathcal{S}_p^{\text{correct}}$.*

Proof. Following Lemma 3.15, we obtain that link trajectories locally asymptotically converge to the desired relative positions z^* when they are initialized in the neighborhood of it. With $z_{ij}^* = d_{ij}^* g_{ij}^*$, it follows that also the robots converge to a point $\hat{p} \in \mathcal{S}_p^{\text{correct}}$. This completes the proof. \square

Employing Lyapunov's indirect method to the moving colinear formations yields the following statement.

Theorem 3.17. *Let $p \in \mathbb{R}^6$ be a configuration yielding a colinear formation satisfying conditions in Table 3.2. Then the configuration p is unstable.*

Proof. We first obtain the matrix A_M and the corresponding characteristic polynomial $\chi_M(\lambda)$. The sub-matrices for the Jacobian matrix (3.46) are $A_{12d} = R_{\text{bd}} \frac{s}{d_{12}} I_2 + 2d_{12}^2 g_{\text{sum}}^* g_{\text{sum}}^{*\top}$, $A_{13d} = R_{\text{bd}} \frac{t}{d_{13}} I_2 + 2d_{13}^2 g_{\text{sum}}^* g_{\text{sum}}^{*\top}$, $A_{12b} = \frac{1}{d_{12}} (I_2 - g_{\text{sum}}^* g_{\text{sum}}^{*\top})$, and $A_{13b} = \frac{1}{d_{13}} (I_2 - g_{\text{sum}}^* g_{\text{sum}}^{*\top})$ with the bearing matrix $g_{\text{sum}}^* g_{\text{sum}}^{*\top} = \begin{bmatrix} k^2 & kl \\ kl & l^2 \end{bmatrix}$. The values for s and t depend on the considered ordering in Table 3.2. Hence, A_M takes the form

$$\begin{aligned}A_M &= -(\text{diag}([(s+1)x \quad (t+1)p]) \otimes I_2) - \\ &\quad \begin{bmatrix} (y-x)k^2 & (y-x)kl & pl^2 & -pkl \\ (y-x)kl & (y-x)l^2 & -pkl & pk^2 \\ xl^2 & -xkl & (q-p)k^2 & (q-p)kl \\ -xkl & xk^2 & (q-p)kl & (q-p)l^2 \end{bmatrix},\end{aligned}\quad (3.51)$$

where the variables x , y , p , and q are defined in (3.29). The characteristic polynomial $\chi_M(\lambda)$ corresponding to matrix A_M is found to be

$$\chi_M(\lambda) = (\lambda + pt + q)(\lambda + xs + y)(\lambda^2 + \mathbb{B}\lambda + \mathbb{C}), \quad (3.52)$$

where $\mathbb{B} = p(t+1) + x(s+1)$ and $\mathbb{C} = px((t+1)(s+1) - 1)$. We explore the nature of the roots, hereby focusing on the coefficients of the quadratic polynomial. Table 3.3 presents the values for \mathbb{B} and \mathbb{C} corresponding to the different robot ordering; the sign of the coefficient is also provided when it can be determined.

Table 3.3: Values for coefficients \mathbb{B} and \mathbb{C} corresponding to the robot orderings in Fig. 3.2

Ordering	\mathbb{B}	\mathbb{C}
I:	$(p+x)(-1+d_{\text{sum}}^*)$	$px \left((-1+d_{\text{sum}}^*)^2 - 1 \right) < 0$
II:	$(p+x)(-1-d_{\text{sum}}^*) < 0$	$px \left((-1-d_{\text{sum}}^*)^2 - 1 \right)$
III:	$(p+x) + (x-p)d_{\text{sum}}^*$	$-(d_{\text{sum}}^*)^2 px < 0$
IV:	$(p+x) - (x-p)d_{\text{sum}}^*$	$-(d_{\text{sum}}^*)^2 px < 0$

By Lemma 3.18, we infer that the quadratic polynomial in (3.52) contains at least a root with positive real part since for each ordering, either coefficient \mathbb{B} or \mathbb{C} is negative. This implies the matrix A_M is not Hurwitz; the colinear formations are unstable. This completes the proof. \square

3.7 Numerical Example

We consider two triangular formation shapes with the same distances d_{12}^* and d_{13}^* but different value for the internal angle θ^* (Note: $\theta^* = \cos^{-1}(g_{12}^{*\top} g_{13}^*)$). In particular, shape \mathbf{T}_1 has bearing vectors such that the internal angle is $\theta_{\mathbf{T}_1}^* = 15^\circ$ while for shape \mathbf{T}_2 , we take $\theta_{\mathbf{T}_2}^* = 45^\circ$. We set the gain ratio R_{bd} to a value 4. Taking the different setups into consideration, the threshold distance such that moving formations (stable or unstable) exist is $\hat{d} = 2\sqrt{3} \approx 3.4641$. We set the desired distances to $d_{12}^* = d_{13}^* = 4$ and assume $\angle g_{12}^* = 0^\circ$. Thus, shape \mathbf{T}_1 and \mathbf{T}_2 has the following desired constraints:

$$\begin{aligned} \mathbf{T}_1 : d_{12}^* = d_{13}^* = 4; \angle g_{12}^* = 0^\circ, \angle g_{13}^* = 15^\circ; \\ \mathbf{T}_2 : d_{12}^* = d_{13}^* = 4; \angle g_{12}^* = 0^\circ, \angle g_{13}^* = 45^\circ. \end{aligned} \quad (3.53)$$

For shape \mathbf{T}_1 , the moving formation for the (1D2B) setup is unstable, since $\cos^2(15^\circ) = 0.9330 > 0.9321$. Hence the constraint in (3.36) is violated. For shape \mathbf{T}_2 , we obtain $\cos^2(45^\circ) = 0.5 < 0.9321$ satisfying constraint (3.36).

We remark that when desired distance constraints are provided, we can also modify the control gains K_d for the distance robot(s) and K_b for the bearing robot(s) such that the desired distances satisfy $d_{ij}^* < \hat{d}$. This prevents the occurrence of (stable or unstable) moving configurations. In the current example, we

intentionally set the gain ratio R_{bd} first and then obtain desired distances d_{ij}^* s in order to show the existence and local asymptotic stability of the moving formations in the (1D2B) setup.

3.7.1 (1D2B) Simulation results

For the three robots in the (1D2B) setup, we focus on the formation shape \mathbf{T}_2 . The Jacobian matrix A_M for the moving formation with distances $d_{12} = d_{13} \approx 3.8686$ is checked to be Hurwitz. Indeed, all values of the first column in the Routh-Hurwitz table (3.37) evaluates to a positive value. Therefore, employing the closed-loop dynamics (3.17) can, depending on the initial configuration $p(0)$, lead to robot trajectories moving with a constant velocity. In Fig. 3.3(b), we show such an outcome for a specific initial configuration $p(0)$. Fig. 3.3(a) depicts an initial configuration $p(0)$ leading to convergence to the correct shape.

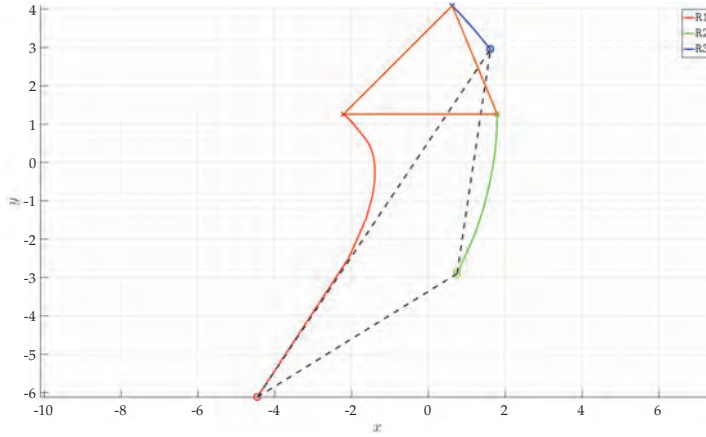
3.7.2 (1B2D) Simulation results

For the three robots in the (1B2D) setup, we focus on the formation shape \mathbf{T}_1 . Recall that for the (1B2D) robot setup, there are two equilibrium formations, namely the correct and desired formation and the flipped formation satisfying only the distance constraints but not the bearing constraints. Fig. 3.4(a) depicts an initial configuration $p(0)$ which converges to this flipped formation. Notice that the signed area corresponding to $p(0)$ is positive (counter-clockwise cyclic ordering of the robots) while the flipped formation has a negative signed area (clockwise cyclic ordering of the robots). Fig. 3.4(b) depicts an initial colinear configuration $p(0)$ leading to robots to move with a constant velocity when employing the closed-loop dynamics (3.40). If the colinear configuration is perturbed, it will converge either to the correct or the flipped formation shape.

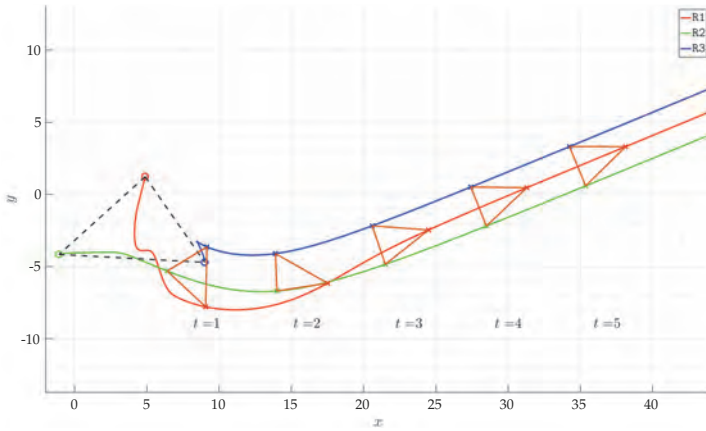
3.8 Full Characterization of the Local Stability of Moving Configurations for the (1D2B) Robot Setup

In Lemma 3.11, we considered only one of four possible combinations (d_{12_M}, d_{13_M}) for the scenario $d_{12}^* > \hat{d}$ and $d_{13}^* > \hat{d}$. Referring to Table 3.1, we can have in total nine¹ possible combinations (d_{12_M}, d_{13_M}) when all the different scenarios are considered. Here, we provide the local stability analysis of the moving formations for the (1D2B) setup for all the remaining combinations and scenarios.

¹In Lemma 3.11, we define the variables m and n . Since they can take values $m \gtrless 0$ and $n \gtrless 0$, we arrive also to the number nine.



(a) Correct Formation



(b) Moving Formation

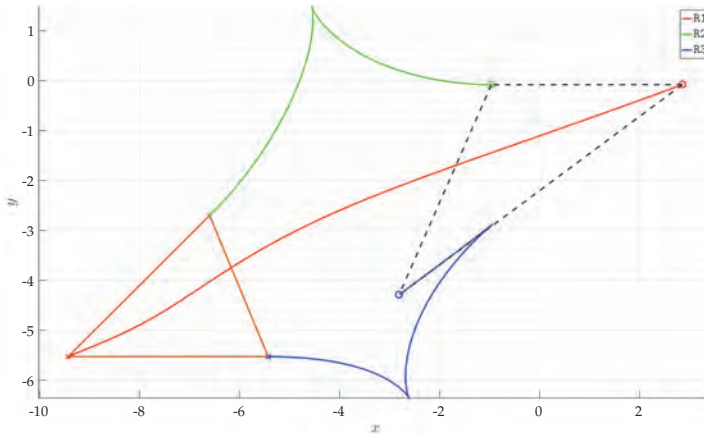
Figure 3.3: Robot trajectories for the (1D2B) setup; \circ represents the initial position and \times is the final position of the robot. On the top panel, we have an initial configuration (connected by dashed lines) where robots converge to the correct formation shape (connected by solid lines) while the bottom panel illustrates an initial configuration where robots converge to the moving configuration with velocity $w = K_b b_{sum}$.

To this end, we first give the following auxiliary result that connects the sign of the coefficients of a polynomial of degree n to its roots.

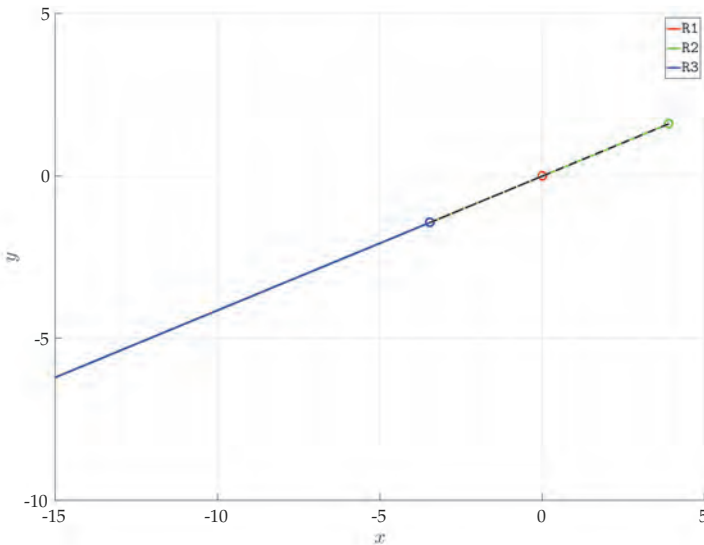
Lemma 3.18. Consider a polynomial of degree n

$$f(y) = y^n + c_1 y^{n-1} + \dots + c_n. \quad (3.54)$$

Suppose the (distinct) roots of the equation $f(y) = 0$ are α_i , $i = 1, \dots, n$. Then the



(a) Flipped Formation



(b) Moving Formation

Figure 3.4: Robot trajectories for the (1B2D) setup; \circ represents the initial position and \times is the final position of the robot. On the top panel, we have an initial configuration (connected by dashed lines) where robots move and converge to the flipped formation shape while the bottom panel illustrates the evolution of the robots when the initial configuration satisfy conditions for ordering III in Table 3.3. The robots move with velocity $w = -K_b b_{\text{sum}}$. If the robots have slightly different initial positions, we will have convergence to an equilibrium configuration since these colinear moving configurations are unstable.

factored form of $f(y)$ is

$$f(y) = (y - \alpha_1)(y - \alpha_2) \cdots (y - \alpha_n), \quad (3.55)$$

and the sum and product of the roots α_i s are related to the coefficients c_1 and c_n as $\sum_{i=1}^n \alpha_i = -c_1$ and $\prod_{i=1}^n \alpha_i = (-1)^n c_n$, respectively. Furthermore, there exists at least a positive real root or a pair of complex roots with positive real part when the coefficient c_1 is negative while an odd number of positive real roots exists when the coefficient c_n is negative.

The proof of Lemma 3.18 is straightforward and therefore omitted.

Proposition 3.19. Consider the desired distance satisfies $d_{ij}^* \geq \hat{d}$ with $\hat{d} = \sqrt[3]{3} \sqrt[3]{\frac{R_{bd}}{2}}$ and let d_{ij} be a feasible solution to the cubic equation (3.25). Define the variable $h(d_{ij}) = 2K_d d_{ij}^2 - K_b \frac{1}{d_{ij}}$. Then,

- $h(d_{ij}) = 0$ when $d_{ij}^* = \hat{d}$;
- $h(d_{ij}) \geq 0$ when $d_{ij}^* > \hat{d} \wedge d_{ij} = y_{p_1}(d_{ij}^*)$ in Lemma 2.2.
- $h(d_{ij}) > 0$ when $d_{ij}^* > \hat{d} \wedge d_{ij} = y_{p_2}(d_{ij}^*)$ in Lemma 2.2;

Proof. The expression $h(d_{ij}) \geq 0$ is equivalent to $d_{ij} \geq \sqrt[3]{\frac{R_{bd}}{2}} = \frac{1}{3}\sqrt{3}\hat{d}$. When $d_{ij}^* = \hat{d}$, we obtain that $d_{ij} = \frac{1}{3}\sqrt{3}\hat{d}$, resulting in the term $h(d_{ij}) = 0$. For $d_{ij}^* > \hat{d}$, Lemma 2.2 provides two feasible distances satisfying the cubic equation (3.25). The ranges of the two feasible distances are $y_{p_1} \in (0, \frac{1}{3}\sqrt{3})d_{ij}^*$ and $y_{p_2} \in (\frac{1}{3}\sqrt{3}, 1)d_{ij}^*$. Since $d_{ij}^* > \hat{d}$, we obtain $y_{p_2} > \frac{1}{3}\sqrt{3}d_{ij}^* > \frac{1}{3}\sqrt{3}\hat{d}$, and therefore $h(y_{p_2}) > 0$. For the feasible distance y_{p_1} , we have $y_{p_1} < \frac{1}{3}\sqrt{3}d_{ij}^*$. It also satisfies $y_{p_1} \geq \frac{1}{3}\sqrt{3}\hat{d}$ and consequently, $h(y_{p_1}) \geq 0$. This completes the proof. \square

Following Proposition 3.19, we define the variables $m := h(d_{12}) = y - x$ and $n := h(d_{13}) = q - p$ in the characteristic polynomial $\chi_M(\lambda)$ (3.34). The case $m > 0$ and $n > 0$ has already been considered in Lemma 3.11.

We are ready to consider the remaining combinations of m and n . First, we assume the bearing vectors g_{12}^* and g_{13}^* are not perpendicular. This is equivalent to $0 < \sin^2 \theta^* < 1$. Table 3.4 provides the sign of the coefficients of $\chi_M(\lambda)$ in (3.35).

Applying Lemma 3.18, we obtain that $\chi_M(\lambda)$ contains at least a root with positive real part for each combination of m and n in Table 3.4. This in turn implies the Jacobian matrix A_M in (3.33) is not Hurwitz, and hence the moving formations are unstable.

We proceed with the case in which $\sin^2 \theta^* = 1$, i.e., the bearing vectors satisfy $g_{12}^* \perp g_{13}^*$. Again, we determine the sign of the coefficients for each combination of m and n ; see Table 3.5.

Applying Lemma 3.18, we obtain that $\chi_M(\lambda)$ contains at least a root with positive real part for all combination of m and n in Table 3.5, except for the cases $(m, n) = \{(0, 0), (> 0, 0), (0, > 0)\}$. Further investigation reveals that for the case $(m, n) = (0, 0)$, we obtain the root $\lambda = 0$ with multiplicity 4 while

Table 3.4: Sign of the coefficients corresponding to the characteristic polynomial $\chi_M(\lambda)$ in (3.35) for $0 < \sin^2 \theta^* < 1$; The ζ symbol means that the sign is indeterminate.

	c_1	c_2	c_3	c_4
$m < 0 \wedge n < 0$	< 0	< 0	> 0	> 0
$m < 0 \wedge n = 0$	< 0	< 0	> 0	$= 0$
$m < 0 \wedge n > 0$	ζ	ζ	ζ	< 0
$m = 0 \wedge n < 0$	< 0	< 0	> 0	$= 0$
$m = 0 \wedge n = 0$	$= 0$	< 0	$= 0$	$= 0$
$m = 0 \wedge n > 0$	> 0	ζ	< 0	$= 0$
$m > 0 \wedge n < 0$	ζ	ζ	ζ	< 0
$m > 0 \wedge n = 0$	> 0	ζ	< 0	$= 0$

Table 3.5: Sign of the coefficients corresponding to the characteristic polynomial $\chi_M(\lambda)$ in (3.35) for $\sin^2 \theta^* = 1$; The ζ symbol means that the sign is indeterminate.

	c_1	c_2	c_3	c_4
$m < 0 \wedge n < 0$	< 0	< 0	> 0	> 0
$m < 0 \wedge n = 0$	< 0	< 0	$= 0$	$= 0$
$m < 0 \wedge n > 0$	ζ	ζ	< 0	< 0
$m = 0 \wedge n < 0$	< 0	< 0	$= 0$	$= 0$
$m = 0 \wedge n = 0$	$= 0$	$= 0$	$= 0$	$= 0$
$m = 0 \wedge n > 0$	> 0	> 0	$= 0$	$= 0$
$m > 0 \wedge n < 0$	ζ	ζ	< 0	< 0
$m > 0 \wedge n = 0$	> 0	> 0	$= 0$	$= 0$

for $(m, n) = \{(> 0, 0), (0, > 0)\}$, the roots to $\chi_M(\lambda)$ are $\lambda_{1,2} = 0$ and $\lambda_{3,4} = \frac{1}{2}(-c_1 \pm \sqrt{c_1^2 - 4c_2})$. Since both $c_1 > 0$ and $c_2 > 0$, we obtain $\sqrt{c_1^2 - 4c_2} < c_1$, and hence $\lambda_{3,4}$ are negative real roots or are roots containing a negative real part. For these specific cases, the Jacobian matrix A_M in (3.33) cannot provide any conclusion on the local stability while for the cases containing a root with positive real part, we conclude those moving formations are unstable. It should be remarked that the case $(m, n) = (0, 0)$ corresponds to the scenario when $d_{12}^* = d_{13}^* = \hat{d}$, $(m, n) = (> 0, 0)$ corresponds to $d_{12}^* > \hat{d}$ and $d_{13}^* = \hat{d}$, and $(m, n) = (0, > 0)$ corresponds to $d_{12}^* = \hat{d}$ and $d_{13}^* > \hat{d}$. In particular, the scenario of $d_{12}^* = d_{13}^* = \hat{d}$ is very specific.

3.9 Conclusions

We have considered the formation shape problem for teams of two and three robots partitioned into two categories, namely distance and bearing robots. Our

aim is to employ gradient-based control laws in a heterogeneous setting and provide a systematic study on the stability of the possible formation shapes that arise as a result. We have shown that under certain conditions on the distance and bearing error signals, we obtain distorted formation shapes moving with a constant velocity w . For the **(1D1B)** and the **(1B2D)** robot setup, these undesired formation shapes are unstable while for the **(1D2B)** robot setup, we derive conditions such that the distorted moving formation shape is locally asymptotically stable. Furthermore, by increasing the value for the gain ratio $R_{bd} = \frac{K_b}{K_d}$, the occurrence of distorted moving formation shapes can be postponed. This may lead to global asymptotic stability of the desired formation shape, depending on the setup considered. We note that the moving configurations in the **(1D2B)** setup and the flipped equilibrium configuration in the **(1B2D)** setup both have a signed area that has an opposite sign compared to the signed area of the desired formation shape.

In the next chapter, we will focus exclusively on the **(1D2B)** setup and introduce an additional signed area constraint for the distance robot. This is done as an attempt to avoid the occurrence of moving formations.

Chapter 4

Securing Isosceles Triangular Formations under Heterogeneous Sensing and Mixed Constraints

In the previous chapter, we obtained that for the **(1D2B)** setup, the incorrect moving formation shape is locally attractive. By including an additional control term that accounts for the signed area, we aim to prevent the occurrence of the incorrect moving formation shapes.

We start this chapter with an introduction and provide some background material in Section 4.2. The **(1D2B)** setup with the added signed area constraint is considered in Section 4.3. We provide preliminary analysis for the specific case of isosceles triangles in Section 4.4. The details for acute isosceles triangles and right and obtuse isosceles triangles are found in Sections 4.5 and 4.6, respectively. The theoretical claims are supported by numerical results in Section 4.7 and we end with the conclusion in Section 4.8.

4.1 Introduction

IN formation control, triangular formations consisting of three autonomous agents serve as a class of benchmarks that can be used to test and compare the performances of different controllers. This apparently simple setup allows detailed rigorous analysis for novel techniques and methodologies as we aim at in this chapter (see [5, 13, 14, 20, 32, 36]), and therefore, it provides a starting point in order to achieve more general formations.

Previously, in Chapter 3, we dealt with the formation control problem in which the team of mobile robots were partitioned in two categories, namely distance robots carrying out distance tasks and bearing robots fulfilling bearing constraints. For the particular case of one distance and two bearing robots, the **(1D2B)** setup, we showed the existence of moving configurations which are locally attractive under certain conditions. One observation on the moving configurations is that the signed area of the corresponding shape has an opposite sign when compared with the desired formation shape; the robots converge to an *incorrect* shape.

In the current chapter, we aim to avoid the occurrence of moving configurations by adding a signed area constraint to the distance robot. We remark that this does

not increase the sensing load on the robot. For the current analysis, we consider isosceles triangles as the desired formation shape. Our main contribution is the identification of bounds on the gain ratio R_{Ad} between the signed area and the distance control term which yields the team of robots to always evolve to the correct isosceles triangular shape.

4.2 Robot Configurations & Signed Area

We briefly consider different configurations of three mobile robots and introduce the signed area of a triangle.

4.2.1 Robot configurations

We consider a team of three robots with R_i as the label for robot i . The robots are moving in the plane \mathbb{R}^2 according to the single integrator dynamics, i.e.,

$$\dot{p}_i(t) = u_i(t), \quad i \in \{1, 2, 3\}, \quad (4.1)$$

where $p_i \in \mathbb{R}^2$ (a point in the plane) and $u_i \in \mathbb{R}^2$ represent the position of and the control input for R_i , respectively. The vector $p = [p_1^\top \ p_2^\top \ p_3^\top]^\top \in \mathbb{R}^6$ represents the *team configuration*. We define p_{ref} as the *reference configuration* where the three positions describe a particular triangle T of interest up to translation. Therefore, the set of *desired configurations* can be formally written from p_{ref} as

$$\mathcal{S}_p := \{p \in \mathbb{R}^6 \mid p = p_{\text{ref}} + (\mathbb{1}_3 \otimes v), v \in \mathbb{R}^2\}, \quad (4.2)$$

where v is a translation vector and \otimes denotes the Kronecker product. Note that the desired configurations can also be described in terms of relative positions (or links) z_{ij} s with $z_{ij} = p_j - p_i \in \mathbb{R}^2$. In particular, it is the singleton \mathcal{S}_z whose one element is

$$z_{\text{ref}} = (H \otimes I_2) p_{\text{ref}}, \quad H = \begin{bmatrix} -1 & 1 & 0 \\ -1 & 0 & 1 \\ 0 & -1 & 1 \end{bmatrix} \quad (4.3)$$

where I_2 is the identity matrix.

Consider the link vector $z(t) := (H \otimes I_2) p(t)$ converging to a point $\tilde{z} \in \mathbb{R}^6$ and $\dot{p}(t) \rightarrow (\mathbb{1}_3 \otimes w)$ as time progresses, where $w \in \mathbb{R}^2$ denotes a constant velocity vector. Let $\tilde{p} \in \mathbb{R}^6$ denotes a configuration yielding \tilde{z} . Then, the team trajectory converges to $p_{\text{traj}}(t) = (\mathbb{1}_3 \otimes c_0) + \tilde{p} + (\mathbb{1}_3 \otimes w)t$, where $c_0 \in \mathbb{R}^2$ is an arbitrary offset given by the initial condition $p(0)$. We have an *equilibrium configuration* when $w = \mathbb{0}_2$, and otherwise, the configuration is *moving*. In the latter case,

$p_{\text{traj}}(t) \rightarrow \infty$ as $t \rightarrow \infty$. Depending on whether $\tilde{z} \in \mathcal{S}_z$ or not, we classify the obtained configuration \tilde{p} as *desired* or *incorrect*.

4.2.2 Signed area of a triangle

For a triangle T with points p_1, p_2 , and p_3 in \mathbb{R}^2 , the *signed area* A is given by

$$A = \frac{1}{2} \mathbf{det} \left(\begin{bmatrix} 1 & 1 & 1 \\ p_1 & p_2 & p_3 \end{bmatrix} \right), \quad (4.4)$$

where $\mathbf{det}(\bullet)$ denotes the determinant of a matrix. Alternative expressions for A are $A = \frac{1}{2} z_{12}^\top J z_{13}$ or $A = \frac{1}{2} \sin \theta_{213} d_{12} d_{13}$ with $\sin \theta_{213} = g_{12}^\top J g_{13}$ and θ_{213} being the *signed angle* enclosed by the bearing vectors g_{12} and g_{13} at point p_1 . Assuming $\angle g_{12} = \alpha$ and $\angle g_{13} = \beta$ with respect to a coordinate frame Σ , it follows that $\sin \theta_{213} = \sin(\beta - \alpha)$. Hence for a counter-clockwise (or clockwise) ordering of points p_1, p_2 , and p_3 , we obtain $\theta_{213} > 0$ and $A > 0$ (or $\theta_{213} < 0$ and $A < 0$).

4.3 The (1D2B) Robot Setup with a Signed Area Constraint

Recall the closed-loop dynamics corresponding to the (1D2B) setup from Chapter 3 is

$$\begin{bmatrix} \dot{p}_1 \\ \dot{p}_2 \\ \dot{p}_3 \end{bmatrix} = \begin{bmatrix} K_d u_{12d} + K_d u_{13d} \\ K_b u_{21b} \\ K_b u_{31b} \end{bmatrix}, \quad (4.5)$$

where $K_d > 0$ and $K_b > 0$ are the gains for the distance and bearing control terms. The *distance control terms* are of the form $u_{ijd} = e_{ijd} z_{ij}$ with the *distance error signal* $e_{ijd} = d_{ij}^2 - (d_{ij}^*)^2$. These are gradient-based control laws obtained from the *distance potential function* $V_{ijd}(e_{ijd}) = \frac{1}{4} e_{ijd}^2$. Similarly, the *bearing control terms* are gradient-based control laws obtained from the *bearing potential function* $V_{ijb}(e_{ijb}) = \frac{1}{2} d_{ij} \|e_{ijb}\|^2$ and are of the form $u_{ijb} = e_{ijb}$ with the *bearing error signal* $e_{ijb} = g_{ij} - g_{ij}^*$. The following findings are reported in the previous chapter on the stability analysis of the closed-loop system (4.5):

1. The equilibrium configurations are the desired configurations in which the error vector is zero; furthermore, they are locally asymptotically stable.
2. The moving configurations occur when the desired distances satisfy $d_{12}^* \geq \hat{d}$ and $d_{13}^* \geq \hat{d}$ with $\hat{d} = \sqrt{3} \sqrt[3]{\frac{R_{bd}}{2}}$ and gain ratio $R_{bd} = \frac{K_b}{K_d}$. The error vector is

of the form

$$\begin{bmatrix} e_{12d} & e_{13d} & e_{12b} & e_{13b} \end{bmatrix} = - \begin{bmatrix} \frac{1}{d_{12}} R_{bd} & \frac{1}{d_{13}} R_{bd} & g_{12}^* + g_{13}^* & g_{12}^* + g_{13}^* \end{bmatrix}, \quad (4.6)$$

and the steady-state translation velocity is $w = K_b g_{12}^* + g_{13}^*$. It is remarked that these moving configurations have a signed area which is opposite in sign to that of the correct shape. When a condition on $\cos \theta^*$ is satisfied, we obtain that the linearization matrix has eigenvalues with negative real parts and hence the moving configurations are locally asymptotically stable.

4.3.1 Adding a signed area constraint to R1

In the works [3, 15, 44, 45], it has been shown that the inclusion of a *signed area constraint* with a proper gain for the resulting control term avoids the occurrence of flipped formations. Since the moving configurations have a signed area which is opposite to that of the correct formation shape, it can be classified as a flipped formation. Hence in the current work, we require R1 to additionally fulfill a signed area constraint A^* involving R2 and R3. This serves as a strategy to avoid flipped formations, and therefore also the moving configurations.

Recall the expression for the signed area is $A = \frac{1}{2} z_{12}^\top J z_{13}$ with J being a rotation matrix. R1 is able to compute this quantity with the available local information. For obtaining the control law, we define the *signed area error signal* as $e_A = A - A^*$. The *signed area potential function* is taken as $V_A(e_A) = e_A^2$. Since R1 will be responsible for the signed area constraint, taking the derivative of V_A with respect to p_1 yields $\frac{\partial}{\partial p_1} V_A = e_A (z_{13} - z_{12})^\top J$. The gradient-based control law for the signed area task is then $u_A = e_A J (z_{13} - z_{12})$.

4.3.2 The (1D2B) robot setup with signed area control term

Adding the control term u_A to R1 in (4.5) results in

$$\begin{bmatrix} \dot{p}_1 \\ \dot{p}_2 \\ \dot{p}_3 \end{bmatrix} = \begin{bmatrix} K_d u_{12d} + K_d u_{13d} + K_A u_A \\ K_b u_{21b} \\ K_b u_{31b} \end{bmatrix}. \quad (4.7)$$

The control gain for the area task is $K_A > 0$ and has dimension $[\text{L}]^{-2} [\text{T}]^{-1}$. Relative to the global coordinate system Σ^g , we have $u_{12b} = -u_{21b}$ and $u_{13b} = -u_{31b}$. The link dynamics corresponding to (4.7) is obtained as

$$\begin{bmatrix} \dot{z}_{12} \\ \dot{z}_{13} \\ \dot{z}_{23} \end{bmatrix} = - \begin{bmatrix} K_b u_{12b} + K_d u_{12d} + K_d u_{13d} + K_A u_A \\ K_b u_{13b} + K_d u_{12d} + K_d u_{13d} + K_A u_A \\ K_b (u_{13b} - u_{12b}) \end{bmatrix}. \quad (4.8)$$

In the remainder of this chapter, we investigate the effect of adding the signed area control term u_A to the closed-loop system (4.5). In particular,

1. we aim to preclude moving configurations by including u_A and a proper tuning of the associated gain K_A in relation to other gains, and
2. as including u_A may introduce other undesired (moving) configurations, we also aim to provide conditions which prevent these possible undesired configurations to occur.

We note that the configurations \hat{p} yielding the collective error variable $e = [e_{12d} \ e_{13d} \ e_A \ e_{12b}^\top \ e_{13b}^\top]^\top \in \mathbb{R}^7$ to be the zero vector are in the set \mathcal{S}_p , i.e., another characterization of the set of desired configurations in terms of the error vector e is $\mathcal{S}_p = \{p \in \mathbb{R}^6 \mid e = 0_7\}$.

To provide answers to the above determined goals, we are required to solve the following vector equation for the distance pair (d_{12}, d_{13}) .

Proposition 4.1. *Consider a team of three robots moving according to (4.7). Define the gain ratios $R_{bd} = \frac{K_b}{K_d} > 0$ and $R_{Ad} = \frac{K_A}{K_d} > 0$. Then for the equilibrium and moving configurations, the feasible distance pairs (d_{12}, d_{13}) are solutions to the vector equation*

$$ag_{12}^* + bg_{13}^* = cg_{12}^{*\perp} + dg_{13}^{*\perp}, \quad (4.9)$$

where the coefficients $a, b, c,$ and d are

$$\begin{aligned} a &= e_{12d}d_{12}, & b &= e_{13d}d_{13}, \\ c &= -R_{Ad}e_A d_{12}, & d &= R_{Ad}e_A d_{13} \end{aligned} \quad (4.10)$$

for equilibrium configurations and

$$\begin{aligned} a &= e_{13d}d_{13} + R_{bd}, & b &= e_{12d}d_{12} + R_{bd}, \\ c &= R_{Ad}e_A d_{13}, & d &= -R_{Ad}e_A d_{12} \end{aligned} \quad (4.11)$$

when considering moving configurations.

Proof. First, we consider equilibrium configurations for which $\dot{p} = 0_6$. From the dynamics for the bearing robots R2 and R3, we immediately obtain $e_{12b} = 0_2$ and $e_{13b} = 0_2$; the bearing constraints are attained. In addition, we have $d_{12} \neq 0$ and $d_{13} \neq 0$. Substituting the correct bearing vectors $g_{12} = g_{12}^*$ and $g_{13} = g_{13}^*$ in the dynamics of R1 and rearranging the terms result in (4.9) with coefficients in (4.10). Next, we consider moving configurations. For this, we focus on the equilibrium points of the link dynamics (4.8) since $\dot{p}_i = \dot{p}_j = w \implies \dot{z}_{ij} = 0_2$. We have already considered the case $w = 0_2$, so our focus will be on $w \neq 0_2$. Setting $\dot{z}_{23} = 0_2$ leads to $g_{12} - g_{13} = g_{12}^* - g_{13}^*$. The possible solutions are found to be the combinations

$(g_{12}, g_{13}) = (g_{12}^*, g_{13}^*)$ and $(g_{12}, g_{13}) = (-g_{13}^*, -g_{12}^*)$. The former corresponds to equilibrium configurations, so $w = \mathbb{0}_2$. The latter results in the bearing error signal $e_{12b} = e_{13b} = -(g_{12}^* + g_{13}^*)$. Substituting the obtained bearing error signal in (4.8) and rearranging terms, we obtain (4.9) with coefficients provided in (4.11). Since the bearing vectors are already known, provided R_{Ad} and R_{bd} are given, the coefficients $\{a, b, c, d\}$ in (4.10) and (4.11) depend solely on the distances d_{12} and d_{13} . This completes the proof. \square

Note that pre-multiplying (4.9) by a rotation matrix Q with angle ξ has no effect on the coefficients $\{a, b, c, d\}$. Hence without loss of generality, we take

$$g_{12}^* = \begin{bmatrix} 1 \\ 0 \end{bmatrix}, g_{13}^* = \begin{bmatrix} \cos \theta^* \\ \sin \theta^* \end{bmatrix}, g_{12}^{*\perp} = \begin{bmatrix} 0 \\ 1 \end{bmatrix}, g_{13}^{*\perp} = \begin{bmatrix} -\sin \theta^* \\ \cos \theta^* \end{bmatrix}. \quad (4.12)$$

This corresponds to $\angle g_{12}^* = 0^\circ$, $\angle g_{13}^* = \theta^*$, $\angle g_{12}^{*\perp} = 90^\circ$, and $\angle g_{13}^{*\perp} = 90^\circ + \theta^*$, where θ^* is the *desired inner angle* enclosed by the bearing vectors g_{12}^* and g_{13}^* . When $\angle g_{12}^* = \alpha \neq 0^\circ$, we can pre-multiply (4.9) by $Q(-\alpha)$ to obtain the bearing vectors in (4.12). Substituting (4.12) in (4.9) yields the set of equations

$$\begin{cases} a + b \cos \theta^* = -d \sin \theta^* \\ b \sin \theta^* = c + d \cos \theta^*. \end{cases} \quad (4.13)$$

Equivalently, we obtain

$$\begin{cases} a \sin \theta^* = -c \cos \theta^* - d \\ b \sin \theta^* = c + d \cos \theta^*. \end{cases} \quad (4.14)$$

In the forthcoming analysis, we aim to find feasible distance pairs (d_{12}, d_{13}) in Proposition 4.1 by solving (4.14). We assume θ^* is in the region $\theta^* \in (0^\circ, 180^\circ)$; the robots are ordered in a counter-clockwise setting and hence the *desired* signed area A^* is positive.

4.4 Analysis on Isosceles Triangles

As a first endeavor, we focus on solving the set of equations (4.14) for the class of *isosceles* triangles. An isosceles triangle has two equal sides of length $\ell > 0$ and two equal angles with value $\gamma \in (0^\circ, 90^\circ)$. The equal sides are called legs and the third side is the base. The equal angles are called base angles and the angle included by the legs is the vertex angle.

In the current setup, we assume the distance constraints d_{12}^* and d_{13}^* are equal, i.e., $d_{12}^* = d_{13}^* = \ell$ are the legs of the triangle and the desired inner angle θ^* is

the vertex angle and satisfies $\theta^* = 180^\circ - 2\gamma$. The isosceles triangle is *acute* when $\theta^* \in (0^\circ, 90^\circ)$, *right* when $\theta^* = 90^\circ$, and *obtuse* when $\theta^* \in (90^\circ, 180^\circ)$.

We first obtain the set of equations (4.14) for the equilibrium and moving configurations corresponding to this class of triangles. To this end, we parameterize the actual distances d_{12} and d_{13} by

$$d_{12} = x\ell, \quad d_{13} = y\ell \quad \text{with } x, y > 0. \quad (4.15)$$

The value $x = 1$ means robot R1 satisfies the distance constraint relative to R2. A similar result concerning R3 holds when $y = 1$.

4.4.1 Equilibrium configurations

For equilibrium configurations, we recall that according to Proposition 4.1, the bearing robots R2 and R3 attain its individual bearing task, i.e. $g_{12} = g_{12}^*$ and $g_{13} = g_{13}^*$. It follows then that $\sin \theta = \sin \theta^*$. With the parameterization in (4.15), the distance and signed area error signals evaluate to $e_{12d} = (x^2 - 1)\ell^2$, $e_{13d} = (y^2 - 1)\ell^2$, and $e_A = \frac{1}{2} \sin \theta^* (xy - 1)\ell^2$. Substituting these relations into (4.14) with coefficients $\{a, b, c, d\}$ defined in (4.10) yields

$$\begin{cases} (x^2 - 1)x = \frac{1}{2}R_{Ad}(xy - 1)(x \cos \theta^* - y) \\ (y^2 - 1)y = \frac{1}{2}R_{Ad}(xy - 1)(y \cos \theta^* - x). \end{cases} \quad (4.16)$$

We find out whether solutions of the form $x = y$ and $x \neq 1$ are feasible. In this case, expression (4.16) reduces to $(1 + \frac{1}{2}R_{Ad}(1 - \cos \theta^*))x = 0$. For it to hold, we require $R_{Ad} = -\frac{2}{1 - \cos \theta^*} < -1$ or $x = 0$. Since $R_{Ad} > 0$ and $x > 0$, it follows both conditions cannot be met. By De Morgan's laws, solutions to (4.16) are either of the form $x \neq y$ or $x = 1$. When $x \neq y$, subtracting the equations in (4.16) results in

$$x^2 + y^2 + xy - 1 = \frac{1}{2}R_{Ad}(1 + \cos \theta^*)(xy - 1). \quad (4.17)$$

In (4.16), we see the presence of $\cos \theta^*$ terms. For acute isosceles triangles, $\cos \theta^* \in (0, 1)$ while for right and obtuse isosceles triangles, $\cos \theta^* \in (-1, 0]$. In the forthcoming sections, we will divide the analysis in these two sub-regions. We state the following result which holds for both sub-regions of $\cos \theta^*$:

Proposition 4.2. *For robot R1, satisfying one of its assigned tasks is equivalent to satisfying all its assigned tasks. In particular, with the parameterization of the distances in (4.15), we have*

$$1. \quad x = 1 \iff y = 1 \wedge xy = 1;$$

$$2. y = 1 \iff x = 1 \wedge xy = 1;$$

$$3. xy = 1 \iff x = 1 \wedge y = 1.$$

Proof. The necessity part (\iff) is immediately observed for all the three statements, so we focus only on the sufficient part (\implies).

$$1. x = 1 \implies y = 1 \wedge xy = 1;$$

Substituting $x = 1$ in (4.16) yields

$$\begin{cases} 0 = \frac{1}{2}R_{Ad}(y-1)(\cos\theta^* - y) \\ (y^2 - 1)y = \frac{1}{2}R_{Ad}(y-1)(y\cos\theta^* - 1). \end{cases} \quad (4.18)$$

The first equation in (4.18) is satisfied when $y = 1$ or $y = \cos\theta^*$. The option $y = 1$ holds for the second equation. In addition, $xy = 1$. Since we know $y > 0$, it follows that option $y = \cos\theta^*$ is feasible only when $\cos\theta^* > 0$. Substituting $y = \cos\theta^*$ in the second equation yields $\cos\theta^* = -\frac{1}{2}R_{Ad}(1 - \cos\theta^*)$. The left-hand side (LHS) is positive while the right-hand side (RHS) is negative since $R_{Ad} > 0$. We infer that $y = \cos\theta^*$ does not satisfy the second equation and hence it is not a solution to (4.18).

$$2. y = 1 \implies x = 1 \wedge xy = 1;$$

Substituting $y = 1$ in (4.16) yields

$$\begin{cases} (x^2 - 1)x = \frac{1}{2}R_{Ad}(x-1)(x\cos\theta^* - 1) \\ 0 = \frac{1}{2}R_{Ad}(x-1)(\cos\theta^* - x). \end{cases} \quad (4.19)$$

The second equation in (4.19) is satisfied when $x = 1$ or $x = \cos\theta^*$. The option $x = 1$ holds for the first equation. In addition, $xy = 1$. Since we know $x > 0$, it follows that $x = \cos\theta^*$ is feasible only when $\cos\theta^* > 0$. Substituting $x = \cos\theta^*$ in the first equation yields $\cos\theta^* = -\frac{1}{2}R_{Ad}(1 - \cos\theta^*)$. The LHS is positive while the RHS is negative since $R_{Ad} > 0$. We infer that $x = \cos\theta^*$ does not satisfy the first equation and hence it is not a solution to (4.19).

$$3. xy = 1 \implies x = 1 \wedge y = 1;$$

Substituting $xy = 1$ in (4.16) yields

$$\begin{cases} (x^2 - 1)x = 0 \\ (y^2 - 1)y = 0 \end{cases} \iff \begin{cases} x = \pm 1 \\ y = \pm 1. \end{cases} \quad (4.20)$$

Since $x > 0$ and $y > 0$ holds, the only possible combination is $x = 1 \wedge y = 1$.

This completes the proof. \square

In Proposition 4.2, at least one of the tasks assigned to R_1 is attained. It remains to investigate the case when none of the assigned tasks is achieved, i.e., the case $x \neq 1, y \neq 1, xy \neq 1$, and $x \neq y$ by De Morgan's laws for the sub-regions of $\cos \theta^*$. We will deal with this in the forthcoming sections.

4.4.2 Moving configurations

Previously, in Proposition 4.1, we have obtained that the bearing vectors corresponding to moving formations are $g_{12} = -g_{13}^*$ and $g_{13} = -g_{12}^*$. It follows that $\sin \theta = -\sin \theta^*$; the formation is flipped and rotated. With the parameterization of the distances $d_{12} = x\ell$ and $d_{13} = y\ell$ in (4.15), we obtain that distance error signals are the same as before while the signed area error signal evaluates to $e_A = \frac{1}{2} \sin \theta^* (-xy - 1) \ell^2$ for moving configurations. The set of equations (4.14) with coefficients $\{a, b, c, d\}$ in (4.11) is found to be

$$\begin{cases} (x^2 - 1)x\ell^3 + R_{bd} = \frac{1}{2}R_{Ad}(xy + 1)(x \cos \theta^* - y)\ell^3 \\ (y^2 - 1)y\ell^3 + R_{bd} = \frac{1}{2}R_{Ad}(xy + 1)(y \cos \theta^* - x)\ell^3. \end{cases} \quad (4.21)$$

Again, we find out whether solutions of the form $x = y$ are feasible. With $x = y$, (4.21) reduces to

$$(x^2 - 1)x\ell^3 + R_{bd} = -\frac{1}{2}R_{Ad}(1 - \cos \theta^*)(x^2 + 1)x\ell^3. \quad (4.22)$$

Observe that the RHS of (4.22) is negative; for the LHS to be negative, $x < 1$ is required. The exact range for x is provided in Corollary 4.4. The difference equation for (4.21) is with $x \neq y$,

$$x^2 + y^2 + xy - 1 = \frac{1}{2}R_{Ad}(1 + \cos \theta^*)(xy + 1). \quad (4.23)$$

Similar to the equilibrium configurations, we will divide the forthcoming analysis on moving configurations in two sub-regions, namely acute isosceles triangles with $\cos \theta^* > 0$ and right and obtuse isosceles triangles having $\cos \theta^* \leq 0$. Before getting into these analyses, we state the following result for the LHS of (4.21):

Proposition 4.3. *Given a cubic equation of the form*

$$f(z) := z^3 - \ell^2 z + R_{bd}, \quad (4.24)$$

where $z = r\ell$ denotes a general variable for the distance and $r \in \{x, y\}$. Let $\hat{d} = \sqrt[3]{\frac{R_{bd}}{2}}$.

Then for $z > 0$, the cubic equation in (4.24) takes values

$$f(z) = \begin{cases} > 0 & \text{if } \ell < \hat{d} \\ \geq 0 & \text{if } \ell = \hat{d} \\ \leq 0 & \text{if } \ell > \hat{d}. \end{cases} \quad (4.25)$$

Proof. By comparison with (2.2), we obtain the coefficients $c = -\ell^2$ and $d = R_{\text{bd}}$ for (4.24). The discriminant evaluates to $\Delta = 4\ell^6 - 27R_{\text{bd}}^2$. Since $c < 0$ and $d > 0$, applying Lemma 2.2 yields for $\Delta \geq 0 \iff \ell \geq \hat{d}$ the positive roots

$$\begin{aligned} z_{\text{p1}} &= \frac{2}{3}\sqrt{3} \cos\left(\frac{1}{3}\varphi - 120^\circ\right) \ell \in \left(0, \frac{1}{3}\sqrt{3}\right] \ell \\ z_{\text{p2}} &= \frac{2}{3}\sqrt{3} \cos\left(\frac{1}{3}\varphi\right) \ell \in \left[\frac{1}{3}\sqrt{3}, 1\right) \ell, \end{aligned} \quad (4.26)$$

where $\varphi = \tan^{-1}\left(-2R_{\text{bd}}^{-1}\sqrt{\frac{\Delta}{108}}\right) \in (90^\circ, 180^\circ]$. Notice that φ depends on both the desired length ℓ and the gain ratio R_{bd} . Before considering the different sub-regions for ℓ , we also compute the derivative of (4.24), yielding $f'(z) = 3z^2 - \ell^2$. The roots are $f'(z) = 0 \iff z = \pm\frac{1}{3}\sqrt{3}\ell$. From the first derivative test, the maximum and minimum are found to be $f_{\text{max}} = f\left(-\frac{1}{3}\sqrt{3}\ell\right) = \frac{2}{9}\sqrt{3}\ell^3 + R_{\text{bd}} > 0$ and $f_{\text{min}} = f\left(\frac{1}{3}\sqrt{3}\ell\right) = -\frac{2}{9}\sqrt{3}\ell^3 + R_{\text{bd}} \geq 0$. The sign of f_{min} depends on the value for ℓ . In addition, $f(0) = f(\ell) = R_{\text{bd}} > 0$. Now we are ready to consider the different sub-regions of ℓ for $z > 0$:

1. $\ell < \hat{d}$; We only have one local minimum for $f(z)$ in the positive range. With $\ell < \hat{d}$, it follows $\ell^3 < \frac{3}{2}\sqrt{3}R_{\text{bd}}$. Correspondingly, we have $f_{\text{min}} = -\frac{2}{9}\sqrt{3}\ell^3 + R_{\text{bd}} > 0$ implying that $f(z) > 0$ for all $z > 0$.
2. $\ell = \hat{d}$; With $\Delta = 0$, we obtain $\varphi = 180^\circ$; the positive roots (4.26) are equal and have value $z_{\text{p1}} = z_{\text{p2}} = \frac{1}{3}\sqrt{3}\ell$. Also, the minimum of $f(z)$ occurs at this point, i.e., $f(z_{\text{p1}}) = f(z_{\text{p2}}) = 0 = f_{\text{min}}$. We thus have $f(z) \geq 0$ for all $z > 0$.
3. $\ell > \hat{d}$; For $\ell > \hat{d}$, we have two distinct positive roots in (4.26). Also, it follows $\ell^3 > \frac{3}{2}\sqrt{3}R_{\text{bd}}$. Correspondingly, we have $f_{\text{min}} = -\frac{2}{9}\sqrt{3}\ell^3 + R_{\text{bd}} < 0$. We note that $z = \frac{1}{3}\sqrt{3}\ell$ lies in the region $(z_{\text{p1}}, z_{\text{p2}})$. The function $f(z)$ thus takes values

$$f(z) = \begin{cases} > 0 & \text{if } z \in (0, z_{\text{p1}}) \cup (z_{\text{p2}}, \infty) \\ = 0 & \text{if } z \in \{z_{\text{p1}}, z_{\text{p2}}\} \\ < 0 & \text{if } z \in (z_{\text{p1}}, z_{\text{p2}}). \end{cases} \quad (4.27)$$

This completes the proof. □

Since $z = r\ell$, we obtain the following corollary:

Corollary 4.4. *The cubic function f in (4.24) takes on values $f(r) > 0$ when $\ell < \hat{d}$, $f(r) \geq 0$ when $\ell = \hat{d}$ and for $\ell > \hat{d}$, we have*

$$f(r) = \begin{cases} > 0 & \text{if } r \in (0, r_1) \cup (r_2, \infty) \\ = 0 & \text{if } r \in \{r_1, r_2\} \\ < 0 & \text{if } r \in (r_1, r_2), \end{cases} \quad (4.28)$$

where $r_1 = \frac{2}{3}\sqrt{3} \cos(\frac{1}{3}\varphi - 120^\circ) \in (0, \frac{1}{3}\sqrt{3})$, $r_2 = \frac{2}{3}\sqrt{3} \cos(\frac{1}{3}\varphi) \in (\frac{1}{3}\sqrt{3}, 1)$, and $\varphi(\ell, R_{bd}) = \tan^{-1}\left(-2R_{bd}^{-1}\sqrt{\frac{\Delta}{108}}\right) \in (90^\circ, 180^\circ)$.

In the upcoming sections, we will study more in detail the set of equations for the equilibrium and the moving configurations for acute, right, and obtuse isosceles triangles.

4.5 Acute Isosceles Triangles

Herein, we focus on acute isosceles triangles in which the vertex angle θ^* is in the range $\theta^* \in (0, 90^\circ) \iff \cos\theta^* \in (0, 1)$.

4.5.1 Stability of equilibrium configurations

Previously, we have shown in Proposition 4.2 that when distance robot R1 attains one of its assigned tasks, it is equivalent to attaining all its assigned tasks. We investigate now whether there exist equilibrium configurations in which none of the tasks assigned to R1 is attained. The following proposition provides necessary conditions which the variables x , y , and the product xy are required to satisfy:

Proposition 4.5. *Assume $x \neq 1$, $y \neq 1$, $xy \neq 1$, and $x \neq y$, where x and y are defined in (4.15). Define $\mathbb{A} = x \cos\theta^* - y$ and $\mathbb{B} = y \cos\theta^* - x$. For the existence of equilibrium configurations in (4.16) satisfying the given constraints, we require that $xy - 1 > 0$ in combination with either 1). $x > 1$, $y < 1$, and $\mathbb{A} > 0$ or 2). $x < 1$, $y > 1$, and $\mathbb{B} > 0$.*

Proof. By direct computation, the following two relations hold: 1). $\mathbb{A} \geq 0 \implies \mathbb{B} < 0$, and 2). $\mathbb{B} \geq 0 \implies \mathbb{A} < 0$. Due to $x \neq 1$, we cannot have $\mathbb{A} = 0$. Similarly, with $y \neq 1$, $\mathbb{B} = 0$ does not hold. Also, the combination $\mathbb{A} < 0$ and $\mathbb{B} < 0$ cannot hold since assuming $xy - 1 > 0$ on the RHS of (4.16) yields $x < 1$ and $y < 1$ on the LHS. With $x < 1$ and $y < 1$, we obtain $xy < 1$ and this contradicts the assumption $xy - 1 > 0$. Similar argument holds when $xy - 1 < 0$ is taken. The remaining feasible combinations are then $\mathbb{A} > 0 \wedge \mathbb{B} < 0$ and $\mathbb{A} < 0 \wedge \mathbb{B} > 0$. It follows that

on the LHS, we either have the combination $x < 1 \wedge y > 1$ or $x > 1 \wedge y < 1$. This depends on the sign of $xy - 1$ as follows:

1. $xy - 1 > 0$;
 - (a) $\mathbb{A} > 0 \wedge \mathbb{B} < 0$ results in $x > 1 \wedge y < 1$.
 - (b) $\mathbb{A} < 0 \wedge \mathbb{B} > 0$ results in $x < 1 \wedge y > 1$.
2. $xy - 1 < 0$;
 - (a) $\mathbb{A} > 0 \wedge \mathbb{B} < 0$ results in $x < 1 \wedge y > 1$.
 - (b) $\mathbb{A} < 0 \wedge \mathbb{B} > 0$ results in $x > 1 \wedge y < 1$.

Consider now $xy - 1 < 0$ holds. Assuming $\mathbb{A} > 0$ leads to $y < x$. However, we have found $x < 1 \wedge y > 1$ on the LHS implying $x < y$ and hence a contradiction. With $\mathbb{B} > 0$, we infer $x < y$ while based on the signs of x and y on the LHS, we have $y < x$ and again a contradiction. For $xy - 1 > 0$, we can find feasible values for x and y satisfying the listed constraints. This completes the proof. \square

A proper choice for the gain ratio R_{Ad} can prevent the occurrence of equilibrium points satisfying the conditions in Proposition 4.5:

Lemma 4.6. *Consider a team of three robots moving according to (4.7) with $K_d > 0$, $K_b > 0$, and $K_A > 0$. Define the gain ratio $R_{Ad} = \frac{K_A}{K_d}$. Furthermore, let the desired formation shape be an isosceles triangle with legs $\ell > 0$ and vertex angle $\theta^* \in (0^\circ, 90^\circ)$. Finally, parameterize the distances d_{12} and d_{13} as in (4.15). If $R_{Ad} \leq \frac{6}{1+\cos\theta^*}$, then the equilibrium configurations $p_{eq} \in \mathcal{S}_p$ in which all the individual assigned tasks are attained.*

Proof. We first consider (4.17). Rearranging the terms yields

$$x^2 + y^2 + (1 - \mathfrak{d})(xy - 1) = 0, \quad (4.29)$$

where $\mathfrak{d} = \frac{1}{2}R_{Ad}(1 + \cos\theta^*) > 0$. Since $x > 0$, $y > 0$, and $xy - 1 > 0$ from Proposition 4.5, it follows that $1 - \mathfrak{d} \geq 0 \iff \mathfrak{d} \leq 1$ will yield the LHS to be positive and hence no feasible combination (\bar{x}, \bar{y}) for (4.29). Adding and subtracting $2xy$ to (4.29) yields

$$(x - y)^2 + (3 - \mathfrak{d})xy - (1 - \mathfrak{d}) = 0. \quad (4.30)$$

Choosing \mathfrak{d} in the range $(1, 3]$, we obtain that all terms on the LHS are non-negative and at least one term is positive; their sum is then also positive and hence we have no combination (\bar{x}, \bar{y}) for (4.30). Notice that $\mathfrak{d} \leq 3 \iff R_{Ad} \leq \frac{6}{1+\cos\theta^*}$. Since solutions to (4.16) should naturally satisfy (4.17), we infer that provided $R_{Ad} \leq \frac{6}{1+\cos\theta^*}$, we do not have feasible combinations (\bar{x}, \bar{y}) with $x \neq y$ satisfying

(4.16). The only possible combination for $x = y$ is the pair $(x, y) = (1, 1)$ which corresponds to robot R_1 satisfying all its assigned tasks. As robots R_2 and R_3 also attain its individual task, we conclude that all robots in the team attain its individual tasks; i.e., $e = 0_7$. This completes the proof. \square

Since we are dealing with acute isosceles triangles, we obtain that the upper bound for R_{Ad} in Lemma 4.6 is in the range $\frac{6}{1+\cos\theta^*} \in (3, 6)$. This seems rather limited. Moreover, in obtaining feasible ranges for R_{Ad} in Lemma 4.6, we only made use of the condition that the product xy is larger than 1 while no specific constraints on x and y in Proposition 4.5 were utilized. We could ask ourselves 1). whether we can expand the region of R_{Ad} by taking into account all the conditions provided in Proposition 4.5. If there are still feasible combinations (\bar{x}, \bar{y}) solving (4.17) while at the same time satisfying all the conditions in Proposition 4.5 with $d > 3$, then a follow-up question would be 2). whether these particular combinations (\bar{x}, \bar{y}) would solve the set of equations (4.16).

For now, we focus on the set of constraints $x > 1, y < 1, A > 0$, and $xy - 1 > 0$ in Proposition 4.5. For a fixed value $x = \bar{x} > 1$, we obtain as solutions to (4.29)

$$y = \frac{d-1}{2}\bar{x} \pm \frac{1}{2}\sqrt{((d+1)(d-3))\bar{x}^2 - 4(d-1)}. \quad (4.31)$$

With $d > 3$, we have $\frac{d-1}{2} > 1$. The feasible value for y which could satisfy $y < 1$ is then $\bar{y} = \alpha\bar{x} - \beta$ with $\alpha = \frac{d-1}{2}$ and $\beta = \frac{1}{2}\sqrt{((d+1)(d-3))\bar{x}^2 - 4(d-1)}$ since the alternative $y = \alpha\bar{x} + \beta > \bar{x} > 1$ and thus violates the constraint. We observe that for specific choices on the values $\bar{x} > 1$ and $d > 3$, we have that \bar{y} satisfies the required constraints. Hence it is possible to find combinations (\bar{x}, \bar{y}) solving the difference equation (4.29) while satisfying the required constraints. The second question now is whether these feasible combinations (\bar{x}, \bar{y}) are also solutions to the set of equations (4.16). Substituting and rearranging the terms yield

$$\frac{1}{1 + \cos\theta^*} (\mathbb{k}\bar{x}^3 + \mathbb{l}\bar{x}^2 + \mathbb{m}\bar{x} + \mathbb{n}) = 0, \quad (4.32)$$

where

$$\begin{aligned} \mathbb{k} &= \frac{1}{2}(d-2)(d+1)(d-(1+\cos\theta^*)), & \mathbb{l} &= -\beta d(d-(1+\cos\theta^*)), \\ \mathbb{m} &= -\frac{1}{2}((3d-2\cos\theta^*)(d-1)+2), & \mathbb{n} &= \beta d. \end{aligned} \quad (4.33)$$

With $d > 3$, we obtain $\mathbb{k} > 0, \mathbb{l} < 0, \mathbb{m} < 0$, and $\mathbb{n} > 0$. Hence we can not provide conclusions on the sign of the cubic term $\mathbb{k}\bar{x}^3 + \mathbb{l}\bar{x}^2 + \mathbb{m}\bar{x} + \mathbb{n}$ on the LHS of (4.32). In Section 4.7, we will numerically evaluate this term. Considering the set of constraints $y > 1, x < 1, \mathbb{B} > 0$, and $xy - 1 > 0$ in Proposition 4.5, we would have

obtained the same result but with the roles for x and y reversed.

4.5.2 Stability of moving configurations

Consider the equations for the moving configurations and again, let $\mathbb{A} = x \cos \theta^* - y$ and $\mathbb{B} = y \cos \theta^* - x$. We obtain $\mathbb{A} \geq 0 \implies \mathbb{B} < 0$ and $\mathbb{B} \geq 0 \implies \mathbb{A} < 0$. Since $x > 0, y > 0$, and $R_{Ad} > 0$, it follows that if one of the RHS is non-negative in (4.21), then the RHS of the other equation needs to be negative. From Proposition 4.3, we obtain that the LHS can be negative only when the legs of the isosceles triangle satisfy $\ell > \hat{d}$. In particular, following Corollary 4.4, the cubic equation on the LHS is negative in the range (r_1, r_2) . When $\ell \leq \hat{d}$, we do not have feasible combinations (\bar{x}, \bar{y}) for the set of equations (4.21) and hence moving configurations cannot occur.

Assume without loss of generality $x \in (r_1, r_2)$. For $y \leq r_1$, we know the LHS of the second equation in (4.21) is positive. On the RHS, we require $\mathbb{B} \geq 0 \implies x < y \implies x < r_1$. This contradicts our assumption that $x \in (r_1, r_2)$ and hence we require $y > r_1$. Following Corollary 4.4, we can divide $y > r_1$ in the three regions $y \in (r_1, r_2)$, $y = r_2$, and $y > r_2$. Before getting into the analysis, we provide the following result concerning the difference equation of (4.21):

Proposition 4.7. *Let $x \in (r_1, r_2) < 1$ in (4.23) and $\mathfrak{d} = \frac{1}{2}R_{Ad}(1 + \cos \theta^*)$. We have the following statements:*

1. Case: $y \leq 1$;

If $\mathfrak{d} \geq 1 \iff R_{Ad} \geq \frac{2}{1 + \cos \theta^*}$, then there are no feasible combinations (\bar{x}, \bar{y}) that satisfy (4.23).

2. Case: $y > 1$;

If $\mathfrak{d} \geq 3 \iff R_{Ad} \geq \frac{6}{1 + \cos \theta^*}$, then the combination (\bar{x}, \bar{y}) where $\bar{y} = \mathfrak{a}\bar{x} + \mathfrak{b}$ with $\mathfrak{a} = \frac{\mathfrak{d}-1}{2}$ and $\mathfrak{b} = \frac{1}{2}\sqrt{(\mathfrak{d}+1)((\mathfrak{d}-3)\bar{x}^2+4)}$ satisfies (4.23).

Proof. Rearranging the terms in (4.23) yields

$$x^2 + y^2 + (1 - \mathfrak{d})xy = 1 + \mathfrak{d}. \quad (4.34)$$

1. Case: $y \leq 1$;

Choosing $\mathfrak{d} \geq 1$, we have $(1 - \mathfrak{d}) \leq 0$. The LHS of (4.34) has upper bound $x^2 + y^2 + (1 - \mathfrak{d})xy \leq x^2 + y^2 < 2$ while the RHS has a value $(1 + \mathfrak{d}) \geq 2$. We infer $\mathfrak{d} \geq 1 \iff R_{Ad} \geq \frac{2}{1 + \cos \theta^*}$ yields no solution for (4.34).

2. Case: $y > 1$;

We consider a specific value for $x = \bar{x}$ in the given range. Note that $\bar{x} < 1$. Solving (4.34) for the unknown y , we obtain

$$y = \frac{\mathfrak{d}-1}{2}\bar{x} \pm \frac{1}{2}\sqrt{(\mathfrak{d}+1)((\mathfrak{d}-3)\bar{x}^2+4)}. \quad (4.35)$$

With $d \geq 3$, we have that the term under the square root is positive. Also, $\frac{d-1}{2} \geq 1$. Applying Descartes' rule of signs, we infer that for $d \geq 3$, we have one positive and one negative root. The positive root is then $\bar{y} = \frac{d-1}{2}\bar{x} + \frac{1}{2}\sqrt{(d+1)((d-3)\bar{x}^2+4)}$.

This completes the proof. \square

For moving configurations, we state the following result:

Lemma 4.8. *Consider a team of three robots moving according to (4.7) with specific gains $K_d > 0$ and $K_b > 0$. Define the gain ratios $R_{bd} = \frac{K_b}{K_d}$ and $R_{Ad} = \frac{K_A}{K_d}$ with $K_A > 0$, and $\hat{d} = \sqrt{3}^3 \sqrt{\frac{R_{bd}}{2}}$. Furthermore, let the desired formation shape be an isosceles triangle with legs $\ell > \hat{d}$ and vertex angle $\theta^* \in (0^\circ, 90^\circ)$. Finally, assume $x \in (r_1, r_2)$ and $y > r_1$, where x and y are defined in (4.15). If $R_{Ad} \geq \max\left\{\frac{6}{1+\cos\theta^*}, \frac{2}{1-\cos\theta^*}\right\}$, then there are no feasible combinations (\bar{x}, \bar{y}) satisfying the set of equations (4.21).*

Proof. The proof will be given for the three regions of $y > r_1$ obtained from Corollary 4.4:

1. $x \in (r_1, r_2)$ and $y \in (r_1, r_2)$;

In this region, we can divide the analysis to the cases $x = y$ and $x \neq y$:

- (a) Case: $x = y$;

Rearranging the terms in (4.22) yields

$$x\ell^3 ((c+1)x^2 + (c-1)) + R_{bd} = 0, \quad (4.36)$$

where $c = \frac{1}{2}R_{Ad}(1 - \cos\theta^*)$. Choosing $c \geq 1$, we have $(c+1) \geq 2$ and $(c-1) \geq 0$. Therefore, all terms in (4.36) are non-negative and at least one term is positive; then the sum on the LHS is also positive. The equation (4.36) does not have roots for $c \geq 1 \iff R_{Ad} \geq \frac{2}{1-\cos\theta^*}$.

- (b) Case: $x \neq y$;

Since both $x < 1$ and $y < 1$, it follows from Proposition 4.7 that the difference equation (4.23) does not have a solution when the gain ratio R_{Ad} satisfies $R_{Ad} \geq \frac{2}{1+\cos\theta^*}$. This implies that the set of equations (4.21) also does not have a solution.

Combining both cases, we infer that $R_{Ad} \geq \frac{2}{1-\cos\theta^*}$ will yield no feasible combinations (\bar{x}, \bar{y}) for (4.21).

2. $x \in (r_1, r_2)$ and $y = r_2$;

We have $x < 1$ and $y = r_2 < 1$. From Proposition 4.7, we infer that when $R_{Ad} \geq \frac{2}{1+\cos\theta^*}$, we have no feasible combinations (\bar{x}, \bar{y}) for (4.21).

3. $x \in (r_1, r_2)$ and $y > r_2$;

We can divide the region for y in two sub-regions, namely $r_2 < y \leq 1$ and $y > 1$.

- (a) Case: $y \in (r_2, 1]$;

Since $x < 1$ and $y \leq 1$, following Proposition 4.7, we infer $R_{Ad} \geq \frac{2}{1+\cos\theta^*}$ is sufficient to obtain no feasible combinations (\bar{x}, \bar{y}) for (4.21).

- (b) Case: $y > 1$;

With the particular choice $R_{Ad} \geq \frac{6}{1+\cos\theta^*} \iff d \geq 3$ from Proposition 4.7, we obtain $\bar{y} = o\bar{x} + \mathbb{b}$ with $o = \frac{d-1}{2}$ and $\mathbb{b} = \frac{1}{2}\sqrt{(d+1)((d-3)\bar{x}^2 + 4)}$ is the solution to (4.23) for a fixed \bar{x} . Substituting the obtained pair (\bar{x}, \bar{y}) back in (4.21) yields

$$\frac{1}{1+\cos\theta^*} (\mathbb{k}\bar{x}^3 + \mathbb{l}\bar{x}^2 + \mathbb{m}\bar{x} + \mathbb{n}) \ell^3 + R_{bd} = 0, \quad (4.37)$$

where

$$\begin{aligned} \mathbb{k} &= \frac{1}{2} (d-2)(d+1)(d-(1+\cos\theta^*)), & \mathbb{l} &= \mathbb{b}d(d-(1+\cos\theta^*)), \\ \mathbb{m} &= \frac{1}{2} (d+1)(3d-2(1+\cos\theta^*)), & \mathbb{n} &= \mathbb{b}d. \end{aligned} \quad (4.38)$$

With $d \geq 3$, we obtain $\mathbb{k} > 0$, $\mathbb{l} > 0$, $\mathbb{m} > 0$, and $\mathbb{n} > 0$. Since the individual terms are positive, it follows the sum is also positive; the combination (\bar{x}, \bar{y}) satisfying (4.23) is not a solution to (4.21). So solutions to (4.21) are of the form $(x, y) \neq (\bar{x}, \bar{y})$. However, these will not solve (4.23), and therefore we conclude that for $R_{Ad} \geq \frac{6}{1+\cos\theta^*}$, the solution set to (4.21) is empty for the mentioned region of x and y .

Combining the results of both parts, we obtain that $R_{Ad} \geq \frac{6}{1+\cos\theta^*}$ is sufficient to obtain no feasible combinations (\bar{x}, \bar{y}) for (4.21).

Gathering the results for all the three considered regions for y , we conclude that $R_{Ad} \geq \max\left\{\frac{6}{1+\cos\theta^*}, \frac{2}{1-\cos\theta^*}\right\}$. This completes the proof. \square

From a design perspective, provided ℓ is given, we can tune the gains K_d and K_b such that $\ell \leq \hat{d}$ is satisfied. In this scenario, any choice of $K_A > 0$ would yield no solutions (x, y) to the set of equations (4.21). This is in agreement with results in Chapter 3 in which moving configurations may occur only when $d_{12}^* \geq \hat{d}$ and $d_{13}^* \geq \hat{d}$ hold. We need Lemma 4.8 when tuning the gains K_d and K_b only is not enough. It provides a lower bound on the gain K_A for a chosen K_d . In the region $\theta^* \in [60^\circ, 90^\circ)$, this lower bound is $K_A \geq \frac{6}{1+\cos\theta^*} K_d$ while $K_A \geq \frac{2}{1-\cos\theta^*} K_d$ when the vertex angle is $\theta^* \in (0, 60)$ in Lemma 4.8. Furthermore, Proposition 4.7

and Lemma 4.8 are results which hold for $x \in (r_1, r_2)$ and $y > r_1$. For the case $y \in (r_1, r_2)$ and $x > r_1$, we obtain the same result, albeit the roles of x and y are reversed.

We conclude this section with the following main result:

Theorem 4.9. *Consider a team of three robots moving according to (4.7) with $K_d > 0$, $K_b > 0$, and $K_A > 0$. Define the gain ratios $R_{bd} = \frac{K_b}{K_d}$ and $R_{Ad} = \frac{K_A}{K_d}$, and also $\hat{d} = \sqrt{3} \sqrt[3]{\frac{R_{bd}}{2}}$. Let the desired formation shape be an acute isosceles triangle with legs $\ell > 0$ and vertex angle θ^* . Finally, parameterize the distances d_{12} and d_{13} as in (4.15). Then starting from all feasible initial configurations, the robots converge to a desired equilibrium configuration $p_{eq} \in \mathcal{S}_p$ in which all the individual tasks are attained if either (K_d, K_b, K_A) is chosen such that $\ell \leq \hat{d}$ and $R_{Ad} \leq \frac{6}{1+\cos \theta^*}$ for $\theta^* \in (0^\circ, 90^\circ)$ or if (K_d, K_b, K_A) is chosen such that $\ell > \hat{d}$ and $R_{Ad} = \frac{6}{1+\cos \theta^*}$ for $\theta^* \in [60^\circ, 90^\circ)$.*

Proof. The proof follows directly from the results obtained in Lemmas 4.6 and 4.8. This completes the proof. \square

With the current constraints imposed on the gain ratio R_{Ad} , we can not provide convergence results for isosceles triangles with legs $\ell > \hat{d}$ and vertex angle $\theta^* \in (0^\circ, 60^\circ)$. We will numerically evaluate this in Section 4.7.

4.6 Right and Obtuse Isosceles Triangles

We continue with right and obtuse isosceles triangles in which the vertex angle θ^* is in the range $\theta^* \in [90^\circ, 180^\circ) \iff \cos \theta^* \in (-1, 0]$.

4.6.1 Stability of equilibrium configurations

We state the following result on equilibrium configurations for right and obtuse isosceles triangles:

Lemma 4.10. *Consider a team of three robots moving according to (4.7) with gains $K_d > 0$, $K_b > 0$, and $K_A > 0$. Let the desired formation shape be an isosceles triangle with legs $\ell > 0$ and vertex angle $\theta^* \in [90^\circ, 180^\circ)$. In addition, parameterize the distances d_{12} and d_{13} as in (4.15). Then all the equilibrium configurations p_{eq} are in \mathcal{S}_p .*

Proof. Given $\theta^* \in [90^\circ, 180^\circ)$, we obtain $\cos \theta^* \in (-1, 0]$. Correspondingly, in (4.16), $\mathbb{A} = x \cos \theta^* - y \leq -y < 0$ and $\mathbb{B} = y \cos \theta^* - x \leq -x < 0$. Assuming $xy - 1 > 0$ on the RHS leads to $x < 1$ and $y < 1$ on the LHS; in turn, this results in $xy < 1$, and therefore contradicting the assumption. Similar arguments hold for $xy - 1 < 0$. Hence there are no feasible combinations (\bar{x}, \bar{y}) satisfying $xy - 1 \neq 0$. In addition, it follows from Proposition 4.2 that $xy - 1 = 0$ is equivalent to the

combination $(x, y) = (1, 1)$; Robot R1 attains all its assigned tasks. With robots R2 and R3 also attaining its individual task, we conclude that all robots in the team attain its individual tasks, i.e., $e = 0_7$. This completes the proof. \square

In Lemma 4.10, we do not have to impose additional constraints on the gains K_d , K_b , and K_A other than that they should be positive.

4.6.2 Stability of moving configurations

For moving configurations, we observe that the sign on the RHS of (4.21) depends only on the terms $\mathbb{A} = x \cos \theta^* - y$ and $\mathbb{B} = y \cos \theta^* - x$. Since $\cos \theta^* \in (-1, 0]$, it follows that $\mathbb{A} < 0$ and $\mathbb{B} < 0$ implying the RHS of (4.21) is negative. For the LHS to be also negative, we require from Proposition 4.3 that the desired length ℓ should satisfy $\ell > \hat{d}$. In particular, the LHS is negative when $x \in (r_1, r_2)$ and $y \in (r_1, r_2)$ with r_1 and r_2 given in Corollary 4.4. The following lemma states a condition on R_{Ad} for precluding moving configurations when $\ell > \hat{d}$:

Lemma 4.11. *Consider a team of three robots moving according to (4.7) with specific gains $K_d > 0$ and $K_b > 0$. Define the gain ratios $R_{bd} = \frac{K_b}{K_d}$ and $R_{Ad} = \frac{K_A}{K_d}$ with $K_A > 0$, and also $\hat{d} = \sqrt{3} \sqrt[3]{\frac{R_{bd}}{2}}$. Furthermore, let the desired formation shape be an isosceles triangle with legs $\ell > \hat{d}$ and vertex angle $\theta^* \in [90^\circ, 180^\circ)$. Finally, parameterize the distances d_{12} and d_{13} as in (4.15). If $R_{Ad} \geq \frac{2}{1 + \cos \theta^*}$, then there are no feasible combinations (\bar{x}, \bar{y}) satisfying the set of equations (4.21).*

Proof. The proof is divided in two parts, namely considering $x = y$ and $x \neq y$ in the feasible region $(r_1, r_2)^2$.

1. Case: $x = y$;

Rearranging the terms in (4.22) yields

$$x\ell^3 ((c + 1)x^2 + (c - 1)) + R_{bd} = 0, \quad (4.39)$$

where $c = \frac{1}{2}R_{Ad}(1 - \cos \theta^*)$. Choosing $c \geq 1$, we have $(c + 1) \geq 2$ and $(c - 1) \geq 0$. Therefore, all terms in (4.39) are non-negative and at least one term is positive; then, the sum on the LHS is also positive. The equation (4.39) does not have roots for $c \geq 1 \iff R_{Ad} \geq \frac{2}{1 - \cos \theta^*}$.

2. Case: $x \neq y$;

It follows from Proposition 4.7 that (4.23) does not have a solution for $R_{Ad} \geq \frac{2}{1 + \cos \theta^*}$ since $x < 1$ and $y < 1$. This in turn implies the set of equations (4.21) does not have a solution.

We have obtained two lower bounds on R_{Ad} . Notice $\frac{2}{1+\cos\theta^*} \geq \frac{2}{1-\cos\theta^*}$ for $\cos\theta^* \leq 0$; choosing $R_{Ad} \geq \frac{2}{1+\cos\theta^*}$ will yield no feasible combinations (\bar{x}, \bar{y}) satisfying the set of equations (4.21). This completes the proof. \square

Similar to acute isosceles triangles, provided ℓ is given, we can first tune the gains K_d and K_b such that $\ell \leq \hat{d}$ is satisfied. Then any choice of $K_A > 0$ would yield no solutions (x, y) to the set of equations (4.21). We need Lemma 4.11 when tuning the gains K_d and K_b only is not enough. In that case, for a specific value $K_d > 0$, we know from the lemma that the gain for the signed area control term needs to satisfy $K_A \geq \frac{2}{1+\cos\theta^*} K_d$. When $\cos\theta^* \rightarrow -1$, i.e., when the vertex angle θ^* of the isosceles triangle is close to 180° , we obtain that $K_A \rightarrow \infty$.

Combining the analyses on the equilibrium and moving configurations, we have the following result for the three-robot formation tasked with displaying a right or obtuse isosceles triangle with legs $\ell > 0$:

Theorem 4.12. *Consider a team of three robots moving according to (4.7) with gains $K_d > 0$, $K_b > 0$, and $K_A > 0$. Define the gain ratios $R_{bd} = \frac{K_b}{K_d}$ and $R_{Ad} = \frac{K_A}{K_d}$, and also $\hat{d} = \sqrt{3} \sqrt[3]{\frac{R_{bd}}{2}}$. Furthermore, let the desired formation shape be an isosceles triangle with legs $\ell > 0$ and vertex angle $\theta^* \in [90^\circ, 180^\circ)$. Finally, parameterize the distances d_{12} and d_{13} as in (4.15). Then, starting from all feasible initial configurations, the robots converge to a desired equilibrium configuration $p_{eq} \in \mathcal{S}_p$ if (K_d, K_b) is chosen such that $\ell \leq \hat{d}$ or if (K_d, K_b, K_A) is chosen such that $\ell > \hat{d}$ and $R_{Ad} \geq \frac{2}{1+\cos\theta^*}$.*

Proof. The proof follows directly from the results obtained in Lemmas 4.10 and 4.11. This completes the proof. \square

In Table 4.1, we summarize the results on the gain ratio R_{Ad} such that convergence to the desired isosceles triangular formation is obtained.

4.7 Numerical Example

4.7.1 Numerical evaluation of (4.32)

Earlier, during the analysis of acute isosceles triangles in Section 4.5, we have found that the difference equation (4.17) contains solutions satisfying Proposition 4.5 for $d > 3$. Substituting these solutions back to the set of equation (4.16) yields the cubic equation (4.32) for which we could not determine its sign since positive and negative coefficients are present. Hence we approach this in a numerical manner. We first choose a value for d satisfying $d > 3$ ($d = \frac{1}{2} R_{Ad} \cos\theta^*$). In the current simulation, we let $d \in \{3.1, 4, 6, 11, 16, 26, 51, 101, 501, 1001\}$. Next, we let x be in the range $x \in (1, 30)$ and compute the corresponding value for y which solves (4.17). By applying the constraints found in Proposition 4.5, we obtain

Table 4.1: Conditions on the gain ratio $R_{Ad} = \frac{K_A}{K_d}$ in Theorems 4.9 and 4.12 for yielding convergence to the desired isosceles triangular formation.

Acute isosceles triangle		Right & obtuse isosceles triangle
$\ell \leq \hat{d}$	$R_{Ad} \in \left(0, \frac{6}{1+\cos\theta^*}\right]$	$R_{Ad} \in (0, \infty)$
$\ell > \hat{d}$	$R_{Ad} = \frac{6}{1+\cos\theta^*}$ for $\theta^* \in [60^\circ, 90^\circ)$	$R_{Ad} \in \left[\frac{2}{1+\cos\theta^*}, \infty\right)$

the feasible combinations (\bar{x}, \bar{y}) for the corresponding value of d . Finally, these combinations (\bar{x}, \bar{y}) are fed back in (4.16). We compute the value on the LHS and on the RHS and take the difference between them. In Fig. 4.1, we have plotted the results for $\theta^* \in \{5^\circ, 15^\circ, 45^\circ, 75^\circ\}$.

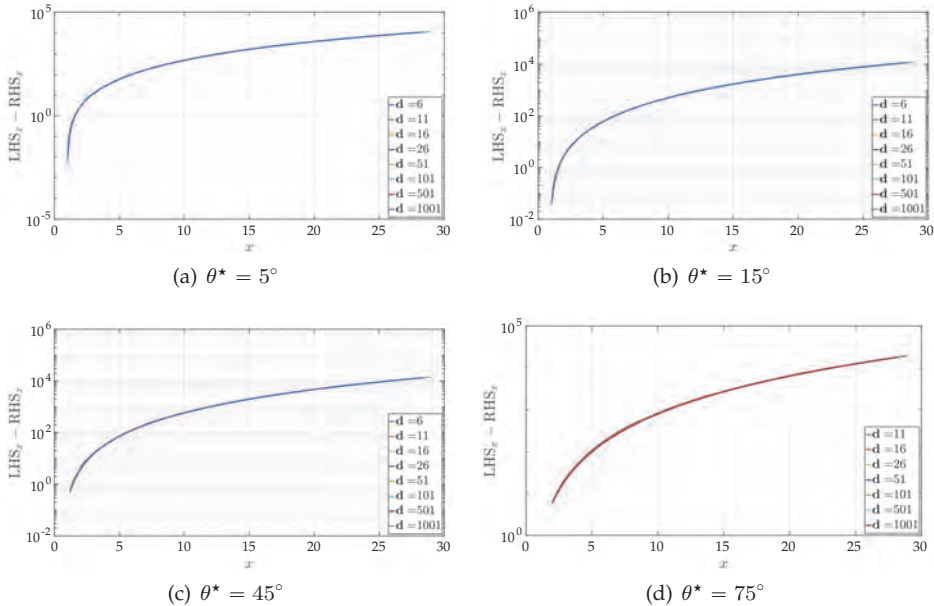


Figure 4.1: Numerical results when evaluating (4.32) for different values of the vertex angle θ^* and gain d

From Fig. 4.1, we observe that the difference between the LHS and the RHS of (4.16) is positive for the different combinations of d and vertex angle θ^* . This difference increases for increasing value of x and also its minimum value increases for increasing value of θ^* . For smaller values of d , we have a smaller set of x -values in the chosen range which satisfy the constraints in Proposition 4.5. From the results of this numerical evaluation, we can conclude that solutions (\bar{x}, \bar{y}) to the

difference equation (4.17) do not satisfy the set of equations (4.16). This also means that the solution set to (4.16) is empty when considering $x \neq 1$, $y \neq 1$, $xy \neq 1$, and $x \neq q$. The upper bound for R_{Ad} in Lemma 4.6 can be extended to ∞ , i.e, we do not need to constrain the gain ratio R_{Ad} . Given this, we can extend the results for Theorem 4.9 as follows:

Corollary 4.13. *Consider a team of three robots moving according to (4.7) with $K_d > 0$, $K_b > 0$, and $K_A > 0$. Define the gain ratios $R_{bd} = \frac{K_b}{K_d}$ and $R_{Ad} = \frac{K_A}{K_d}$, and also $\hat{d} = \sqrt{3} \sqrt[3]{\frac{R_{bd}}{2}}$. Furthermore, let the desired formation shape be an acute isosceles triangle with legs $\ell > 0$ and vertex angle $\theta^* \in (0^\circ, 90^\circ)$. Finally, parameterize the distances d_{12} and d_{13} as in (4.15). Then, starting from all feasible initial configurations, the robots converge to a desired equilibrium configuration $p_{eq} \in \mathcal{S}_p$ in which all the individual tasks are attained if either (K_d, K_b) is chosen such that $\ell \leq \hat{d}$ or if (K_d, K_b, K_A) is chosen such that $\ell > \hat{d}$ and $R_{Ad} \geq \max \left\{ \frac{6}{1+\cos \theta^*}, \frac{2}{1-\cos \theta^*} \right\}$.*

4.7.2 Simulation setup

For illustrating the theoretical claims, we consider simulations of isosceles triangles with different values for the legs ℓ and the vertex angle θ^* . The gains are taken as $K_d = 3$ and $K_b = 48$ yielding the threshold distance $\hat{d} = 2\sqrt{3} \approx 3.4641$. We let the legs ℓ and vertex angle θ^* of the isosceles triangle take values $\ell \in \{3, 6, 10\}$, $\theta^* \in \{5^\circ, 10^\circ, 30^\circ, 60^\circ, 90^\circ, 120^\circ, 150^\circ\}$ while the gain ratio R_{Ad} can be chosen from $R_{Ad} \in \left\{ 0.05, 0.1, 0.3, 0.5, 0.7, 0.9, 1, 3, 6, 10, 20, 50, \frac{2}{1-\cos \theta^*}, \frac{2}{1+\cos \theta^*}, \frac{6}{1+\cos \theta^*} \right\}$. The initial positions of the robots are in the square $[-100, 100]^2$ and we consider simulations from 5000 starting positions for the team of robots.

4.7.3 Simulation results

Here we present the results from the numerical set up. For the isosceles triangle with legs $\ell = 3 < \hat{d}$, we obtain that starting from all the considered initial positions, the robots converge to a desired equilibrium configuration in \mathcal{S}_p . For isosceles triangles with legs $\ell = 6$ and $\ell = 10$, we observe that for values of R_{Ad} less than 1, we have convergence to moving configurations. For $\ell = 6$, this is $R_{Ad} \leq 0.5$ while for $\ell = 10$, we have $R_{Ad} \leq 0.7$. To be safe, we can infer from the current results that starting from $R_{Ad} = 1$, we only have convergence to a desired equilibrium. This value is smaller than the lower bound that we have obtained in Lemmas 4.8 and 4.11. To better illustrate the convergence observation, we plot the results of two simulations in Fig. 4.2(a). The desired shape is an equilateral triangle with legs $\ell = 10$. We start from the same initial position. In order to show the simulation results clearly, we plot them side-by-side by shifting the trajectories horizontally.

For $R_{Ad} = 0.5$, we observe that the robots converge to a moving configuration while choosing $R_{Ad} = 1$ results in convergence to the desired formation shape.

In order to observe whether for larger values of ℓ we also have this result, we consider taking $\theta^* = 60^\circ$; this corresponds to an equilateral triangle. Now, we let ℓ and R_{Ad} take values $\ell \in \{3, 4, 6, 8, 10, 15, 20, 25, 50, 75, 100\}$ and $R_{Ad} \in \{0.25, 0.5, 0.75, 1, 2, 4\}$. We observe that convergence to moving configurations occur when $R_{Ad} \leq 0.75$ while starting from $R_{Ad} = 1$, all initial configurations evolve to a desired configuration in the set \mathcal{S}_p . From Lemma 4.8, we have that the theoretical lower bound is $R_{Ad} = 4$ while numerically $R_{Ad} = 1$ suffices.

From these numerical results, we can say that the bounds for R_{Ad} obtained during the theoretical analyses are conservative and that a value $R_{Ad} \geq 1$ suffices to prevent the occurrence of moving configurations for isosceles triangles.

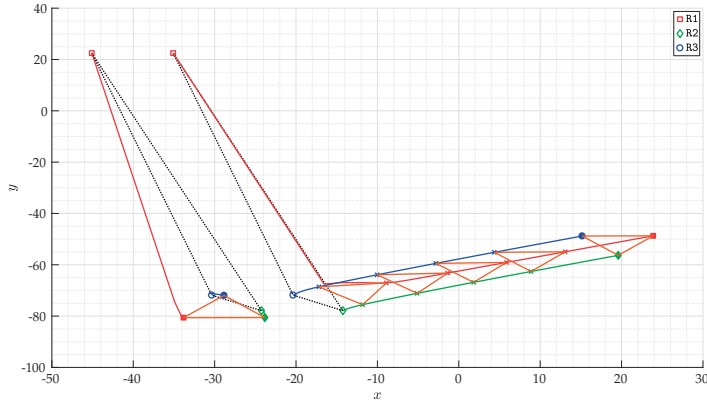
4.7.4 Extension to general triangles

So far, we have obtained results for the analysis of the (1D2B) setup with a signed area constraint when the desired formation shape is an isosceles triangle. To demonstrate that the proposed closed-loop formation system (4.7) may also work for general triangles, we have carried out some simulations. In Fig. 4.2(b), we plot the result of two simulations.

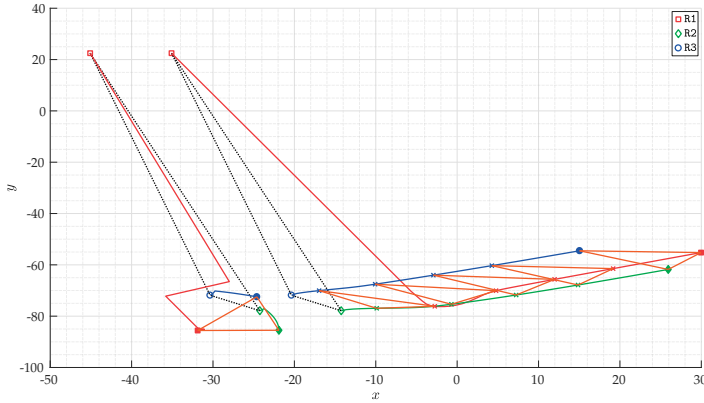
The desired formation shape is a general triangle with lengths $d_{12}^* = 10$ and $d_{13}^* = 15$ and angle $\theta_{213} = 60^\circ$. The moving configuration is obtained when $R_{Ad} = 0.2$ while we observe convergence to the desired shape when $R_{Ad} = 1$. This illustrates that by a proper tuning of the gains, we could also have convergence results to \mathcal{S}_p for general triangles. Furthermore, we notice that when one of the desired lengths is less than \hat{d} , we always have convergence to the desired formation shape. This was also found in the previous chapter.

4.8 Conclusions

We have provided a comprehensive analysis for the formation shape control problem involving a team of three robots partitioned into one distance and two bearing robots. We let the distance robot also maintained a signed area constraint next to the existing distance constraints considered previously, and studied the effect of this new constraint for the class of isosceles triangles. We have shown theoretically and using numerical simulations that the existing equilibrium configurations are maintained and no other undesired equilibrium configurations are introduced by the addition of the signed area control term. Moreover, we have derived sufficient conditions on the gain ratio R_{Ad} for preventing moving configurations to occur when the leg ℓ of the triangle is larger than a threshold distance \hat{d} . As a



(a) Equilateral Triangle



(b) General Triangle

Figure 4.2: Robot trajectories for the (1D2B) setup; **Top:** Desired shape is an equilateral triangle with leg $\ell = 10$. For $R_{Ad} = 0.5$, the trajectories converge to an incorrect moving configuration while for $R_{Ad} = 1$, the trajectories converge to the desired equilateral triangle. **Bottom:** Desired shape is a general triangle with $d_{12}^* = 10$, $d_{13}^* = 15$, and $\theta_{213} = 60^\circ$. The incorrect moving configuration occurs when $R_{Ad} = 0.2$ while convergence to the desired shape is obtained when $R_{Ad} = 1$.

result, convergence results to the desired set \mathcal{S}_p have been established for arbitrary isosceles triangular formations. Numerical results indicated that a lower bound of $R_{Ad} = 1$ suffices for preventing convergence to moving configurations while the theoretical analyses resulted in a more restrictive value that depends on the vertex angle θ^* . Furthermore, simulations have shown that the proposed strategy could also work for general triangles. The formal analysis of general triangles is the subject of future work.

Chapter 5

Angle-Constrained Formation Control for Circular Mobile Robots

In Chapters 3 and 4, we considered the formation shape control problem where the robots have heterogeneous sensing mechanism. By contrast, in this chapter, we assume all robots have the same sensing mechanism. Another difference is that the robots are modeled as circular disks as opposed to regarding them as kinematic point masses moving in the plane. As a consequence, each robot can extract multiple features from its neighboring robots; these will be used for the control design. In the current setup, we can construct formations using a set of inner angle constraints that are closely related to constructing formations using a set of distance constraints. We will show how to obtain a gradient-based control law which only uses the available bearing measurements that the individual robot extract from its neighbors. Consequently, we will provide local stability guarantees using the proposed control law.

We begin the chapter with an introduction, followed by a brief exposition of distance rigidity theory in Section 5.2. Next, in Section 5.3, we show how a desired formation can be described in terms of a set of internal angle constraints; also, the problem is formulated. The gradient-based control design and subsequent analysis are detailed in Section 5.4. We give a numerical example in Section 5.5 and end this chapter with concluding remarks in Section 5.6.

5.1 Introduction

OVER the years, different approaches for formation control have been studied, and these can be classified according to the sensing and control variables that are related to a geometrical property of the desired deployment for the robots [38]. One class of formation control strategies is the rigidity-based control strategies. In this class, rigidity theory plays a key role in characterizing a (at least locally) unique target deployment which can be achieved by a systematic design of distributed control laws. Utilizing the *distance* [38, 48] (or *bearing* [54, 55]) *rigidity theory*, we can define a specific deployment or *target formation shape* in terms of a set of inter-robot distance (or bearing) constraints. The robots use available relative position or distance (or relative bearing) measurements in the design and

execution of the distributed control laws. Recently, new rigidity theories, such as *angle rigidity* [16], *ratio-of-distance-rigidity* [11], and *bearing-ratio-of-distance-rigidity theory* [12] have also been developed for characterizing a (at least locally) unique target formation shape using a set of angle, ratio-of-distance, and bearing-ratio-of-distance constraints, respectively. These theories focus on providing more flexibility to the target deployment by allowing scaling or rotational motions.

One common aspect in the above-mentioned rigidity-based formation control theories is that the mobile robots are assumed to be simple points. As each robot is represented by a point in the plane, there can be only one relative position, distance, or bearing measurement between a pair of neighboring mobile robots. Instead of treating each robot as a point, in this chapter, we treat robots as objects with area so that multiple features in the area can be measured by its neighbors. In particular, we assume each mobile robot to have a circular shape and move with single-integrator dynamics in the plane. Furthermore, each mobile robot can observe *two* distinctive features from its designated neighboring robots. These are the outermost points of the neighboring robots' disk that can be seen from its centroid. In other words, we have the internal angle information of the neighboring robots. The desired formation shape can then be described in terms of feasible internal angle constraints which have a close relationship to the distance constraints that are used in distance-based formation control. This approach enables us to make the following novel contribution in the field of formation control:

We provide an angle-constrained formation control algorithm which resembles distance-based formation control. The main feature of our algorithm is that it requires only direction/bearing/unit vectors as measurements instead of a vector (that requires range and direction). Furthermore, our algorithm provides collision avoidance guarantees where the clearance distance (which is twice the radius) between neighboring robots is not breached by design.

5.2 Distance Rigidity Theory

Recall from Section 2.2.1 that a framework \mathcal{F}_p in the plane is an embedding of a graph \mathcal{G} through assigning a location p_i to each vertex i of the graph. Related to \mathcal{F}_p , we can define the *distance rigidity function* $r_{\text{dist}} : \mathbb{R}^{2n} \rightarrow \mathbb{R}_{>0}^m$ as

$$r_{\text{dist}}(p) := \frac{1}{2} \left[\cdots \quad \|p_j - p_i\|^2 \quad \cdots \right]^\top, \quad \forall \{i, j\} \in \mathcal{E}, \quad (5.1)$$

with each entry of the vector being half the squared distance between two points. Given the distance rigidity function (5.1), we say a framework \mathcal{F}_p is *distance rigid*, if there exists a neighborhood \mathcal{U}_p of p such that, if $q \in \mathcal{U}_p$ and $r_{\text{dist}}(p) = r_{\text{dist}}(q)$, then \mathcal{F}_q is congruent to \mathcal{F}_p . Let $z_{ij} = p_j - p_i \in \mathbb{R}^2$ be the relative position vec-

tor associated to $\{i, j\} \in \mathcal{E}$, and $z \in \mathbb{R}^{2m}$ be the stacked vector of z_{ij} s. Using the incidence matrix $\tilde{H} \in \mathbb{R}^{2m \times 2n}$, we obtain $z = \tilde{H}p$. Besides, let $Z(z) = \mathbf{blkdiag}(\{z_{ij}\}_{\{i, j\} \in \mathcal{E}}) \in \mathbb{R}^{2m \times m}$. Using these expressions, (5.1) can be written in compact form as $r_{\text{dist}}(p) = \frac{1}{2}Z^\top(z)z$. By taking the Jacobian of (5.1), we obtain the *distance rigidity matrix* $R_{\text{dist}}(p)$ as

$$R_{\text{dist}}(p) := \frac{\partial r_{\text{dist}}(p)}{\partial p} = Z^\top(z)\tilde{H} \in \mathbb{R}^{m \times 2n}. \quad (5.2)$$

Let $\delta p \in \mathbb{R}^{2n}$ be an infinitesimal variation of p . A motion δp is said to be *trivial* if $R_{\text{dist}}(p)\delta p = \mathbb{0}_m$ corresponds to a translation and/or a rotation of the entire framework. Trivial motions in the plane are a translation in the x - and in the y -direction, a rotation, and the combination thereof, all applied to the entire framework. We say a framework \mathcal{F}_p is *infinitesimally distance rigid* if and only if the set of infinitesimally distance rigid motions consists of only the trivial motions. This can be translated to the following condition on the distance rigidity matrix: $\mathbf{rank}(R_{\text{dist}}(p)) = 2n - 3$. Furthermore, an infinitesimally distance rigid framework must have at least $2n - 3$ edges. If the number of edges m is exactly $2n - 3$, then the framework is said to be *minimally and infinitesimally distance rigid*.

5.3 Problem Formulation

We consider a group of n mobile robots moving in the plane. Each robot has a circular shape with center specified by $p_i \in \mathbb{R}^2$ and radius by $r_i \in \mathbb{R}_{>0}$. For simplicity, we assume the radii of the robots have the same value and let $r \in \mathbb{R}_{>0}$ represent this common value. We assume the robots are moving with single-integrator dynamics, i.e.,

$$\dot{p}_i(t) = u_i(t), \quad \forall i \in \mathcal{V}, \quad (5.3)$$

where $u_i \in \mathbb{R}^2$ is the controlled velocity to be designed. The group dynamics is given by $\dot{p}(t) = u(t)$ with the stacked vectors $p = [p_1^\top \ \cdots \ p_n^\top]^\top \in \mathbb{R}^{2n}$ and $u = [u_1^\top \ \cdots \ u_n^\top]^\top \in \mathbb{R}^{2n}$.

Each robot is equipped with a sensory system mounted at the center p_i of the robot. With the equipped sensory system, we assume the robots are able to detect two points on the surface of each of its designated neighbors. To illustrate this, let us consider without loss of generality a pair of robots labeled i and j within the group of robots, see Fig. 5.1. We assume robot i has the role of ‘observer’ and robot j is the ‘observed’ robot. Since robot i is the observer, it is able to detect two points on the surface of robot j . We denote the position of the detected points as

p_{jL_i} and p_{jR_i} to indicate these are the positions of robot j as detected by robot i . The measurements from robot j that are available to robot i are the *relative bearing measurements* $g_{ijL} = \frac{z_{ijL}}{\|z_{ijL}\|}$ and $g_{ijR} = \frac{z_{ijR}}{\|z_{ijR}\|}$, with $z_{ijL} = p_{jL_i} - p_i$ and $z_{ijR} = p_{jR_i} - p_i$ being the relative position from the detected points to the center of robot i . The two bearing vectors form an angle θ_{ij} centered at p_i , as can be seen in Fig. 5.1.

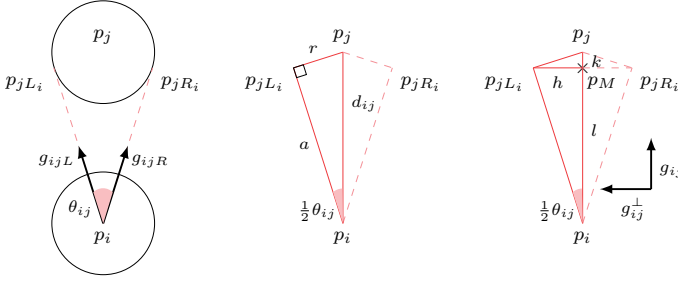


Figure 5.1: Sensing setup with robot i being the ‘observer’ and robot j the ‘observed’ robot. On the left panel, robot i detects the points p_{jL_i} and p_{jR_i} of robot j and the internal angle θ_{ij} can be obtained from the bearing measurements g_{ijL} and g_{ijR} . In the middle panel, we use geometrical arguments to relate θ_{ij} to the inter-center distance d_{ij} and the radius r . On the right panel, we have a geometrical view supporting Proposition 5.4.

By the inner product rule, we obtain

$$\cos \theta_{ij} = g_{ijL}^\top g_{ijR}. \quad (5.4)$$

Remark 5.1. It should be noted the lines in the direction of the unit vectors g_{ijL} and g_{ijR} are both tangent lines from point p_i to robot j . Hence these lines are perpendicular to the radius of the circle, i.e., $(p_{jL_i} - p_j) \perp z_{ijL}$ and $(p_{jR_i} - p_j) \perp z_{ijR}$. Furthermore, the triangle $\Delta p_j p_{jL_i} p_i$ with vertices p_j , p_i , and p_{jL_i} and the triangle $\Delta p_j p_{jR_i} p_i$ with vertices p_j , p_i , and p_{jR_i} are reflections of each other with the line connecting p_j and p_i as the line of reflection. Hence the angle $\angle p_{jL_i} p_i p_j = \angle p_j p_i p_{jR_i} = \frac{1}{2} \theta_{ij}$.

By considering the geometry, we obtain an alternative expression for $\cos \theta_{ij}$, which is related to the radii of and the inter-center distance between the robots.

Proposition 5.2. *The internal angle θ_{ij} is related to the inter-center distance d_{ij} between the robots i and j and the radii r of the robots as*

$$\cos \theta_{ij} = 1 - 2 \left(\frac{r}{d_{ij}} \right)^2. \quad (5.5)$$

Proof. The desired result can be obtained by employing the cosine double-angle

identity $\cos \alpha = 1 - 2 \sin^2 \frac{1}{2} \alpha$ and noting from Remark 5.1 that $\Delta p_j p_j L_i p_i$ is a right triangle with $\sin \frac{1}{2} \theta_{ij} = \frac{r}{d_{ij}}$. Fig. 5.1 provides the geometric illustration. This completes the proof. \square

Note that (5.4) and (5.5) are equivalent for obtaining the internal angle θ_{ij} ; the former is based on available bearing measurements while the latter is based on geometry.

Remark 5.3. As robots i and j have a circular shape, the feasible interval for the inter-center distance d_{ij} is $d_{ij}^{\text{feas}} \in (2r, \infty)$. This also poses restrictions on the value for θ_{ij} and $\cos \theta_{ij}$. From (5.5), it follows that $d_{ij}^{\text{feas}} \in (2r, \infty)$ implies $\cos \theta_{ij}^{\text{feas}} \in (\frac{1}{2}, 1)$ and $\theta_{ij}^{\text{feas}} \in (0, 60^\circ)$. Correspondingly, an increase in the value of d_{ij} results in an increase of $\cos \theta_{ij}$ and a decrease of θ_{ij} .

We can rewrite (5.5) as $d_{ij} = \sqrt{\frac{2r^2}{1 - \cos \theta_{ij}}}$. By obtaining $\cos \theta_{ij}$ from (5.4) and knowing r , we can infer the inter-center distance d_{ij} . With this observation, we define an *internal angle rigidity function* $r_{\text{angle}} : \mathbb{R}^{2n} \rightarrow \mathbb{R}_{>0}^m$ given by

$$r_{\text{angle}}(p) = [\dots \cos(\theta_{ij}) \dots]^\top, \quad \forall \{i, j\} \in \mathcal{E} \quad (5.6)$$

for describing a framework $\mathcal{F}_p(\mathcal{G}, p)$. By Remark 5.3, there is a one-to-one relationship between the newly defined rigidity function (5.6) and the distance rigidity function (5.1). The Jacobian of (5.6) is

$$R_{\text{angle}}(p) = \frac{\partial r_{\text{angle}}(p)}{\partial p} = \frac{\partial r_{\text{angle}}(p)}{\partial q} \frac{\partial q}{\partial p} = D(d) R_{\text{dist}}, \quad (5.7)$$

with $d \in \mathbb{R}^m$ being the stacked vector of distances d_{ij} s, $q = (\mathbf{diag}(d) d) \in \mathbb{R}^m$, and $D(d) = 4r^2 \mathbf{diag}(\{d_{ij}^{-4}\}_{\{i, j\} \in \mathcal{E}}) \in \mathbb{R}^{m \times m}$. The matrix $D(d)$ is positive definite as each $d_{ij} > 2r > 0$; we have $\mathbf{rank}(R_{\text{angle}}) = \mathbf{rank}(R_{\text{dist}})$.

Now we can define the desired target formation shape by a framework $\mathcal{F}_{p^*}(\mathcal{G}, p^*)$ where the vector $p^* \in \mathbb{R}^{2n}$ satisfies a set of desired internal angle constraints $r_{\text{angle}}(p^*)$. One way to obtain the internal angle constraints is to employ (5.5) when the desired distance constraints are given. Moreover, the formation \mathcal{F}_{p^*} is *minimally* and *infinitesimally* rigid in the distance rigidity sense. The formation control problem that is considered in this chapter can be formulated as follows:

Angle-constrained Formation Control Problem with Collision Avoidance:

Given a set of feasible internal angle constraints¹ $\{\theta_{ij}^*\}_{\{i, j\} \in \mathcal{E}}$ obtained using (5.5) from a minimally and infinitesimally rigid framework \mathcal{F}_{p^*} and an initial configuration $p(0) \in \mathbb{R}^{2n}$ with $\|p_j(0) - p_i(0)\| > 2r, \forall \{i, j\} \in \mathcal{E}$. Design a control law

¹We give a formal definition of such a set in Section 5.4.5.

$u_i(t)$, $\forall i \in \mathcal{V}$ utilizing only the neighboring measurements obtained as in (5.4) such that $\forall \{i, j\} \in \mathcal{E}$, we have

- *Collision avoidance*: $\|p_j(t) - p_i(t)\| > 2r, \forall t \geq 0$;
- *Convergence*: $\theta_{ij}(t) \rightarrow \theta_{ij}^*$ as $t \rightarrow \infty$.

5.4 Gradient-Based Control Design

In this section, we pursue a gradient-based control design approach utilizing angle-based potential functions for solving the formation control problem. To each edge $\{i, j\} \in \mathcal{E}$, we define the error signal $e_{ij}(t) = \cos \theta_{ij}(t) - \cos \theta_{ij}^*$. By Remark 5.3, we deduce the feasible region for the error signal is $e_{ij}^{\text{feas}} \in (-c_{ij}, f_{ij})$ with $c_{ij} = \cos \theta_{ij}^* - \frac{1}{2}$ and $f_{ij} = 1 - \cos \theta_{ij}^*$. Both c_{ij} and f_{ij} are strictly positive.

5.4.1 Proposed angle-based potential function

For a robot pair $\{i, j\}$, we take as potential function

$$V_{ij}(e_{ij}) = \frac{1}{2}r \left(\frac{\cos \theta_{ij} - \cos \theta_{ij}^*}{\cos \theta_{ij} - \frac{1}{2}} \right)^2 = \frac{1}{2}r \left(\frac{e_{ij}}{e_{ij} + c_{ij}} \right)^2. \quad (5.8)$$

The denominator term $\cos \theta_{ij} - \frac{1}{2}$ ensures collision avoidance between the neighboring robots i and j , i.e., $\|p_j(t) - p_i(t)\| > 2r, \forall t > 0$ given that $\|p_j(0) - p_i(0)\| > 2r$. The function $V_{ij}(e_{ij})$ is non-negative in e_{ij}^{feas} . Furthermore, $V_{ij}(e_{ij}) = 0$ if and only if $e_{ij} = 0$ and $V_{ij}(e_{ij}) \rightarrow \infty$ if e_{ij} approaches the lower bound $-c_{ij}$ from above, i.e., when the mobile robots are approaching each other. The first derivative $v_{ij}(e_{ij}) := \frac{\partial}{\partial e_{ij}} V_{ij}(e_{ij})$ can be obtained as

$$v_{ij}(e_{ij}) = r \frac{e_{ij} c_{ij}}{(e_{ij} + c_{ij})^3}.$$

The value of $v_{ij}(e_{ij})$ equals zero if and only if $e_{ij} = 0$ and the sign of v_{ij} depends on the sign of e_{ij} . The second derivative $k_{ij}(e_{ij}) := \frac{\partial^2}{\partial e_{ij}^2} V_{ij}(e_{ij})$ is given as

$$k_{ij}(e_{ij}) = r \frac{c_{ij}}{(e_{ij} + c_{ij})^4} (-2e_{ij} + c_{ij}).$$

$k_{ij}(e_{ij})$ is positive when $e_{ij} < \frac{1}{2}c_{ij}$. Recall $e_{ij}^{\text{feas}} \in (-c_{ij}, f_{ij})$; therefore we need to determine when $\frac{1}{2}c_{ij} \leq f_{ij}$. By some algebraic computations, we obtain $\frac{1}{2}c_{ij} \leq f_{ij}$ if and only if $\cos \theta_{ij}^* \leq \frac{5}{6}$. When $\cos \theta_{ij}^* < \frac{5}{6}$, we have the region for which $k_{ij}(e_{ij})$ is positive is a subset of e_{ij}^{feas} , whereas when $\cos \theta_{ij}^* \geq \frac{5}{6}$, we have $k_{ij}(e_{ij})$ is positive over the entire domain e_{ij}^{feas} .

The properties of (5.8) will be used later for deriving the exponential convergence of the error dynamics.

5.4.2 Gradient-based control law for each robot

The local potential function for each robot i is $V_i(e) = \sum_{j \in \mathcal{N}_i} V_{ij}(e_{ij})$ with $e \in \mathbb{R}^m$ being the stacked vector of error signals e_{ij} s. The control input $u_i(t)$ is then

$$u_i(t) = -\left(\frac{\partial}{\partial p_i} V_i(e)\right)^\top = -\sum_{j \in \mathcal{N}_i} \left(\frac{\partial}{\partial p_i} V_{ij}(e_{ij})\right)^\top. \quad (5.9)$$

Utilizing (5.5), the term $\frac{\partial}{\partial p_i} V_{ij}(e_{ij})$ can be evaluated as

$$u_{ij}^\top := \frac{\partial}{\partial p_i} V_{ij}(e_{ij}) = -v_{ij}(e_{ij}) \frac{4r^2}{d_{ij}^4} z_{ij}^\top. \quad (5.10)$$

Note that (5.10) requires relative state variables d_{ij} , z_{ij} , and the knowledge of r . However, robot i has access to only the relative bearing measurements g_{ijL} and g_{ijR} for each $j \in \mathcal{N}_i$. Nonetheless, we show that the gradient-control law (5.9) can be implemented using these available measurements.

Proposition 5.4. *The gradient-based control law (5.9) can be implemented by each robot $i \in \mathcal{V}$ using the set of available measurements $\left\{ \{g_{ijL}\}_{j \in \mathcal{N}_i}, \{g_{ijR}\}_{j \in \mathcal{N}_i} \right\}$.*

Proof. To implement (5.9), we need to rewrite (5.10) in terms of the available measurements g_{ijL} and g_{ijR} . To this end, first, we seek expressions for the positions p_{jL_i} and p_{jR_i} . Let us consider again Fig. 5.1. Denote the intersection between the lines connecting the center of the robots and the two intersection points as p_M (marked with the \times -symbol in the right panel of Fig. 5.1). Let $\|p_{jL_i} - p_M\| = h$, $\|p_j - p_M\| = k$, and $\|p_i - p_M\| = l$ satisfying $k + l = d_{ij}$. l can also be written as a fraction of the inter-center distance d_{ij} , i.e., $l = s d_{ij}$ with $s \in (0, 1)$. We can now express the positions p_{jL_i} and p_{jR_i} as $p_{jL_i} = p_j - k g_{ij} + h g_{ij}^\perp$, and $p_{jR_i} = p_j - k g_{ij} - h g_{ij}^\perp$. Recall g_{ij} is the unit vector between the centers of the robots. Subsequently, the relative position z_{ijL} and z_{ijR} can be obtained as $z_{ijL} = l g_{ij} + h g_{ij}^\perp$, and $z_{ijR} = l g_{ij} - h g_{ij}^\perp$, while their sum equals $z_{ij+} = z_{ijL} + z_{ijR} = 2s z_{ij}$. Due to the reflection observation in Remark 5.1, we have $\|z_{ijL}\| = \|z_{ijR}\| = \sqrt{l^2 + h^2} =: a$. Using the previous computations, we obtain for the sum of the relative bearing measurements $g_{ij+} = g_{ijL} + g_{ijR} = 2 \frac{s}{a} z_{ij}$. In addition, $\frac{g_{ij+}}{\|g_{ij+}\|^2} = \frac{2 \frac{s}{a} z_{ij}}{4 \left(\frac{s}{a}\right)^2 a_{ij}^2} \iff 2 \frac{z_{ij}}{a_{ij}^2} = 4 \frac{s}{a} \frac{g_{ij+}}{\|g_{ij+}\|^2}$. Since $s = \frac{l}{d_{ij}}$, we can rewrite $\frac{s}{a}$ as $\frac{s}{a} = \frac{l}{d_{ij} a} \frac{r}{r} = \frac{1}{r} \sin \frac{1}{2} \theta_{ij} \cos \frac{1}{2} \theta_{ij} = \frac{1}{2r} \sin \theta_{ij}$ by using $\sin \frac{1}{2} \theta_{ij} = \frac{r}{d_{ij}}$, $\cos \frac{1}{2} \theta_{ij} = \frac{a}{d_{ij}} = \frac{l}{a}$, and the sine double-angle identity $\sin 2\alpha = 2 \sin \alpha \cos \alpha$. Sub-

stituting the obtained expressions in (5.10) and utilizing (5.5) yield

$$u_{ij}^\top = -2\widehat{v}_{ij}(e_{ij})(1 - \cos \theta_{ij}) \sin \theta_{ij} \|g_{ij+}\|^{-2} g_{ij+}, \quad (5.11)$$

where $\widehat{v}_{ij}(e_{ij}) = \frac{v_{ij}(e_{ij})}{r} = \frac{e_{ij}c_{ij}}{(e_{ij}+c_{ij})^3}$. Using (5.11), we can implement (5.9) without knowledge of the range information and the radii of the robots. This completes the proof. \square

5.4.3 Gradient-based control law for the group of robots

The overall potential function $V(e)$ can be expressed as the sum of all the individual potential functions $V_{ij}(e_{ij})$, i.e., $V(e) = \sum_{\{i,j\} \in \mathcal{E}} V_{ij}(e_{ij})$. The control law $u_i(t)$ in (5.9) is then $u_i(t) = -\left(\frac{\partial}{\partial p_i} V(e)\right)^\top$. Noting $\frac{\partial}{\partial p} V(e) = \frac{\partial V(e)}{\partial e} \frac{\partial e}{\partial q} \frac{\partial q}{\partial p}$, we obtain the following compact form for the closed-loop formation control system:

$$\dot{p}(t) = -R_{\text{angle}}^\top v(e), \quad (5.12)$$

with the vector $v(e) \in \mathbb{R}^m$ denoting the gradients of (5.8) for each robot pair $\{i, j\} \in \mathcal{E}$.

Lemma 5.5. *The closed-loop formation control system (5.12) has the following properties:*

1. *The formation centroid $p_{\text{cent}} = \frac{1}{n} \mathbb{1}_n^\top p$ is stationary, i.e., $p_{\text{cent}}(t) = p_{\text{cent}}(0)$, $\forall t \geq 0$;*
2. *Each mobile robot can have its own local coordinate system for obtaining the required relative state measurements and implementing the desired control action.*

Proof. The proof is similar to Lemma 4 in [49], and therefore not provided here. \square

5.4.4 Internal angle error system

Using the definition of the error vector e , and expressions (5.5) and (5.12), we obtain the error dynamics as

$$\dot{e}(t) = \frac{\partial e}{\partial p} \dot{p} = -R_{\text{angle}} R_{\text{angle}}^\top v(e) = -Fv(e). \quad (5.13)$$

The matrix $F = R_{\text{angle}} R_{\text{angle}}^\top = D(d) R_{\text{dist}} R_{\text{dist}}^\top D(d) \in \mathbb{R}^{m \times m}$ is symmetric and at least positive semidefinite. Moreover, for any infinitesimally and minimally distance rigid framework \mathcal{F}_{p^*} , F can be shown to be a function of the error vector e around the origin by employing the law of cosines. By this observation, we conclude the error dynamics given by (5.13) constitute an autonomous system.

The main result will be the local exponential stability of the error dynamics (5.13). To this end, we first construct a compact and invariant sub-level set for the

overall potential function $V(e)$. Previously, we have $k_{ij}(e_{ij}) > 0$ holds if and only if $e_{ij} < b_{ij} := \min\{\frac{1}{2}c_{ij}, f_{ij}\}$ for all $\{i, j\} \in \mathcal{E}$. Let $b = \min\{b_{ij}\}_{\{i, j\} \in \mathcal{E}} > 0$. We define the ‘hypercube’ as

$$\mathcal{H}_b = \{e \in \mathcal{CF} \mid |e_k| < b, k \in \mathcal{K}\}, \quad (5.14)$$

with \mathcal{CF} being the Cartesian product $(-c_1, f_1) \times \cdots \times (-c_m, f_m)$ and $\mathcal{K} = \{1, \dots, m\}$ being the ordered edge index set. Choose $q \in (0, b)$ such that

$$\mathcal{B}_q = \{e \in \mathcal{H}_b \mid \|e\| \leq q\} \subset \mathcal{H}_b. \quad (5.15)$$

Let $\alpha = \min_{\|e\|=q} V(e)$. As $q \neq 0$, we have $V(e) > 0$ and also $\alpha > 0$. Choose $\beta \in (0, \alpha)$ and define

$$\Omega_\beta = \{e \in \mathcal{B}_q \mid V(e) \leq \beta\}. \quad (5.16)$$

By definition, the sub-level set Ω_β is closed and since $\Omega_\beta \subset \mathcal{B}_q$, it is also bounded. Thus, Ω_β is a compact set. The time derivative of $V(e)$ is obtained as

$$\dot{V}(e) = \frac{\partial}{\partial e} V(e) \dot{e} = -v^\top(e) F(e) v(e) \leq 0. \quad (5.17)$$

This implies $V(e(t)) \leq V(e(0))$. Whenever $e(0) \in \Omega_\beta$, we have by (5.17) that $e(t) \in \Omega_\beta$; therefore, the set Ω_β is also positive invariant. As $V(e) \geq 0$ and $\dot{V}(e) \leq 0$, the overall potential function can serve as a candidate Lyapunov function. We are ready to state and prove the main result.

Theorem 5.6. *Consider a group of circular shaped robots modeled with single-integrator dynamics (5.3) and having a graph topology \mathcal{G} such that the desired formation is minimally and infinitesimally rigid in the distance rigidity sense. Let $e(0)$ be such that it is in the compact and invariant set Ω_β (5.16). Then $e = \mathbb{0}_m$ is a locally exponential stable equilibrium point of the error dynamics (5.13).*

Proof. The proof can be divided into three main stages. *First*, we consider the asymptotic stability of the origin $e = \mathbb{0}_m$. The set Ω_β has the property of being compact and positive invariant. In addition, the value for β can be chosen such that for every vector $e \in \Omega_\beta$, the formation is minimally and infinitesimally rigid in the distance rigidity sense, and close to the target formation. Due to our choice of β , we have that R_{dist} has full row rank. Since $R_{\text{angle}} = D(d) R_{\text{dist}}$ and $D(d)$ positive definite, also R_{angle} has full row rank. This in turn implies $F(e) = R_{\text{angle}} R_{\text{angle}}^\top$ is positive definite. Let λ be the minimal eigenvalue of the matrix $F(e)$ in Ω_β , i.e., $\lambda = \min_{e \in \Omega_\beta} \mathbf{eig}(F(e)) > 0$. It follows from (5.17) that

$$\dot{V}(e) = -v^\top(e) F(e) v(e) \leq -\lambda \|v(e)\|^2 \quad (5.18)$$

holds. The value $\dot{V}(e)$ is negative definite for all $e \in \Omega_\beta \setminus \{0_m\}$; therefore local asymptotic stability of the origin is attained.

Next, we aim to show the following two inequalities as is done in [48]:

$$c_1 \|e\|^2 \leq V(e) \leq c_2 \|e\|^2; \quad \|v(e)\|^2 \geq \rho \|e\|^2, \quad (5.19)$$

with c_1 , c_2 , and ρ being positive constants that we need to determine. These inequalities facilitate the proof to exponential stability of the origin. To this end, recall the overall potential function $V(e)$

$$V(e) = \sum_{k \in \mathcal{K}} V_k(e_k) = \sum_{k \in \mathcal{K}} \int_0^{e_k} v_k(s) \, ds. \quad (5.20)$$

Within the set Ω_β , we can find a value for δ such that

$$\mathcal{H}_\delta = \{e \in \Omega_\beta \mid |e_k| \leq \delta, k \in \mathcal{K}\}. \quad (5.21)$$

By Lemma 3.2 in [26], we have the function $v_k(e_k)$ is Lipschitz continuous in \mathcal{H}_δ . In addition, the function $k_k(e_k)$ is positive within the set Ω_β , and thus also in the subset \mathcal{H}_δ . The remainder of the proof for obtaining the positive constants c_1 , c_2 , and ρ of (5.19) follows closely [48] and for this reason, it is omitted.

Finally, we can show exponential stability of the origin as a result of the previous two steps. Substituting (5.19) in (5.18), we obtain

$$\dot{V}(e) \leq -\lambda \|v(e)\|^2 \leq -\lambda \rho \|e\|^2. \quad (5.22)$$

By Theorem 4.10 in [26], we conclude that the origin is exponentially stable in \mathcal{H}_δ . The error norm is bounded by an exponential decreasing function as

$$\|e(t)\| \leq \left(\frac{c_2}{c_1}\right)^{\frac{1}{2}} \|e(0)\| \exp\left(-\frac{\gamma}{2}t\right), \quad (5.23)$$

with $\gamma = \frac{\lambda \rho}{c_2}$. This completes the proof. \square

5.4.5 Equilibrium sets

Theorem 5.6 concerns the local exponential convergence of the formation control system to the desired formation shape. In general, the set of equilibrium points of the mobile robots can be given by $\mathcal{W} := \{p \in \mathbb{R}^{2n} \mid R_{\text{angle}}^\top v(e) = 0_{2n}\}$. The set of *correct* formation shapes is given by $\mathcal{W}_c := \{p \in \mathbb{R}^{2n} \mid e = 0_m\}$ while the set of *incorrect* formation shapes is $\mathcal{W}_i := \mathcal{W} \setminus \mathcal{W}_c$. Considering the target formation shape is minimally and infinitesimally rigid, we conclude that the formation shapes in

\mathcal{W}_i are not infinitesimally rigid, since the null space of R_{angle}^\top also consists of a non-trivial vector $v(e) \neq \mathbb{0}_m$. Similar to distance-based control, the set \mathcal{W}_i includes configurations where all the robots' center are colinear. Moreover, we can obtain the following on the equilibrium set of the p -dynamics and the e -dynamics:

Lemma 5.7. *The equilibrium sets of the error system (5.13) is the same as the equilibrium sets of the closed-loop formation control system (5.12).*

Proof. Since $\dot{e}(t) = R_{\text{angle}}\dot{p}(t)$, obviously $\dot{p}(t) = \mathbb{0}_{2n} \implies \dot{e}(t) = \mathbb{0}_m$. It remains to show $\dot{e}(t) = \mathbb{0}_m \implies \dot{p}(t) = \mathbb{0}_{2n}$. Assume $\exists \dot{p}(t) \neq \mathbb{0}_{2n}$ such that $\dot{p}(t) \in \text{Null}(R_{\text{angle}})$ holds. From (5.12), we also have $\dot{p}(t) \in \text{Col}(R_{\text{angle}}^\top)$. Since $\text{Null}(R_{\text{angle}}) \perp \text{Col}(R_{\text{angle}}^\top)$, we obtain $\text{Null}(R_{\text{angle}}) \cap \text{Col}(R_{\text{angle}}^\top) = \{\mathbb{0}_{2n}\}$, contradicting the assumption $\dot{p}(t) \neq \mathbb{0}_{2n}$. This completes the proof. \square

5.5 Numerical Example

5.5.1 Simulation setup

We apply the proposed control law to a team of 4 circular robots with radii $r = 1$. The collective goal is to form a rectangular shape with the inter-center distances given as $d_{12}^* = d_{34}^* = 3$, $d_{13}^* = d_{24}^* = 4$, and $d_{14}^* = 5$. Using (5.5), we obtain $\cos \theta_{12}^* = \cos \theta_{34}^* = 0.7778$, $\cos \theta_{13}^* = \cos \theta_{24}^* = 0.8750$, and $\cos \theta_{14}^* = 0.9200$. The initial configuration, depicted as dashed circles in Fig. 5.2(a), has center positions $p_1(0) = [0, 0]^\top$, $p_2(0) = [2.05, 0]^\top$, $p_3(0) = [-2.05, 0.05]^\top$, and $p_4(0) = [-1, 1.85]^\top$. Using this initial configuration, we illustrate the collision avoidance feature of the proposed control law and the convergence to the desired formation shape, even though $p(0) \notin \mathcal{H}_b$. We obtain $b = 0.08$, and set the gain $K = 50$ for speeding up the convergence.

5.5.2 Simulation results

The trajectories of the robots are depicted in Fig. 5.2(a). In addition, the inter-center distances and the internal angle errors between the robots are given in Figs. 5.2(b) and 5.2(c), respectively.

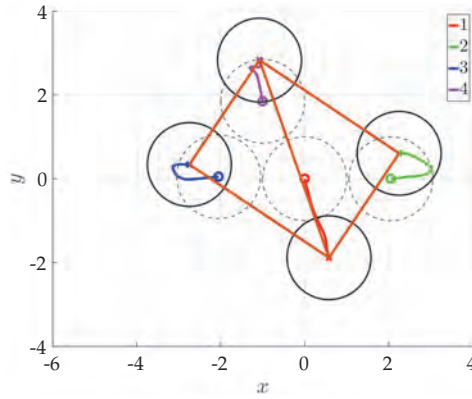
Let us focus on robot 2, the green robot in Fig. 5.2(a). It has the neighboring robots 1 (red robot) and 4 (magenta robot). From the figure, we observe that since robots 2 and 1 are close to each other initially, robot 2 quickly moves away from robot 1, and almost attains the desired constraint with robot 1. However, due to this motion, its distance to the neighboring robot 4 has increased to about 4.9. This can also be observed from Fig. 5.2(c), where we see an increase in the magenta colored signal representing error $|e_{24}|$. Since robot 2 is now sufficiently far from

robot 1, it then tries to satisfy the internal angle constraint with robot 4 as can be observed in both Figs. 5.2(b) and 5.2(c) . By zooming in on Fig. 5.2(c), we can observe exponential convergence of the error signals starting around $t = 3$ s. All the error signals are then well below the threshold value of $b = 0.08$.

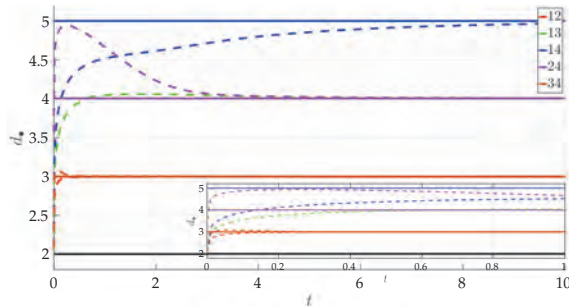
5.6 Conclusions

We have solved the formation control problem for circular mobile robots subjected to internal angle constraints. A gradient-descent control law requiring only relative bearing measurements for implementation has been proposed. This control law enjoys local exponential convergence for the error dynamics and ensures collision avoidance between neighboring robots.

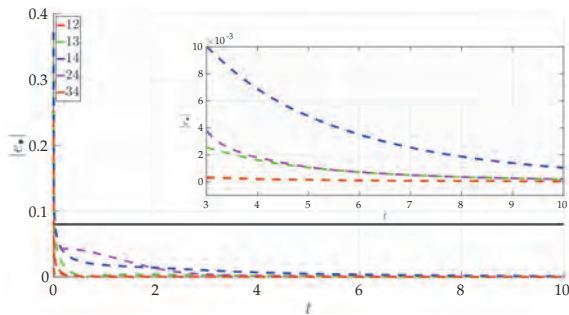
One possible direction for future work is to consider circular robots of different sizes.



(a) Robot trajectories



(b) Inter-center distances



(c) Internal angle errors

Figure 5.2: Simulation of a team of 4 circular mobile robots having radii $r = 1$. On the top panel, we have the robot trajectories; dashed circles represent initial configuration while solid circles are final robot positions. The solid lines are the robot center trajectories. In the center panel, the convergence of the distances d_{ij} (dashed) to their desired values d_{ij}^* (solid) is depicted. The black solid line represents $d_{\min} = 2$ between the robots. The bottom panel shows the convergence of the internal angle errors. The black solid line depicts the value $b = 0.08$ for the hypercube \mathcal{H}_b .

Chapter 6

Distributed Formation with Diffusive Obstacle Avoidance Control in Coordinated Mobile Robots

The previous chapters considered the problem of designing control laws for achieving the desired formation shape on the group level. In a practical scenario, achieving a desired formation is one of the tasks that we require the mobile robots to accomplish. Besides this, we can require the mobile robots to move to a specific location. During this transition, they can encounter obstacles. Avoiding these obstacles should also be part of the requirements for the team. In this chapter, we deal with the above-mentioned multi-objective problem where a group of mobile robots has to move as a collective to a desired final position. We will consider a modular approach for obtaining the sub-controllers. The resulting controller will be obtained by a linear combination of these sub-controllers and we will show that this combined controller solve our considered problem.

We start this chapter with an introduction. In Section 6.2, we formulate the problem of steering a group of mobile robots towards a desired destination. The different sub-controllers are given in Section 6.3. Furthermore, the detailed analysis on the combined controller is provided. We compare our approach with another controller in Section 6.4 and close the chapter with some conclusions.

6.1 Introduction

IN recent decades, the field of networked multi-agent systems has attracted a lot of research attention in various domains. Compared to a single robot, a group of networked robots has the advantages of being flexible, redundant and fault tolerant [7]; therefore, it can be employed to perform complex tasks [37] in a centralized or in a distributed manner. In particular, sensing and controlling the group of networked robots in a distributed manner is of interest and various application area can be found, such as detection of events in wireless sensor networks or execution of search and rescue operations in disasters.

Along this line, we consider the problem of steering a group of mobile robots as a formation towards a final desired destination while avoiding obstacles along the course of motion. A possible application can be found in smart manufacturing

systems where the group as a collective is required to work together to transport an object from position A to position B. In such smart manufacturing systems, there may be barriers which the mobile robots individually and as a group should avoid while carrying out the requested task.

In literature, numerous references are found for achieving each of the individual tasks (formation control, group motion control, obstacle avoidance) or combinations thereof. See, for example, the paper [38] for an overview of various approaches for achieving the formation control task based on the interconnection topology and sensing capability of the robots. In [7, 52], the weighted centroid tracking problem has been considered in which the formation centroid was required to track an assigned task function. In [25], a decentralized controller has been constructed based on the notion of *navigation function*. This controller guarantees the convergence of the multi-agent system to the desired formation while maintaining network connectivity and avoiding obstacles. In [37], the multi-agent collision avoidance problem was introduced and formulated as a nonlinear differential game. Dynamic feedback strategies were constructed guaranteeing the avoidance of collisions with obstacles or other agents while the individual agents reached their target. In [40], Lyapunov-like barrier functions were introduced such that the objective of avoiding obstacles could be composed together with other control objectives of the multi-agent systems into a single function for every agent.

Furthermore, avoiding obstacles can be regarded as part of the requirements for guaranteeing safety of a (non)linear system; other requirements being the state and input constraints on the system. In [2, 43], the problem of synthesizing controllers for safety critical systems has been considered. In both papers, the control design was based on the unification of both Control Lyapunov functions and Control Barrier functions for satisfying the performance/stability properties and safety objectives, respectively.

In this chapter, we propose a new distributed control law for solving the obstacle avoidance task that can be combined linearly with standard formation control law and group motion control law. In our setting, each individual robot is assumed to be able to measure the relative position with respect to the obstacle and the robot is equipped with a potential-based distributed control law that is used to compute local obstacle avoidance maneuver. Correspondingly, we introduce a distributed dynamic controller that allows the diffusion of such obstacle avoidance maneuver action to the neighbors and to the rest of the network. In comparison to the approach proposed in [37], our obstacle avoidance approach is completely decentralized and we prove rigorously that our approach can be combined linearly with other distributed control laws for simultaneously solving the multitasking problem. By contrast, in [37], the agents were not required to achieve a network objective (such as, a desired formation or consensus) while moving to the individual target positions. As will be shown later in our simulation results, by diffusing

the obstacle avoidance maneuver to the network through a dynamic controller, we are able to minimize the deformation in the formation shape that is mainly caused by the local obstacle avoidance movement. In contrast to the work in [25], we consider also the movement of the formation as a whole towards a desired destination in the plane. For the moment, the group motion control is achieved by a centralized control law.

6.2 Problem Formulation

We consider a group of n identical agents¹ moving in the 2-dimensional plane. Each robot is modeled as a single integrator, i.e.,

$$\dot{p}_i = u_i, \quad i \in \mathcal{V} := \{1, \dots, n\}, \quad (6.1)$$

where $p_i \in \mathbb{R}^2$ and $u_i \in \mathbb{R}^2$ denote the position and controlled velocity of robot i , respectively. In the following, we will introduce the three tasks that will be handled simultaneously by our proposed controller.

Obstacle Avoidance Control Problem

Without loss of generality, we consider obstacles that can be encapsulated by circles in the plane. The centroid and radii of each circle \mathcal{O}_k , $k = 1, \dots, K$ is given by $p_k^{\text{obs}} \in \mathbb{R}^2$ and $R_k^{\text{obs}} \in \mathbb{R}_{>0}$, respectively. The boundary of the k -th obstacle is defined by the set

$$\partial\mathcal{O}_k := \left\{ x \mid \|x - p_k^{\text{obs}}\| = R_k^{\text{obs}} \right\}.$$

For our later description of distributed obstacle avoidance control law, we associate to each robot i a parameter $R_i^{\text{safe}} \in \mathbb{R}_{>0}$ which defines the safe distance to the boundary of any obstacle. Roughly speaking, when the robot's distance to the boundary of an obstacle is less than R_i^{safe} , then the distributed obstacle avoidance control will set in for the i -th robot. In the current setup, we consider the case $R_i^{\text{safe}} = R^{\text{safe}}$ for all $i \in \mathcal{V}$.

For the following definitions, let \mathcal{P}_0 denote the set of initial conditions which do not intersect \mathcal{O}_k for all k .

Definition 6.1 (local obstacle avoidance). *The i -th robot is said to avoid collision with obstacle \mathcal{O}_k if for almost all $p_i(0) \in \mathcal{P}_0$ the trajectories $p_i(t)$ do not enter \mathcal{O}_k for all $t \in \mathbb{R}_{\geq 0}$, i.e., $p_i(t) \notin \mathcal{O}_k$ for all $t \in \mathbb{R}_{\geq 0}$.*

Definition 6.2 (obstacle avoidance task). *The group of n agents is said to achieve obstacle avoidance if every i -th robot avoids collision with all obstacles \mathcal{O}_k , $k = 1, \dots, K$.*

¹We use the term 'agent' and (mobile) robot interchangeably.

Formation Control Problem

The interaction among the agents is represented by an undirected and connected graph $\mathcal{G}(\mathcal{V}, \mathcal{E})$. In the present study, we assume that the agents can obtain relative position information from its neighbors, i.e., robot i has access to $p_j - p_i, \forall j \in \mathcal{N}_i$. The desired relative position among the agents is encoded in a vector $p^* \in \mathbb{R}^{2n}$. Note that p^* has to satisfy geometric constraints that define the shape of the formation; we assume p^* is well-posed, i.e., the formation shape is geometrically feasible. We refer to the exposition in [6, 19, 39] on the graph formalism of mobile robots' formation. For a given p^* , the group of n -agents is said to be in *the desired formation* if $p_j - p_i = p_j^* - p_i^*, \forall (i, j) \in \mathcal{E}$.

Definition 6.3 (formation task). *For a given p^* , the group of n -agents is said to achieve formation w.r.t. p^* if all agents' trajectories asymptotically converge to the desired formation, i.e., $\lim_{t \rightarrow \infty} (p_j(t) - p_i(t)) = p_j^* - p_i^*, \forall (i, j) \in \mathcal{E}$.*

Group Stabilization Control Problem

In addition to the above distributed control tasks, we can add a group motion task where the group's centroid and orientation are controlled to achieve certain control behavior, such as following a given reference trajectory or converging to a desired point (e.g., group stabilization).

Definition 6.4 (group stabilization task). *The group of n -agents is said to achieve group stabilization if the centroid of the group $p_{cen} := \frac{1}{n} \mathbb{1}_n^T p$ converges asymptotically to the origin, i.e., $p_{cen}(t) \rightarrow \mathbb{0}_2$ as $t \rightarrow \infty$.*

In the following section, we present our control design framework which accomplish all three different control tasks. Both the obstacle avoidance and formation task are solved by distributed control laws while the group stabilization task is solved by a coordinated control law.

Assumption 6.5. During the transition, the formation centroid p_{cen} is allowed to cross the obstacles.

6.3 Distributed Obstacle Avoidance-Formation Control Design

The navigation function as used in [25] requires us to have prior information of all tasks so that we can embed this information to the navigation function. In contrast to this approach, we will pursue a control design that is modular where one can add and remove the control law for a particular task directly without jeopardizing

the completion of other tasks. Therefore, we assume that the control law for each robot is a linear combination of control laws of different tasks, i.e.,

$$u_i = u_i^f + u_i^g + u_i^o, \quad \forall i \in \mathcal{V}, \quad (6.2)$$

where u_i^f is the local control law for solving formation task, u_i^g is the local control law for solving group stabilization task, and u_i^o is the local control law for solving obstacle avoidance task of the i -th robot.

In the following sub-sections, we present a particular control law for each of the aforementioned tasks that will be used in our unified control framework. While our framework is not restricted to these control laws, we will focus mainly on these laws in this chapter where we can demonstrate the applicability of our approach.

6.3.1 Distributed formation control law

For achieving the formation task, we consider the following standard relative position-based formation control law

$$u_i^f = c_f \sum_{j \in \mathcal{N}_i} w_{ij} ((p_j - p_i) - (p_j^* - p_i^*)) \quad (6.3)$$

where $c_f \in \mathbb{R}_{>0}$ is the formation gain and $w_{ij} \in \mathbb{R}_{>0}$ is the weight of the edge $(i, j) \in \mathcal{E}$. In compact form, the above law can be written as

$$U^f = c_f \tilde{L} (p^* - p) \quad (6.4)$$

where U^f is the stacked vector of u_i^f s and $\tilde{L} = L \otimes I_2$. The stability analysis of closed-loop system using only this formation control law can be found, among others, in [38].

6.3.2 Coordinated group stabilization control law

For stabilizing the group, we assume the existence of a central coordinator. The role of the central coordinator is to calculate the formation centroid p_{cen} based on the position of the agents and use this information to compute the stabilizing control law for the group.

The design of the control law for group stabilization is based on the assumption that the desired formation has been reached and there is no obstacle. In this case, using (6.1), (6.2), (6.3) and $u_i^o = 0_2$, the dynamics of the centroid position is given by

$$\dot{p}_{\text{cen}} = \frac{1}{n} \tilde{\mathbb{1}}_n^\top \dot{p} = u^g, \quad (6.5)$$

where we assume that the control law u^g will be communicated to all the agents, and therefore $u_1^g = u_2^g = \dots = u_n^g = u^g$.

We propose the following group motion control law:

$$\begin{cases} u^g = -c_P p_{\text{cen}} + c_I \gamma \\ \dot{\gamma} = -p_{\text{cen}}, \end{cases} \quad (6.6)$$

where $c_P \in \mathbb{R}_{>0}$ and $c_I \in \mathbb{R}_{>0}$ are the group proportional and integral gain, respectively. In compact form, we can write the group stabilization control law for the whole group as

$$U^g = \tilde{\mathbb{1}}_n (-c_P p_{\text{cen}} + c_I \gamma), \quad (6.7)$$

where U^g is the stacked vector of u_i^g s.

If we do not need to solve for the obstacle avoidance task then the group stabilization task can be solved simply by using a proportional controller. As it will be clear later, the integral action is needed in our control law for compensating the drift that is introduced by the distributed control law for the obstacle avoidance given in the next subsection. We also remark that as each robot gets u^g , the formation control is not affected by the group motion control. Therefore, both control laws are complementary to each other.

6.3.3 Distributed obstacle avoidance control law

While the agents are maintaining the formation shape and moving together towards the desired destination, all agents should locally avoid any obstacle that they encounter during the course of transition. Let us consider for the moment a robot i and an obstacle \mathcal{O}_k . As defined before, the robot i avoids obstacle \mathcal{O}_k when $p_i(t) \notin \mathcal{O}_k$ for all $t \in \mathbb{R}_{\geq 0}$. Note that the distance from p_i to \mathcal{O}_k is

$$d_k(p_i) := \min_{x \in \partial \mathcal{O}_k} \lim \|x - p_i\|. \quad (6.8)$$

while the point in \mathcal{O}_k that is closest to p_i is denoted by

$$x_k^*(p_i) := \arg \min_{x \in \partial \mathcal{O}_k} \|x - p_i\|. \quad (6.9)$$

Using these notations, robot i avoids obstacle \mathcal{O}_k implies that $d_k(p_i(t)) > 0$ for all $t \in \mathbb{R}_{\geq 0}$. For constructing a local obstacle avoidance control law, we consider a potential function which is a logarithmic barrier function given by

$$W_k(p_i) = -c_\alpha \log \left(\frac{d_k(p_i)}{R^{\text{safe}}} \right). \quad (6.10)$$

It can be checked that as $p_i \rightarrow \partial\mathcal{O}_k$, $W_k(p_i) \rightarrow \infty$. Using such potential function, the following gradient-based control law for robot i when it is within the vicinity to the obstacle \mathcal{O}_k has been used for mobile robots to avoid obstacles (see, for instance, [27, 50]).

$$u_i^o = \alpha_i^k(p_i), \quad (6.11)$$

where $\alpha_i^k(p_i)$ is given by

$$\alpha_i^k(p_i) = \begin{cases} 0_2 & \text{if } d_k(p_i) > R^{\text{safe}} \\ -\left(\frac{\partial W_k(p_i)}{\partial p_i}\right)^\top & \text{otherwise.} \end{cases} \quad (6.12)$$

The constant $c_\alpha \in \mathbb{R}_{>0}$ in (6.10) defines the controller gain and it can be checked that

$$\frac{\partial W_k(p_i)}{\partial p_i} = c_\alpha \frac{(x_k^*(p_i) - p_i)^\top}{d_k^2(p_i)}$$

based on the use of potential function W_k as in (6.10).

So when the relative distance between a robot i and the obstacle k is less than the threshold R^{safe} , robot i will activate the obstacle avoidance action. However, if we apply this obstacle avoidance control law locally on robot i , then the rest of the agents will only be driven by the formation and group stabilization control laws (c.f. (6.2)). As a consequence, the unexpected obstacle avoidance maneuver by robot i that is not communicated to the others will introduce undesirable deformation to the formation shape. On the other hand, the real-time communication of the obstacle avoidance control action to all agents should be prohibited as it will unnecessarily consume the communication channel and is not scalable.

In order to “diffuse” the obstacle avoidance action to the other agents, we introduce a dynamic obstacle avoidance controller whose state variable ζ_i is communicated to its neighbors. More precisely, the local dynamic obstacle avoidance controller is described by

$$\begin{cases} \dot{\zeta}_i &= c_\zeta \sum_{j \in \mathcal{N}_i} w_{ij} (\zeta_j - \zeta_i) + u_{\alpha_i} \\ u_i^o &= \zeta_i, \end{cases} \quad (6.13)$$

where $c_\zeta \in \mathbb{R}_{>0}$ is the diffusion gain of obstacle avoidance control law, $w_{ij} \in \mathbb{R}_{>0}$ is the weight of the edge $(i, j) \in \mathcal{E}$ and u_{α_i} is given by

$$u_{\alpha_i} = \sum_{k=1}^K \alpha_i^k(p_i) = - \sum_{k=1}^K \left(\frac{\partial W_k(p_i)}{\partial p_i} \right)^\top.$$

In compact form, the distributed dynamic obstacle avoidance control law is given

by

$$\begin{cases} \dot{\zeta} &= -c_\zeta \tilde{L}\zeta + U_\alpha \\ U^\circ &= \zeta, \end{cases} \quad (6.14)$$

where U° and U_α are the stacked vector of u_i° s and u_{α_i} s, respectively. The state variable ζ can be seen as an aggregation of the obstacle behavior of the individual robot. When we pre-multiply the first equation in (6.13) by $\frac{1}{n}\tilde{\mathbb{1}}_n^\top$, we obtain

$$\frac{1}{n}\tilde{\mathbb{1}}_n^\top \dot{\zeta} = \frac{1}{n}\tilde{\mathbb{1}}_n^\top \left(-c_\zeta \tilde{L}\zeta + U_\alpha \right) \implies \dot{\zeta}_{\text{avg}} = \frac{1}{n} \sum_{i=1}^n u_{\alpha_i},$$

where $\zeta_{\text{avg}} := \frac{1}{n}\tilde{\mathbb{1}}_n^\top \zeta$. Thus, whenever the agents are already free from obstacles after some finite time $\tilde{t} > 0$, then $U_\alpha(t) = \mathbb{0}_{2n}$ for all $t > \tilde{t}$. In this case, the distributed obstacle avoidance control law becomes a consensus system which implies that ζ_i will converge to a common value given by $\frac{1}{n} \sum_{j=1}^n \zeta_j(\tilde{t})$ as a consequence of the average consensus protocol. Due to the integral action in the group stabilization controller, such constant bias from the asymptote of $\zeta_i(t)$ will be compensated and the integral controller ensures that the formation will not be deformed and the group centroid converges to the origin.

6.3.4 Stability analysis of the unified control law

We will prove that the unified control law (6.2), where the individual control laws u_i^f, u_i^g, u_i° are as in (6.3), (6.6) and (6.13), is able to achieve the control objectives of reaching and maintaining desired formation, of coordinated group stabilization and of performing obstacle avoidance. We state the following main result:

Theorem 6.6. *Consider a group of n -agents modeled as single integrators as in (6.1) and the multitasking control problem as given before with obstacles $\mathcal{O}_k, k = 1, \dots, K$ and the target formation shape encoded in the desired relative position p^* . Then the unified control law (6.2) with u_i^f, u_i^g, u_i° given by (6.3), (6.6) and (6.13), respectively, solve simultaneously the obstacle avoidance, formation and group stabilization control problems globally. More precisely, for all initial conditions $p_i(0) \in \mathbb{R}^2 \setminus \bigcup_k \mathcal{O}_k$,*

- (O1) $\lim_{t \rightarrow \infty} \tilde{H}(p^* - p(t)) = \mathbb{0}_{2m}$; the desired formation is asymptotically reached;
- (O2) $p_{\text{cen}}(t) = \frac{1}{n}\tilde{\mathbb{1}}_n^\top p(t) \rightarrow \mathbb{0}_2$ as $t \rightarrow \infty$; the group centroid converges to the origin;
- (O3) $d_k(p_i(t)) > 0$ for all i, k and $t \in \mathbb{R}_{\geq 0}$; every robot avoids all obstacles at all time.

Before giving the proof of Theorem 6.6, we first present the following auxiliary result. Using the incidence matrix H , we can transform the dynamics on the agents

p_i to dynamics on the edges of the form $p_j - p_i$. Let us define $z := \tilde{H}p \in \mathbb{R}^{2m}$. The z -dynamics are then given by

$$\begin{aligned}\dot{z} &= \tilde{H}\dot{p} = \tilde{H} \left(c_f \tilde{L}(p^* - p) + \tilde{\mathbb{1}}_n (-c_P p_{\text{cen}} + c_1 \gamma) + \zeta \right) \\ &= c_f \tilde{H} \tilde{L}(p^* - p) + \tilde{H} \zeta.\end{aligned}\quad (6.15)$$

Lemma 6.7. *Assume the group of agents successfully carried out the obstacle avoidance task. Then the equilibrium points of the closed loop system satisfy $H(p^* - p) = \mathbb{0}_{2m}$ and $p_{\text{cen}} = \frac{1}{n} \tilde{\mathbb{1}}_n^\top p = \mathbb{0}_2$.*

Proof. Firstly, it can be checked that the time derivative of \dot{p} is given by

$$\ddot{p} = -c_f \tilde{L}\dot{p} + \tilde{\mathbb{1}}_n (-c_P \dot{p}_{\text{cen}} - c_1 \dot{p}_{\text{cen}}) - c_\zeta \tilde{L}\zeta + U_\alpha. \quad (6.16)$$

The term $\tilde{L}\zeta$ can be rewritten as

$$\tilde{L}\zeta = \tilde{H}^\top \tilde{W} \tilde{H} \zeta = \tilde{H}^\top \tilde{W} \left(\dot{z} - c_f \tilde{H} \tilde{L}(p^* - p) \right) = \tilde{L}\dot{p} - c_f \tilde{L}^2(p^* - p). \quad (6.17)$$

Substituting (6.17) in (6.16) yields

$$\begin{aligned}\ddot{p} &= -c_f \tilde{L}\dot{p} + \tilde{\mathbb{1}}_n (-c_P \dot{p}_{\text{cen}} - c_1 \dot{p}_{\text{cen}}) - c_\zeta \left(\tilde{L}\dot{p} - c_f \tilde{L}^2(p^* - p) \right) + U_\alpha \\ &= -(c_f + c_\zeta) \tilde{L}\dot{p} - c_f c_\zeta \tilde{L}^2 p + \tilde{\mathbb{1}}_n (-c_P \dot{p}_{\text{cen}} - c_1 \dot{p}_{\text{cen}}) + c_f c_\zeta \tilde{L}^2 p^* + U_\alpha \\ &= - \left[(c_f + c_\zeta) \tilde{L} + c_P \tilde{Q} \right] \dot{p} - \left[c_f c_\zeta \tilde{L}^2 + c_1 \tilde{Q} \right] p + c_f c_\zeta \tilde{L}^2 p^* + U_\alpha,\end{aligned}\quad (6.18)$$

where $\tilde{Q} = \frac{1}{n} \tilde{\mathbb{1}}_n \tilde{\mathbb{1}}_n^\top$. Moving the terms of p and \dot{p} to the left-hand side of the equation, we obtain

$$\ddot{p} + \mathcal{A}\dot{p} + \mathcal{B}p = c_f c_\zeta \tilde{L}^2 p^* + U_\alpha, \quad (6.19)$$

where $\mathcal{A} = (c_f + c_\zeta) \tilde{L} + c_P \tilde{Q}$, $\mathcal{B} = c_f c_\zeta \tilde{L}^2 + c_1 \tilde{Q}$. As the obstacle avoidance task is successfully carried out, $U_\alpha = \mathbb{0}_{2N}$. Setting also \dot{p} and \ddot{p} to zero to determine equilibrium points, we have

$$\left(c_f c_\zeta \tilde{L}^2 + \frac{c_1}{N} \tilde{\mathbb{1}}_n \tilde{\mathbb{1}}_n^\top \right) p = c_f c_\zeta \tilde{L}^2 p^* \iff c_1 \tilde{\mathbb{1}}_n p_{\text{cen}} = c_f c_\zeta \tilde{L} \tilde{H}^\top \tilde{W} \tilde{H} (p^* - p).$$

By the hypothesis that the formation is feasible, we can readily observe the existence of a \hat{p} which satisfies both $\tilde{H}(p^* - \hat{p}) = \mathbb{0}_{2m}$ and $\tilde{\mathbb{1}}_n \hat{p} = \mathbb{0}_2$. \hat{p} is also unique. This completes the proof. \square

Now, we are ready to proof Theorem 6.6 as follows.

Proof. From the proof of Lemma 6.7, we can consider the dynamics of the closed-

loop system as given by (6.19). Take as Lyapunov function candidate

$$\begin{aligned} V(p, \dot{p}) &= \frac{1}{2} \dot{p}^\top \dot{p} + \frac{1}{2} c_f c_\zeta (p^* - p)^\top \tilde{L}^2 (p^* - p)^\top \\ &\quad + \frac{1}{2} c_1 n p_{\text{cen}}^\top p_{\text{cen}} + \sum_{i=1}^n \sum_{k=1}^K W_k(p_i) \end{aligned} \quad (6.20)$$

where $W_k(p_i)$ is the logarithmic barrier function (6.10) which is active when $d_k(p_i) \leq R^{\text{safe}}$ and else 0. The time derivative of V is

$$\begin{aligned} \dot{V} &= \dot{p}^\top \ddot{p} - c_f c_\zeta (p^* - p)^\top \tilde{L}^2 \dot{p} + c_1 n p_{\text{cen}}^\top \dot{p}_{\text{cen}} + \sum_{i=1}^n \sum_{k=1}^K \frac{d}{dt} W_k(p_i) \\ &= \dot{p}^\top \left[-\mathcal{A}\dot{p} - \mathcal{B}p + c_f c_\zeta \tilde{L}^2 p^* + U_\alpha \right] - c_f c_\zeta \dot{p}^\top \tilde{L}^2 (p^* - p) \\ &\quad + c_1 n \left(\frac{1}{n} \tilde{\mathbb{1}}_n^\top \right)^\top \left(\frac{1}{n} \tilde{\mathbb{1}}_n^\top \dot{p} \right) + \sum_{i=1}^n \sum_{k=1}^K \frac{\partial W_k}{\partial p_i} \dot{p}_i \\ &= \dot{p}^\top \left[-\mathcal{A}\dot{p} - c_1 \tilde{Q}p + U_\alpha \right] + c_1 p^\top \tilde{Q} \dot{p} - \sum_{i=1}^n u_{\alpha_i}^\top \dot{p}_i \\ &= -\dot{p}^\top \mathcal{A} \dot{p} < -\ell \|\dot{p}\|^2, \end{aligned} \quad (6.21)$$

where $\ell > 0$. The last inequality is due to the fact that \mathcal{A} is positive definite by Lemma 2.1. Since the function V is proper and \dot{V} is non-increasing, it follows immediately that **(O3)** is achieved. Moreover, the application of La-Salle invariance principle implies that the state trajectories $(p(t), \dot{p}(t))$ converges to the largest invariant set where $\dot{p} = \mathbb{0}_{2n}$. By Lemma 6.7, such invariant set is given by $\tilde{H}(p^* - p) = \mathbb{0}_{2m}$ and $p_{\text{cen}} = \mathbb{0}_2$. This implies that both **(O1)** and **(O2)** hold. This completes the proof. \square

6.4 Numerical Example

6.4.1 Simulation setup

To demonstrate the applicability of the proposed control law, we perform numerical simulations with a network of 3 mobile robots. We consider two circular obstacles in the plane with center at $p_{\text{obs}_1} = (4, 7)$ and $p_{\text{obs}_2} = (1, 4)$ (shown in red in the figures). The radii of the obstacles is set equally to $R_{\text{obs}} = 0.75$. For the obstacle avoidance control law, we take $R^{\text{safe}} = 0.75$. In the figures, the blue annulus shows the area within R^{safe} from the obstacles where the obstacle avoidance control law is activated. We set the gains of the control law to

$c_f = 10$, $c_P = 1$, $c_1 = 0.8$, $c_\alpha = 100$, $c_\zeta = 10$, and the initial positions of the are $p_1 = [5, 10]^\top$, $p_2 = [5, 13]^\top$, and $p_3 = [3, 10]^\top$. The desired relative positions for the formation are set to $z_{12}^* = [0, 3]^\top$, $z_{13}^* = [-2, 0]^\top$.

6.4.2 Simulation results

The proposed control law (6.2) is compared against the control mechanism where the obstacle avoidance control law is only locally applied to the robot which is within a distance R^{safe} from an obstacle. No diffusion of this control action takes place to the neighbors and hence the other agents will solely be driven by the formation control law (6.3) and the group stabilization control law (6.6) when they are individually not in close vicinity to any obstacles. From the figure, we observe that whenever an robot is within a distance R^{safe} from the boundary of the obstacle (the blue region) then the obstacle avoidance behavior of the particular robot is ‘activated’. In the top right figure, as a direct consequence of the diffusive action in the proposed control law, the neighboring agents undergo similar trajectories as that of the maneuvering robot. However, this is not the case in the bottom left figure. Because of this, we observe larger distortion caused by the obstacle maneuver to the formation (compare the top right and the bottom right figure) for the “diffusiveless” case. Besides, in the top right figure, the length of the edge between agents 2 and 3 is not affected by the obstacle maneuver due to the fact that we started with the prescribed configuration, set the initial condition for ζ_i , $i = 2, 3$ for both agents to be the same (0_2) and both agents are connected to robot 1. In the bottom right figure, during the time interval $[0.14, 0.6]$ s, the edge between robot 2 and 3 is not affected by the obstacle maneuver of robot 1. This also occurs at the time interval $[1.0, 1.4]$ s, but now for the edge between 1 and 3 while robot 2 is avoiding obstacle \mathcal{O}_2 . Finally, one can observe that the group stabilization control law is able to steer the whole group towards the origin.

6.5 Conclusions

In this chapter, we propose a new distributed control design law for achieving formation while avoiding obstacles for a group of agents. The local obstacle avoidance is achieved by a potential-based control law. By employing a dynamical controller, the local obstacle behavior of a particular robot is diffused through the network. In combination with a coordinated group controller, we are able to steer the formation centroid to the origin while maintaining formation shape during and after the obstacle avoidance maneuver. This is shown through an example in which we compare the proposed control law with the case when the local obstacle avoidance behavior is not diffused.

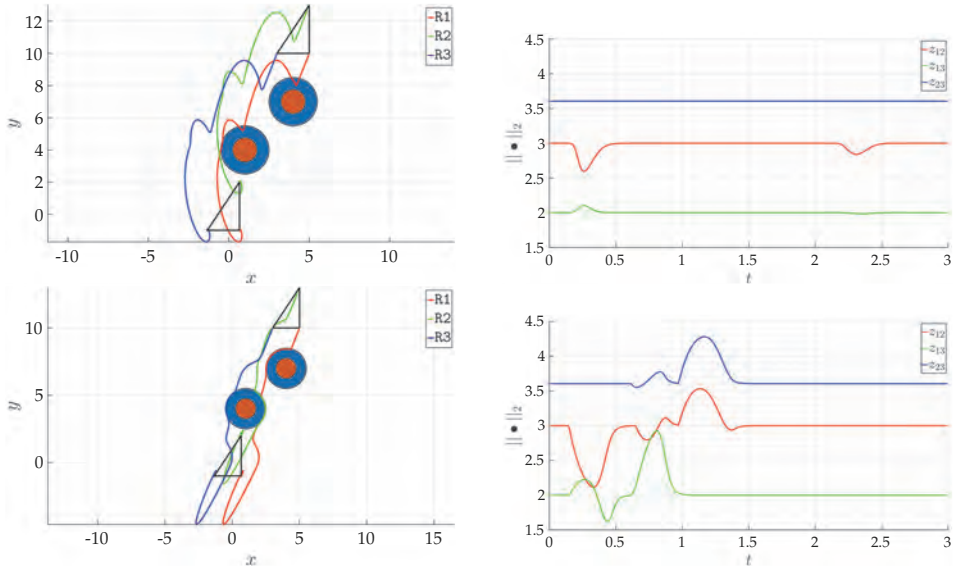


Figure 6.1: Simulation results of simultaneous obstacle avoidance, formation and group stabilization control tasks problem where we compare the performance of our diffusive obstacle avoidance distributed control approach with that of standard gradient-based local obstacle avoidance control method. Left column: The plot of three agents' position trajectories transitioning from a given initial position to the desired formation and final desired centroid position; Right column: The plot of distances between the agents; Top row: The simulation result using our proposed diffusive obstacle avoidance distributed control law; Bottom row: The simulation result using local obstacle avoidance control method and hence no "diffusion" to the neighbors.

Chapter 7

Conclusions

In this thesis, we have studied three problems; two problems concern securing a desired formation shape and the remaining one focuses on maneuvering the formation to a desired position. The following sections summarize the main findings of our study and some ideas for future work.

7.1 Main Findings

IN Chapter 3, we have investigated the problem of reaching a formation by a team of robots which can be divided in two sub teams, namely a team of robots carrying out distance related tasks while the other team of robots carries out bearing related tasks. We have employed existing gradient-based control laws for performing the individual tasks. Analyses performed on teams consisting of two and three robots have revealed that besides the desired formation shape, the robots may also display incorrect shapes; these can move with a constant velocity. One additional observation is that the incorrect formation shapes all have a signed area which has an opposite sign compared to the desired shape. After identifying these different shapes, we have used the linearization method to study the local stability of the desired and incorrect shapes. For the **(1D1B)** and the **(1B2D)** setup, we have found that the incorrect moving shapes are unstable while the flipped formation shape that has been encountered in the **(1B2D)** setup is stable. For the **(1D2B)** setup, we have found through the linearization method that most of the incorrect moving shapes are unstable. Only one of the moving shapes is locally attractive when certain conditions are met. We also note that the occurrence of the moving shapes can be prevented by choosing the control gains for the distance and bearing robots such that its ratio exceeds a certain threshold value related to the distance. However, in this case, the robots need to have knowledge of each other's gain parameter.

We have paid further attention to the **(1D2B)** setup in Chapter 4. In particular, we have added a signed area constraint which the distance robot also needs to satisfy and for which no additional sensing is required. In the current case, we have limited ourselves to isosceles triangles as the desired shape. Again, we start with identifying the formation shapes that the team may display. Hereafter, we

have obtained conditions which prevent the team to display incorrect moving shapes. By tuning the gain ratio between the signed area control term and the distance control term, we can guarantee that the team will only display the desired isosceles triangle. This tuning can be carried out independently of the control gain for the bearing robots.

In Chapter 5, we have studied the formation shape control problem in which the robots are modeled as circular disks. By allowing robots to take two measurements from each of its neighbors, we obtain information on the internal angle. We have established that the desired formation shape can also be given in terms of desired internal angles; these have a close relationship with formations described in terms of distances. We have proposed a gradient-based controller which utilizes only the locally available bearing measurements. Analyses performed on the associated error system show the local exponential convergence of the formation system to the desired formation shape. In addition, collision avoidance is guaranteed for each pair of neighboring robots.

Finally, we have focused on a multi-objective formation-motion control problem in Chapter 6. The goal here has been to steer the whole formation to a desired final position while avoiding obstacles. We have proposed a dynamic obstacle avoidance controller for each robot to avoid circular obstacles during the transition. By communicating this control action to the rest of the team, we show that the distortion on the formation shape is reduced. This obstacle avoidance controller can be combined with the other tasks that the robots need to carry out.

7.2 Outlook

In what follows, we provide some ideas for future work.

- Chapter 3: For the **(1B2D)** setup, we have observed that the flipped formation is also locally attractive. Recently, the authors in [30] have introduced the concept of a signed angle which is related to the signed area of a triangle. As one direction, we could study the effect of introducing such a signed angle constraint for the bearing robot in the **(1B2D)** setup.
- Chapter 4: For the **(1D2B)** setup, numerical analyses have shown that the signed area constraint may also be beneficial for the general triangle case. The formal analysis of this could be done following closely the workflow we have executed for the case of isosceles triangles. We may need to introduce a new parameter corresponding to the desired distances, i.e., $d_{12}^* = t d_{13}^*$. Note that for isosceles triangles, the parameter t has the value 1.
- Chapters 3 and 4: In these chapters, we have performed analyses on setups of two and three mobile robots. It is of interest to study setups with more

than three heterogeneous sensing robots. A systematic approach for augmenting the three mobile robot setup could be a first step in this endeavor. Inspirations for this could be drawn from the Henneberg operations for growing minimally distance-rigid graphs .

- Chapter 5: In this chapter, the robots are taken as circular disks with a common value for the radius. It would be of interest to consider circular robots with different sizes. One of the challenges here is that the same distance translates to a different internal angle for each of the robot maintaining the same distance. Perhaps considering the interconnection to be directed instead of undirected would be more beneficial. Another extension would be to consider robots moving in the 3D-space rather than the plane. The robots could be considered as spherical objects with a common radii. It is possible to obtain an internal angle based on two measurements similar to the 2D-plane case.
- Chapter 6: For the formation-maneuvering problem, we could employ distance-based formation control instead of formation control in terms of relative positions. The group control is currently carried out by an external coordinator. It would be an idea to accomplish this task by allowing one or several robots to be 'leaders' of the team while the remaining robots are 'followers'. For the circular robots in Chapter 5, we could also explore the formation-maneuvering problem.

Bibliography

- [1] H.-S. Ahn. *Formation Control*. Springer-Verlag GmbH, 2019.
- [2] A. D. Ames, X. Xu, J. W. Grizzle, and P. Tabuada. Control Barrier Function Based Quadratic Programs for Safety Critical Systems. *IEEE Transactions on Automatic Control*, 62(8):3861–3876, Aug. 2017.
- [3] B. D. O. Anderson, Z. Sun, T. Sugie, S.-I. Azuma, and K. Sakurama. Distance-based rigid formation control with signed area constraints. In *2017 56th IEEE Conference on Decision and Control (CDC)*, pages 2830–2835, Dec. 2017.
- [4] B. D. O. Anderson, Z. Sun, T. Sugie, S.-I. Azuma, and K. Sakurama. Formation shape control with distance and area constraints. *IFAC Journal of Systems and Control*, 1:2–12, Sept. 2017.
- [5] B. D. O. Anderson, C. Yu, S. Dasgupta, and A. S. Morse. Control of a three-coleader formation in the plane. *Systems & Control Letters*, 56(9):573–578, 2007.
- [6] B. D. O. Anderson, C. Yu, B. Fidan, and J. M. Hendrickx. Rigid graph control architectures for autonomous formations. *IEEE Control Systems Magazine*, 28:48–63, 2008.
- [7] G. Antonelli, F. Arrichiello, F. Caccavale, and A. Marino. Decentralized time-varying formation control for multi-robot systems. *The International Journal of Robotics Research*, 33(7):1029–1043, May 2014.
- [8] M.-A. Belabbas, S. Mou, A. S. Morse, and B. D. O. Anderson. Robustness issues with undirected formations. In *2012 51st IEEE Conference on Decision and Control (CDC)*, pages 1445–1450. IEEE, Dec. 2012.

- [9] A. N. Bishop, M. Deghat, B. D. O. Anderson, and Y. Hong. Distributed formation control with relaxed motion requirements. *International Journal of Robust and Nonlinear Control*, 25(17):3210–3230, Nov. 2015.
- [10] A. N. Bishop, T. H. Summers, and B. D. O. Anderson. Stabilization of stiff formations with a mix of direction and distance constraints. In *2013 IEEE International Conference on Control Applications (CCA)*, pages 1194–1199, Aug. 2013.
- [11] K. Cao, Z. Han, X. Li, and L. Xie. Ratio-of-Distance Rigidity in Distributed Formation Control. In *2018 15th International Conference on Control, Automation, Robotics and Vision (ICARCV)*, pages 1016–1021. IEEE, Nov. 2018.
- [12] K. Cao, D. Li, and L. Xie. Bearing-ratio-of-distance rigidity theory with application to directly similar formation control. *Automatica*, 109:108540, Nov. 2019.
- [13] M. Cao, A. S. Morse, C. Yu, B. D. O. Anderson, and S. Dasgupta. Controlling a triangular formation of mobile autonomous agents. In *2007 46th IEEE Conference on Decision and Control (CDC)*, pages 3603–3608, 2007.
- [14] M. Cao, C. Yu, A. S. Morse, B. D. O. Anderson, and S. Dasgupta. Generalized Controller for Directed Triangle Formations. *IFAC Proceedings Volumes*, 41(2):6590–6595, 2008.
- [15] Y. Cao, Z. Sun, B. D. O. Anderson, and T. Sugie. Almost Global Convergence For Distance- and Area-Constrained Hierarchical Formations Without Reflection. In *2019 15th IEEE International Conference on Control and Automation (ICCA)*, pages 1534–1539, July 2019.
- [16] L. Chen, M. Cao, and C. Li. Angle rigidity and its usage to stabilize multi-agent formations in 2D. *IEEE Transactions on Automatic Control*, pages 1–1, 2020.
- [17] H. G. de Marina. Maneuvering and robustness issues in undirected displacement-consensus-based formation control. *To appear in IEEE Transactions on Automatic Control*, 2021.
- [18] H. G. de Marina, M. Cao, and B. Jayawardhana. Controlling Rigid Formations of Mobile Agents Under Inconsistent Measurements. *IEEE Transactions on Robotics*, 31(1):31–39, Feb. 2015.
- [19] H. G. de Marina, B. Jayawardhana, and M. Cao. Distributed Rotational and Translational Maneuvering of Rigid Formations and Their Applications. *IEEE Transactions on Robotics*, 32(3):684–696, June 2016.

- [20] H. G. de Marina, Z. Sun, M. Cao, and B. D. O. Anderson. Controlling a triangular flexible formation of autonomous agents. *IFAC-PapersOnLine*, 50(1):594–600, July 2017.
- [21] M. de Queiroz, X. Cai, and M. Feemster. *Formation Control of Multi-Agent Systems*. John Wiley & Sons, Ltd, Jan. 2019.
- [22] L. E. Dickson. *First Course in the Theory of Equations*. John Wiley & Sons, Incorporated, 1922.
- [23] F. Dörfler and B. A. Francis. Formation control of autonomous robots based on cooperative behavior. In *2009 European Control Conference (ECC)*, pages 2432–2437. IEEE, Aug. 2009.
- [24] D. Frank, D. Zelazo, and F. Allgöwer. Bearing-Only Formation Control with Limited Visual Sensing: Two Agent Case. *IFAC-PapersOnLine*, 51(23):28–33, 2018.
- [25] Z. Kan, A. P. Dani, J. M. Shea, and W. E. Dixon. Network Connectivity Preserving Formation Stabilization and Obstacle Avoidance via a Decentralized Controller. *IEEE Transactions on Automatic Control*, 57(7):1827–1832, July 2012.
- [26] H. K. Khalil. *Nonlinear Systems*. Prentice Hall, Upper Saddle River, New Jersey, 3 edition, 2002.
- [27] O. Khatib. Real-Time Obstacle Avoidance for Manipulators and Mobile Robots. *The International Journal of Robotics Research*, 5(1):90–98, Mar. 1986.
- [28] L. Krick, M. E. Broucke, and B. A. Francis. Stabilisation of infinitesimally rigid formations of multi-robot networks. *International Journal of Control*, 82(3):423–439, Feb. 2009.
- [29] S.-H. Kwon and H.-S. Ahn. Generalized Rigidity and Stability Analysis on Formation Control Systems with Multiple Agents. In *2019 18th European Control Conference (ECC)*, pages 3952–3957, June 2019.
- [30] S.-H. Kwon, Z. Sun, B. D. O. Anderson, and H.-S. Ahn. Hybrid distance-angle rigidity theory with signed constraints and its applications to formation shape control. <https://arxiv.org/abs/1912.12952>, 2019.
- [31] S.-H. Kwon, M. H. Trinh, K.-H. Oh, S. Zhao, and H.-S. Ahn. Infinitesimal Weak Rigidity and Stability Analysis on Three-Agent Formations. In *2018 57th Annual Conference of the Society of Instrument and Control Engineers of Japan (SICE)*, pages 266–271, Sept. 2018.

- [32] H. Liu, H. G. de Marina, and M. Cao. Controlling triangular formations of autonomous agents in finite time using coarse measurements. In *2014 IEEE International Conference on Robotics and Automation (ICRA)*, pages 3601–3606. IEEE, 2014.
- [33] T. Liu and M. de Queiroz. Distance + Angle-Based Control of 2-D Rigid Formations. *IEEE Transactions on Cybernetics*, pages 1–10, 2020.
- [34] F. Mehdifar, C. P. Bechlioulis, F. Hashemzadeh, and M. Baradarannia. Prescribed performance distance-based formation control of Multi-Agent Systems. *Automatica*, 119:109086, Sept. 2020.
- [35] S. Mou, M.-A. Belabbas, A. S. Morse, Z. Sun, and B. D. O. Anderson. Undirected Rigid Formations Are Problematic. *IEEE Transactions on Automatic Control*, 61(10):2821–2836, Oct. 2016.
- [36] S. Mou, A. S. Morse, M.-A. Belabbas, and B. D. O. Anderson. Undirected rigid formations are problematic. In *2014 53rd IEEE Conference on Decision and Control (CDC)*, pages 637–642, Dec. 2014.
- [37] T. Mylvaganam, M. Sassano, and A. Astolfi. A Differential Game Approach to Multi-agent Collision Avoidance. *IEEE Transactions on Automatic Control*, 62(8):4229–4235, Aug. 2017.
- [38] K.-K. Oh, M.-C. Park, and H.-S. Ahn. A survey of multi-agent formation control. *Automatica*, 53:424–440, Mar. 2015.
- [39] R. Olfati-Saber and R. M. Murray. Graph rigidity and distributed formation stabilization of multi-vehicle systems. In *2002 41st IEEE Conference on Decision and Control (CDC)*, volume 3, pages 2965–2971. IEEE, Dec. 2002.
- [40] D. Panagou, D. M. Stipanović, and P. G. Voulgaris. Distributed Coordination Control for Multi-Robot Networks Using Lyapunov-Like Barrier Functions. *IEEE Transactions on Automatic Control*, 61(3):617–632, Mar. 2016.
- [41] W. Ren and R. W. Beard. *Distributed Consensus in Multi-vehicle Cooperative Control*. Springer, London, 2008.
- [42] W. Ren, R. W. Beard, and E. M. Atkins. Information Consensus in Multivehicle Cooperative Control. *IEEE Control Systems Magazine*, 27(2):71–82, Apr. 2007.
- [43] M. Z. Romdlony and B. Jayawardhana. Stabilization with guaranteed safety using Control Lyapunov–Barrier Function. *Automatica*, 66:39–47, Apr. 2016.
- [44] T. Sugie, B. D. O. Anderson, Z. Sun, and H. Dong. On a hierarchical control strategy for multi-agent formation without reflection. In *2018 57th IEEE Conference on Decision and Control (CDC)*, pages 2023–2028, Dec. 2018.

- [45] T. Sugie, F. Tong, B. D. O. Anderson, and Z. Sun. On global convergence of area-constrained formations of hierarchical multi-agent systems. *To be presented at 2020 59th IEEE Conference on Decision and Control*; <https://arxiv.org/abs/2009.03048>, 2020.
- [46] D. J. T. Sumpter. The principles of collective animal behaviour. *Philosophical Transactions of the Royal Society of London. Series B, Biological sciences*, 361:5–22, Jan. 2006.
- [47] Z. Sun, B. D. O. Anderson, S. Mou, and A. S. Morse. Robustness issues in double-integrator undirected rigid formation systems. *IFAC-PapersOnline*, 50(1):1334–1339, July 2017.
- [48] Z. Sun, S. Mou, B. D. O. Anderson, and M. Cao. Exponential stability for formation control systems with generalized controllers: A unified approach. *Systems & Control Letters*, 93:50–57, July 2016.
- [49] Z. Sun, S. Mou, M. Deghat, and B. D. O. Anderson. Finite time distributed distance-constrained shape stabilization and flocking control for d-dimensional undirected rigid formations. *International Journal of Robust and Nonlinear Control*, 26(13):2824–2844, Sept. 2016.
- [50] K. P. Tee, S. S. Ge, and E. H. Tay. Barrier Lyapunov Functions for the control of output-constrained nonlinear systems. *Automatica*, 45(4):918–927, Apr. 2009.
- [51] T. Vicsek. A question of scale. *Nature*, 411(6836):421–421, May 2001.
- [52] Q. Yang, M. Cao, H. Fang, and J. Chen. Weighted centroid tracking control for multi-agent systems. In *2016 55th IEEE Conference on Decision and Control (CDC)*, pages 939–944. IEEE, Dec. 2016.
- [53] S. Zhao, Z. Li, and Z. Ding. A Revisit to Gradient-Descent Bearing-Only Formation Control. In *2018 IEEE 14th International Conference on Control and Automation (ICCA)*, pages 710–715. IEEE, June 2018.
- [54] S. Zhao and D. Zelazo. Bearing Rigidity and Almost Global Bearing-Only Formation Stabilization. *IEEE Transactions on Automatic Control*, 61(5):1255–1268, May 2016.
- [55] S. Zhao and D. Zelazo. Bearing Rigidity Theory and Its Applications for Control and Estimation of Network Systems: Life Beyond Distance Rigidity. *IEEE Control Systems Magazine*, 39(2):66–83, Apr. 2019.

Summary

This thesis focuses on securing and maneuvering geometrical shapes for a group of mobile robots.

We first consider a setup in which the team is divided in two types of robots, each carrying out tasks of a different type. In particular, we have so called distance robots whose task is to maintain desired distances with certain robots within the team and we have bearing robots whose task is to maintain desired directions. Existing gradient-based control laws are employed in carrying out the different tasks. For teams of two and three robots, we show that besides displaying the desired geometrical shape, the team can also display incorrect shapes. Furthermore, when displaying these incorrect shapes, the team may move with a constant velocity. We perform stability analyses on these incorrect shapes in order to determine whether the team can converge to these incorrect moving shapes.

For the team consisting of one distance and two bearing robots, we extend the task requirements by including an additional signed area constraint for the distance robot. For this setup with the additional signed area constraint, we provide a comprehensive analysis when the desired shape is an isosceles triangle. We show that by properly choosing the control gains of the distance robot, the team of robots will only display the desired shape.

Next, we consider mobile robots which have a circular shape instead of being modeled as a point mass. Due to this modeling, the robots are able to obtain more than one measurement from its neighbors. We present a setup where the robots obtain two direction measurements from each of its neighbors. Based on these measurements, we propose and subsequently perform analysis on a gradient-based controller for attaining the desired shape which is given in terms of internal angles. We are able to let the robots converge to the desired shape when the initial geometry is close to it.

Finally, we consider the team moving as a collective to a desired final position. During the transition, the team may encounter obstacles. Avoiding these obstacles

is essential for completing the assigned mission. We propose a modular framework for achieving each of the task assigned to the robot. In this scenario, we identify three tasks, namely, securing the formation, moving as a formation, and avoiding possible obstacles. We design an obstacle-avoidance controller which makes the individual robot avoid the obstacle. By letting the robot communicate this action to its neighbors, we reduce the distortion of the formation shape during movements.

Samenvatting

Dit proefschrift gaat over het formeren en bewegen van geometrische vormen door een groep van mobiele robots.

We bestuderen eerst een opstelling waarbij de groep van robots onderverdeeld is in twee typen; elk type voert bepaalde taken uit. We hebben enerzijds 'afstand-robots' welke de taken krijgen om gewenste afstanden tot andere robots te behouden en we hebben anderzijds 'richting-robots' welke in plaats van afstanden, gewenste richtingen (tot de andere robots) in stand houden. Bestaande op gradiënt gebaseerde regelaars zijn gebruikt om de verschillende taken uit te voeren. Voor teams welke uit twee of drie robots bestaan, hebben we aangetoond dat deze naast gewenste vormen, ook incorrecte vormen kunnen aannemen. Wanneer de teams deze incorrecte vorm aannemen, kunnen ze als geheel ook bewegen. Middels stabiliteitsanalyses willen we nagaan of het team van robots kan convergeren tot deze incorrecte vormen.

Voor de groep welke uit één 'afstand-robot' en twee 'richting-robots' bestaat, hebben we het takenpakket uitgebreid door toevoeging van een 'signed' oppervlakte beperking voor de 'afstand-robot'. We hebben het team als geheel uitvoerig geanalyseerd ingeval de gewenste vorm voor de groep een gelijkbenige driehoek is. Door de juiste vermenigvuldigingsfactoren voor de regelaars van de 'afstand-robot' te kiezen tonen we aan dat de groep altijd de gewenste gelijkbenige driehoek als vorm aanneemt.

Hierna kijken we naar het vraagstuk waarbij de mobiele robots worden gemodelleerd als cirkels in plaats van als punten. Als gevolg hiervan kunnen de robots meer dan één meting van hun burens waarnemen. We presenteren een opstelling waarbij de robots steeds twee richting-metingen waarnemen van elk van hun burens. Gebruikmakend van deze metingen, stellen we een op gradiënt gebaseerde regelaar voor voor het aannemen van de gewenste vorm; deze gewenste vorm wordt beschreven middels een verzameling van interne hoeken. We hebben de regelaar ook geanalyseerd en komen tot de conclusie dat de gewenste vorm kan

worden vertoond door de groep van robots indien de initiële vorm redelijk dichtbij is.

Tot slot beschouwen we een groep van robots die als een collectief bij een gewenste eindpositie moet uitkomen. Tijdens het manoeuvreren kan de groep hindernissen tegenkomen. Hierbij is het vermijden van deze hindernissen essentieel om het doel succesvol te realiseren. We stellen een modulair raamwerk voor om de individuele taken van elke robot te volbrengen. In het huidige scenario hebben we drie taken geïdentificeerd, namelijk: de formatie vormen, het bewegen als een collectief, en mogelijke hindernissen vermijden. We ontwerpen een regelaar die het mogelijk maakt dat elke robot de hindernis vermijdt. Door het communiceren van deze regelaar naar de burens beperken we de deformatie van de vorm gedurende de transitie.